PHOTOELECTROCATALYTIC DEGRADATION OF ORGANIC MICROPOLLUTANTS IN AQUEOUS SOLUTIONS USING BISMUTH VANADATE PHOTOANODES

By

Sadhna Jagannathan

Thesis Committee Members

Prof. Dr. Ir. Jan Peter van der Hoek

Dr. Ir. Henri Spanjers

Prof. Dr. Ir. Ruud van Ommen

Ir. Agha Zeeshan Ali

Submitted by: June 2022

Program: MSc. Applied Earth Sciences

Track: Environmental Engineering

Faculty: Civil Engineering & Geosciences

Department: Water Management

ACKNOWLEDGEMENT

My journey of MSc Environmental Engineering at TU Delft has been strenuous and challenging, yet enlightening all at once. This journey was filled with ups, downs and lessons, and as I look back, this was the best decision that I could have taken, and I am grateful for the experience. I was fortunate to be able to conduct my thesis in water treatment, a field with so much potential, and I am grateful to have had a wonderful team of supervisors to accomplish my goals.

I extend my heartfelt gratitude to my daily supervisor, Ir. Agha Zeeshan Ali for his constant guidance, patience and kindness throughout my thesis, for teaching me many skills that I know today, and for motivating me to always aim high and be perseverant in work. I sincerely thank Dr. Ir. Henri Spanjers and Prof. Dr. Ir. Jan Peter van der Hoek, for their expert advice and feedback during my thesis which immensely helped me in my work, along with their kind and encouraging words that motivated me. I also thank Prof. Dr. Ir. Ruud van Ommen and Dr. Ir. Yasmina Bennani for their valuable suggestions in solidifying my thesis matter.

I thank the Waterlab technicians for answering my doubts regarding lab information, location of chemicals and technical issues. I thank Patricia and Jane for operating the LC-MS for my samples, and Armand for providing me with the necessary equipment. I also thank Ruud Henrikx, Bahiya Ibrahim, Arjan Thijssen and Stefaan Heirman for carrying out important analyses.

This rollercoaster would not have been possible to ride without a solid support system, both in Delft and back home. First and foremost, I thank my amazing parents, who taught me the value of hard work, for providing me with unconditional love and care, and encouraging words of support and advice from overseas. I thank Sarah for always unfailingly being there for me during my work, be it in my sickness, self-doubt or happiness, and for giving me advice which was crucial for my thesis. I thank my amazing friends Srilekha, Ravi, Aditya, Rahul, and Yuga, my family in Delft, for our friendship, warmth and chai sessions. I thank my lovely juniors, Monica and Maitry, who became my support system through the course of my lab work, kept watch over me and pulled me back up whenever I fell. I thank Yiqian for her assistance and our teamwork in lab experiments. Finally, I was lucky to have awesome friends in my class, and I thank Eman, Hannah, Fabio, Feiyang, and Chris for their immense help and partnership in my courses.

ABSTRACT

As industrialization advances rapidly in pursuit of refining the quality of human life, there has been a release of organic micropollutants (OMPs) such as pharmaceuticals into various water reserves. This has endangered the ecosystem and the possibilities of water recovery. Commonly used tertiary wastewater treatment technologies have proven to, not under all conditions, be less effective in OMP removal. Hence, Advanced Oxidation Processes (AOPs) have gained attention in the recent past due to their production of reactive oxidative species (ROS) that unselectively degrade OMPs. Photocatalysis (PC), an AOP that uses solar radiation to produce ROS, has been investigated earlier, but shows low efficiency due to fast electron-hole recombination. Photoelectrocatalysis (PEC) is a modified version that additionally uses electrical energy, thereby reducing the recombination and improving the OMP removal efficiency. Bismuth vanadate ($BiVO_4$) photocatalyst has gained importance due to its narrow band gap of 2.4 eV and hence, efficient absorption in visible light spectrum. Thus, this research focused on investigating PEC using $BiVO_4$ electrodes for the removal of OMPs in aqueous solutions. The $BiVO_4$ electrodes were fabricated using dip-coating from 1 to 5 layers, and electrodeposition at -0.2 V and -0.4 V, each at durations of 2, 5, 7, 10 and 15 minutes. They were then characterized using analytical techniques to investigate their structural, optical and optoelectronic properties. Subsequently, all the $BiVO_4$ electrodes were used for the photoelectrocatalytic degradation of Acetaminophen (ACT). The electrodes fabricated by dip-coating were shown to achieve superior degradation efficiencies of ACT of over 99% in 5 hours, due to optimum surface morphology and band gap. It was seen that their varied surface structures played an important role in improving OMP degradation, and compensated for their low average quantum efficiency at 7%, as compared to that of electrodeposition at 14%. Next, the photoelectrocatalytic degradation of multiple OMPs in a solution was studied, and it was determined that although the ROS unselectively targeted all the OMPs, some were degraded quicker than others due to their chemical structure. Scavenging experiments were also carried out that affirmed the role played by ROS in the photoelectrocatalytic degradation of the OMPs. Eventually, the degradation of OMPs in secondary wastewater treatment effluent was conducted to test its usage in purification applications. Overall, PEC using $BiVO_4$ electrodes was found to be feasible and successful in OMP degradation, and has the potential to be developed for usage in environmental remediation strategies like water treatment and recovery.

Table of Contents

ACKNOWLEDGEMENT ..... **I**

ABSTRACT ..... **II**

LIST OF ACRONYMS ..... **V**

CHAPTER 1: INTRODUCTION **1**

CHAPTER 2: LITERATURE **4**

2.1. Background 4
2.2. Photocatalysts and Photoelectrocatalysis 9
2.3. Bismuth Vanadate ($BiVO_4$) Electrode 10
2.3.1. Structural Properties 11
2.3.2. Optical and Electronic Properties 12
2.3.3. Fabrication of $BiVO_4$ electrodes 13
2.3.4. Review of $BiVO_4$ in Photocatalysis and Photoelectrocatalysis 15
2.4. Selected OMPs 17
2.4.1. Acetaminophen 17
2.4.2. Propranolol 17
2.4.3. Benzotriazole 18
2.5. Usage of AOPs for OMP Removal from SWTE 18

CHAPTER 3: RESEARCH MOTIVE **20**

3.1. Knowledge Gaps 20
3.2. Research Questions 20
3.3. Objectives 21
3.4. Hypothesis 22

CHAPTER 4: MATERIALS AND METHODS **23**

4.1. Chemicals 23
4.2. Electrode Fabrication 23
4.2.1. Dip-coating 24
4.2.2. Electrodeposition 25
4.3. Electrode Characterization 27
4.3.1. X-Ray Diffraction 27
4.3.2. Surface Profilometry 28
4.3.3. Energy Dispersive X-Ray Analysis 29
4.3.4. X-Ray Fluorescence 29
4.3.5. Scanning Electron Microscopy 30
4.3.6. UV-Visible Spectroscopy 31
4.3.7. Incident Photon to Current Efficiency Measurement 32
4.3.8. Linear Sweep Voltammetry 33
4.4. Degradation Experiments 33
4.5. Analytical Method: LC-MS 37

CHAPTER 5: RESULTS AND DISCUSSION **38**

5.1. Structural Characterization of Electrodes 38
5.1.1. Crystallinity 38

5.1.2. Film Thickness 40
5.1.3. Chemical Composition 40
5.1.4. Surface Morphology 44
5.2. Optical Characterization of Electrodes 46
5.3. Optoelectronic Characterization of Electrodes 49
5.3.1. Band Potentials 49
5.3.2. Incident Photon to Current Efficiency 50
5.4. Photoelectrochemical Characterization of Electrodes 52
5.5. Degradation of Single Component System 53
5.5.1. Degradation of Phenol 53
5.5.2. Effect of Electrode Fabrication on Degradation 54
5.6. Degradation of Multiple Component System 60
5.6.1. Photoelectrocatalytic Degradation of Multiple OMPs 60
5.6.2. Photoelectrocatalytic Degradation of ACT, PRO and BTA 62
5.6.3. Reusability of Electrode in Photoelectrocatalytic Degradation 65
5.7. Scavenger Studies 66
5.8. Photoelectrocatalytic degradation of OMPs in SWTE 71

CHAPTER 6: CONCLUSION 74

CHAPTER 7: RECOMMENDATIONS 76

REFERENCES 77

APPENDICES 87

APPENDIX A: MOLECULAR STRUCTURES OF ACT, PRO AND BTA 87

APPENDIX B: FABRICATION OF $BiVO_4$ ELECTRODES 88

APPENDIX C: CHARACTERIZATION OF $BiVO_4$ ELECTRODES 90

APPENDIX D: PHOTOELECTROCATALYTIC DEGRADATION USING $BiVO_4$ ELECTRODES 92

List of Acronyms

OMP	Organic Micropollutant
AOP	Advanced Oxidation Process
ROS	Reactive Oxidative Species
•OH	Hydroxyl
$O_2^{\bullet -}$	Superoxide
PEC	Photoelectrocatalysis
PC	Photocatalysis
$BiVO_4$	Bismuth vanadate
FTO	Fluorine doped tin oxide
SWTE	Secondary wastewater treatment effluent
IPCE	Incident photon-to-current efficiency
SEM	Scanning Electron Microscopy
XRD	X-Ray Diffraction
XRF	X-Ray Fluorescence
EDX	Energy Dispersive X-Ray Analysis
LSV	Linear Sweep Voltammetry
UV	Ultraviolet
ACT	Acetaminophen
PRO	Propranolol
BTA	Benzotriazole

CHAPTER 1: INTRODUCTION

Water remains an indispensable natural resource for the sustenance of human and animal lives. In the recent years, water contamination of surface, underground as well as drinking water owing to the rapid urbanization and industrialization has been recognized as one of the biggest threats faced by the society (Samsudin et al., 2018; Malathy et al., 2018). These human activities have led to the excessive release of toxic and harmful chemicals like pharmaceuticals, dyes, heavy metals, pesticides, personal care products and surfactants, many of which consist of, and constitute, recalcitrant organic micropollutants. Organic micropollutants (OMPs) is the term used to refer to a variety of compounds that are present in low concentration, from approximately 0.01 to 3 µg/L (Ashton et al., 2004), that possess threats to the environmental ecosystem, but are only partly covered in the current rules on water quality, and tend to be resistant to biodegradation (Anjum et al., 2017). These OMPs contaminate the biosphere via different sources. Some of these sources are through discharge of secondary wastewater treatment effluent (SWTE), agricultural runoff mixed with surface water, and industrial wastewater, as shown in Figure 1 (Khanzada et al., 2020). The United Nations' World Water Development has maintained that the disruption of the water cycle would lead to further adverse effects on other environmental remediation goals like clean energy production, sustainable development, as well as on economic development goals like food security and human health (Geissen et al., 2015).

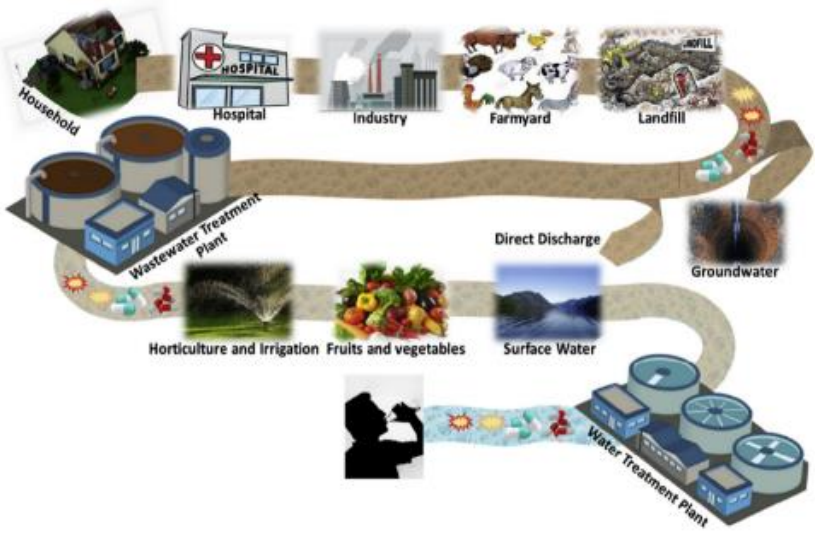

Figure 1: Potential sources and pathways of OMPs into the hydrosphere (Khanzada et al., 2020)

Therefore, it is imperative to discover and carry out innovative treatment methods for the removal of OMP to mitigate the damage caused by their emissions. Treating the SWTE also provides options for water reuse and reclamation, to mitigate the global issue of water shortage (Ren et al., 2021). Commonly employed technologies SWTE treatment include coagulation-flocculation, membrane-based technologies and adsorption technologies (Samsudin et al., 2018). However, they are rendered less efficient in the removal of OMPs due to their negative impacts such as the fouling of membranes, and the increased concentration of metal ions from coagulants in water (Khanzada et al., 2020). The OMPs are present in trace levels, and are therefore persistent, which further reduces the efficiency in removing them. Hence, a group of technologies called Advanced Oxidation Processes, which have accomplished success in the degradation of organic pollutants, have been reviewed as a solution for the removal of OMPs (Khanzada et al., 2020).

Advanced oxidation processes (AOPs) form a current innovative water treatment technology, and were first proposed in the 1980s for drinking water treatment, and were later studied for treatment of different wastewaters (Deng and Zhao, 2015). AOPs consist of in-situ generation of reactive oxidizing species (ROS), called radicals, which are capable of attacking recalcitrant organic species in water, resulting in their degradation. The most common type of ROS consists of hydroxyl (•OH) radicals, which have a high standard reduction potential of 2.8 eV (vs Standard Hydrogen Electrode). This makes them powerful oxidizing agents that have the ability to convert the organic pollutants unselectively into their oxidation products. Moreover, the short lifetime of these generated radicals allows their self-elimination during the AOPs treatment (Orimolade and Arotiba, 2020). Hence, along with being environmentally and economically feasible, the ability of AOPs in degrading OMPs has led to its consideration as the tertiary treatment step in wastewater treatment. Existing research by (Sánchez-Polo et al., 2006) shows the success of AOPs involving ozone in combination with granular activated carbon (O_3|GAC), in oxidizing various contaminants present in the water of Lake Zurich.

Photocatalysis (PC) is an AOP occurring when light interacts with the surface of semiconductor materials, called photocatalysts, and generates electron – hole pairs, which on interaction with water results in ROS generation. Semiconductors are materials where the excitation spectrum of the electrons is not continuous, but appears in the form of bands separated by gaps (Yu and Cardona, 2005). The first band, or the valence band, consists of occupied molecular orbitals. When

incident radiation having energy greater than that of the semiconductor band gap falls onto the surface of the semiconductor, the electrons are excited to the conduction band, creating vacancies or holes that are positively charged (Ren et al., 2021). PC has intrigued much attention due to its relative ease of process integration and capability of degrading the recalcitrant pollutant without producing any harmful by-product, and in an eco-friendly and renewable manner due to the utilization of solar energy (Samsudin et al., 2018). Titanium dioxide (TiO_2) has been widely used as a photocatalyst in the degradation of various dyes due to its excellent physical and chemical stability and inexpensiveness (Zhao et al., 2017). However, TiO_2 has a large band gap energy of 3.2 eV, which limits its use mainly in the ultraviolet spectrum, when the solar radiation consists of light in majorly the visible spectrum (Malathi et al., 2018). Hence, bismuth vanadate ($BiVO_4$), another metal oxide, has gained interest as a photocatalyst in organic pollutant photodegradation due to its relatively small band gap.

However, PC presents a key limitation that is rapid electron – hole pair recombination. This diminishes the interactions of the holes and electrons with water to form oxidant species that degrade the organics (Samsudin et al., 2018). Thus, there is a recent interest in a modified and innovative alternative, called photoelectrocatalysis (PEC). PEC is a process that adds the element of electrochemistry to the existing principle of PC, and has achieved significant recognition for its ability to slowing the recombination. This is achieved by applying an external bias potential to the anodic photocatalyst (Malathi et al., 2018). As a consequence of the external bias, the lifetime of the electrons and holes is lengthened, and this allows more degradation of organic pollutants, due to the production of more ROS (Jafar et al., 2013). During PEC, the organics are degraded by various reactions that involve the electrons and holes generated on illumination of the photocatalyst (Samsudin et al., 2018). Therefore, it is of interest to observe the efficiency of PEC using $BiVO_4$ in the degradation of OMPs, which is studied in this research.

CHAPTER 2: LITERATURE

2.1. Background

The photocatalysts used in PEC fall under the category of materials known as semiconductors (Wang et al., 2018). Semiconductors are characterized as materials that possess values of conductivity lower than those of metals and metalloids, but higher than the insulators such as non-metals (Rahman, 2014). The ability to conduct heat and electricity arises due to the carrier charge density and carrier mobility in the material (Cattarin and Decker, 2009). When an electron moves from its location, it leaves behind a positively charged vacancy in its original position, which are referred to as holes. Thus, the two charge carriers of a semiconductor are the photogenerated electrons and holes (Yoon et al., 2010). The carrier charge densities of semiconductors lie between 10^{13} and 10^{21} carriers/cm^3 (Optical Materials, 2021). The valence electrons of a crystalline semiconductor material are present in distinct bands of fixed energies, known as the valence band and the conduction band, as depicted in Figure 2. The energy gap between the valence and conduction bands, where no other energy levels exist, is known as the band gap energy, or the band width energy (What Is Conduction and Valence Band in Semiconductors - Definition, 2019). On supplying a certain excitation energy to a semiconductor that exceeds its band gap energy of a semiconductor, the electrons get excited and move from the valence band to a higher energy state in the conduction band (Edebali et al., 2018).

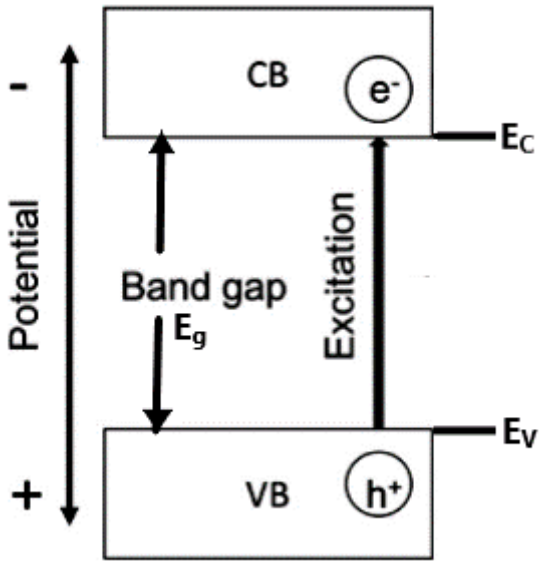

Figure 2: Illustration of the valence band and conduction bands of a semiconductor, denoted by VB and CB respectively, adapted from (Optical Materials, 2021). E_g is the band gap energy, whereas E_C and E_V are the conduction and valence band energies, respectively.

This review will focus on semiconductors made of metal oxides, due to their usage in photocatalytic and photoelectrocatalytic setups. Metal oxides are commonly used in carrying out various processes for environmental remediation, such as decarbonization, energy storage, pollution monitoring in the biosphere, and degradation of harmful pollutants. They are also used in AOPs like PC and PEC (Danish et al., 2020). Metal oxides show a wide range of variation in their structural, photochemical and electronic properties, which chiefly depend on their synthesis, as well as the various parameters of their synthesis (Nunes, 2019). Fujishima and Honda (1972) have reported that metal oxides have garnered attention for their inexpensive cost with high abundance, optical absorption properties, suitable band edge positions for redox reactions with water, and good charge separation. Metal oxide photocatalysts have also been used in the photocatalytic degradation of organic dyes such as Rhodamine B in aqueous solutions (Bordbar et al., 2017). However, most research has been conducted in the application of PEC in water splitting, whereas few articles report the degradation of organics using PEC.

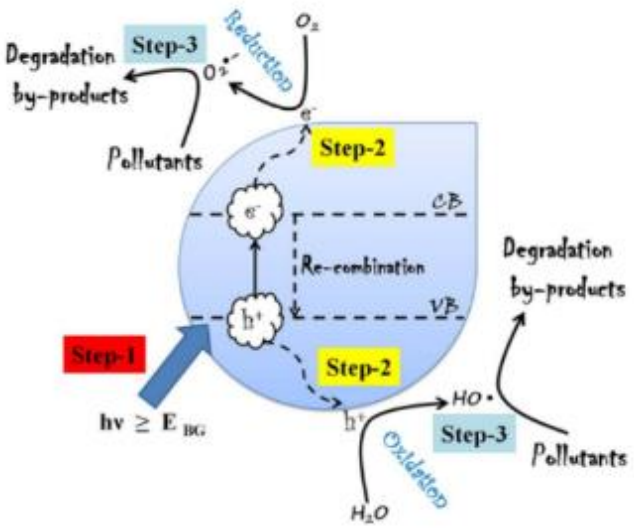

Figure 3: Reactions taking place in photocatalytic degradation of organic molecules (Malathi et al., 2018)

When a metal oxide photocatalyst in an aqueous photoelectrocatalytic cell is illuminated with irradiation, the key principle maintains that if the energy of the irradiation is equal to or greater than the band gap energy of the photocatalyst, there will be an ejection of the electron from the fully filled valence band to the empty conduction band, thus creating a positively charged hole in its place in the valence band (Optical Materials, 2021). Assuming that irradiation of frequency ν illuminates a photocatalyst with energy higher than the band gap energy, the equations of the reactions are summarized in Figure 3 and mentioned as follows:

$$\text{Photocatalyst} + h\nu \rightarrow e^-_{CB} + h^+_{VB} \quad (1)$$

Where hν is the minimum energy of irradiation needed to excite the electrons, and e^-_{CB} and h^+_{VB} are the ejected electron in the conduction band, and the positive hole that remains in the valence band, respectively (Peleyeju and Arotiba, 2018). The generated carriers undergo reactions to generate radicals that are responsible for the degradation and mineralization of the organics. There is also direct oxidation of the organics by the holes, which are strongly oxidizing species themselves (Samsudin et al., 2018). It has been noted by several researchers that oxidation processes at the anode are considered a benefitting innovation in the field of water purification (Danish et al., 2020). The major reactions taking place during the process of PEC are as follows:

$h^+_{VB} + ORG \rightarrow CO_2 + H_2O$ (2)

$h^+_{VB} + H_2O \rightarrow \bullet OH + H^+$ (3)

$e^-_{CB} + O_2 \rightarrow O_2\bullet^-$ (4)

$\bullet OH + ORG \rightarrow CO_2 + H_2O$ (5)

$O_2\bullet^- + ORG \rightarrow CO_2 + H_2O$ (6)

Where •OH, $O_2\bullet^-$, H^+, ORG, CO_2, O_2 and H_2O are the hydroxyl radical, superoxide radical, hydrogen ion, organic pollutants, carbon dioxide, oxygen and water respectively (Garcia-Segura and Brillas, 2017). The •OH radical is produced by the reaction of the holes with water molecules, whereas the $O_2\bullet^-$ radical is produced by the reaction of the conduction band electrons with the oxygen molecules. The organic molecules are adsorbed on the surface of the photoanode, where the •OH and $O_2\bullet^-$ radicals produced oxidize and degrade the pollutants, along with the additional direct oxidation of OMPs by the positively charged holes (Samsudin et al., 2018). From Equation 3, it can be inferred that the higher is the amount of •OH radicals produced, the lower is the pH of the solution. There are also less powerful oxidizing radicals and compounds, namely the hydroperoxyl radical ($HO_2\bullet$) and hydrogen peroxide (H_2O_2) that may contribute to a smaller extent to the degradation of organics. Figure 3 shows the stepwise operation of PC, starting with the electron and hole pair production on irradiation, with the electron reducing O_2 to form the $O_2\bullet^-$ radical, and the hole oxidizing the H_2O molecule to form •OH radicals. As previously mentioned, a major drawback of the PC process is the quick electron-hole recombination, which is also suggested in Figure 3. The conduction band electron, which is at a higher energy state, is relatively unstable. It is in the nature of any species to attain the ground state or stable state of that species. Hence, the conduction band electron returns to the valence band, along with the emission of heat, as shown in the following equation (Samsudin et al., 2018).

$e^-_{CB} + h^+_{VB} \rightarrow$ Photocatalyst + heat (6)

This leads to a desire for a modification that will allow longer lifetimes of the photogenerated electrons and holes, which is done in PEC. The concept of PEC involves the addition of an electrochemical component to the principle of PC (Malathi et al., 2018). A positively charged external anodic bias potential is applied to the photocatalyst that acts as the photoanode in the

photocatalytic degradation of organics. This potential facilitates the extraction of the conduction band electrons through the circuit by the cathode due to the potential gradient. This delays the recombination of those electrons with the valence band holes (Egerton et al., 2006). In this way, the lifetime of holes and electrons is prolonged, which in turn allows the production of more radicals. Thus, this leads to a higher efficiency of degradation of OMPs, as compared to PC. Figure 4 shows the process of PEC using $BiVO_4$ as the photoanode.

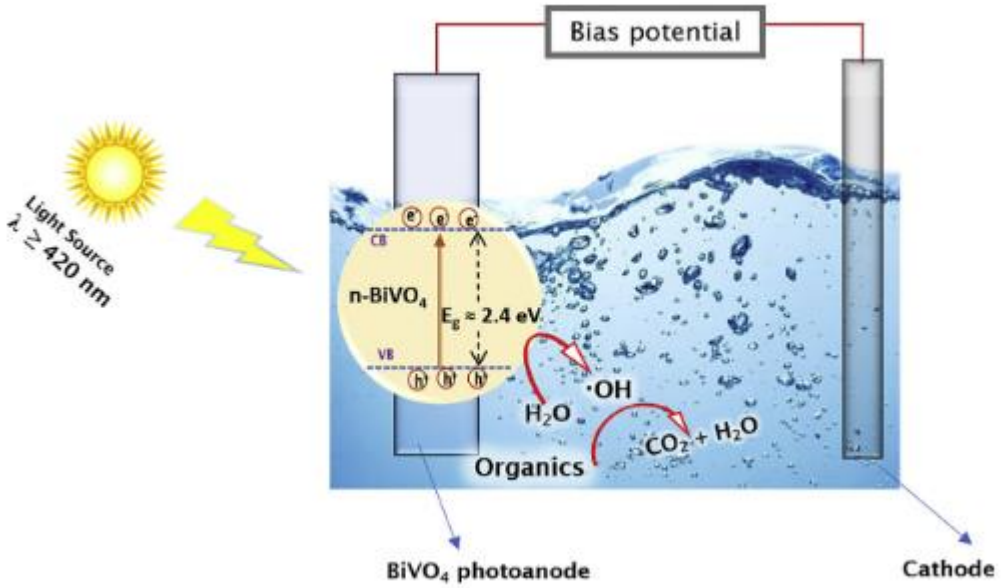

Figure 4: Principle of PEC in organics degradation using $BiVO_4$ electrodes (Orimolade and Arotiba, 2020)

The photoelectrocatalytic setup involves the connection of the photoanode to a potentiostat. The photocatalyst is prepared as a photoanode in the form of thin films onto a conductive substrate. The substrate commonly used for this purpose is made of glass, with an active site consisting of fluorine doped tin oxide (FTO) (Jafar et al., 2013). This is different from the process of PC, where the photocatalyst is frequently in the form of nanoparticles. The usage of thin films is an added advantage of PEC, due to the possibility of reusing the photocatalyst for further experiments, because it is in the form of a solid electrode. This would not be possible in the case of nanoparticles, and thus the wastage of material is prevented in PEC (Xu et al., 2011).

2.2. Photocatalysts and Photoelectrocatalysis

Although PC and PEC using metal oxide photoanodes have proven to be successful in the degradation of organic pollutants (Danish et al., 2020), the process depends on the type of photocatalyst used, and their optoelectronic properties (Danish et al., 2020). The material used should have a band gap suitable for the irradiation spectrum, and band edge locations suitable for water oxidation and oxygen reduction. The material should also be stable and have ample surface area for the organic molecules to get adsorbed, from where they are oxidized by the radicals produced during PEC. In the recent past, apart from TiO_2, other transition metal oxides such as α-Fe_2O_3, $BiVO_4$, WO_3, ZnO, and CuO were extensively used and studied in their application as photocatalysts (Samsudin et al., 2018). Figure 5 depicts these commonly used photocatalysts with their band gap and band edge location.

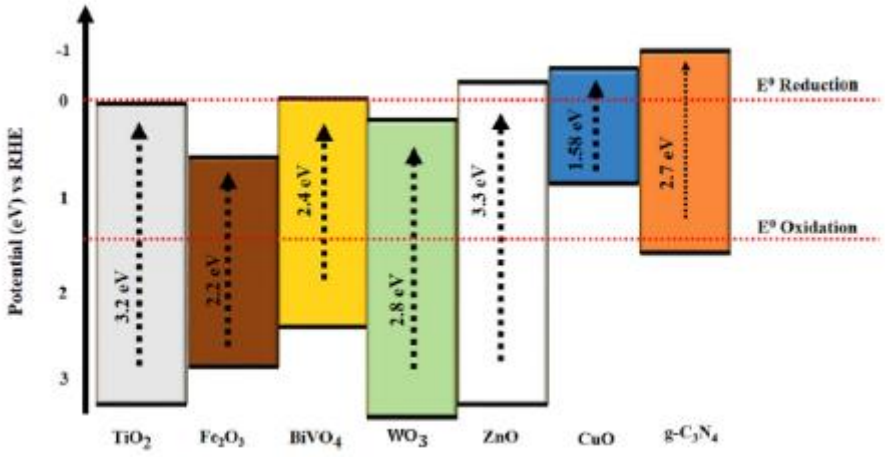

Figure 5: Band gap energy of various metal oxides photocatalysts (Samsudin et al., 2018)

Zinc oxide (ZnO) is another metal oxide photocatalyst that proves to be advantageous in terms of low cost and non-toxicity, which gives it consideration in environment purification technologies (Mou et al., 2018). However, ZnO has a band gap of 3.3 eV which is higher than that of TiO_2, and thus exhibits limited absorption in the solar spectrum (Atchudan et al., 2018). It is also amphoteric and forms conjugate acids and bases in aqueous solution (Danish et al., 2020). This compromises its chemical stability and thus its photocatalytic ability in water treatment (Danish et al., 2020). Therefore, limited research has been conducted using ZnO in the process of PEC for water

treatment. However, ZnO has been used in heterojunction with another compound in the photocatalytic degradation of dyes (Mou et al., 2018). A heterojunction is created when two photocatalysts of different band gaps are combined, for superior photocatalytic properties (Orimolade and Arotiba, 2020).

Tungsten trioxide (WO_3) has been considered for the PC with acidic aqueous solutions due to its chemical stability (Dong et al., 2017). It is also cheap, and has a narrow band gap that is suitable for absorption in the visible spectrum. However, it is susceptible to rapid recombination, and the material also possesses toxicity and experiences corrosion in the presence of light (Xu et al., 2011). Cupric oxide (CuO), with a narrow band gap, has also proven to be effective in the removal of inorganic ions and dyes, and has gained interest due to its abundance, inexpensiveness and easy fabrication (Kumar et al., 2019). However, is it mostly used in heterojunction with another material, due to rapid recombination when used on its own (Li et al., 2017). The hematite form of Ferric Oxide (α-Fe_2O_3) is another metal oxide that has shown promising results in the photodegradation of alkaline solutions and dyes, and has high absorption in the visible light spectrum. However, the slow mobility of charge carriers on light absorption reduces the efficiency of PC (Zhang et al., 2015).

Bismuth vanadate ($BiVO_4$) is a non-toxic and low-cost n-type semiconductor with outstanding chemical and photostability (Trześniewski and Smith, 2016). $BiVO_4$ is a promising candidate for PC, due to its suitably narrow band gap, proper band location for water oxidation as shown in Figure 5, as well as other properties like low toxicity and good physicochemical stability (Samsudin et al., 2018). Its low band gap energy of 2.4 eV allows for more efficient usage of the solar radiation in the visible spectrum (Tan et al., 2017). It has also proven to have good photocatalytic properties, showing high activity for water oxidation and organics degradation (Tan et al., 2017; Orimolade and Arotiba, 2020).

2.3. Bismuth Vanadate ($BiVO_4$) Electrode

In light of its advantageous features, $BiVO_4$ has gained attention due to its efficient visible-light photocatalytic degradation of organic pollutants, as well as in PEC for water splitting and hydrogen evolution (Orimolade and Arotiba, 2020). Further studies have been conducted, increasingly over

the recent years, on the application of $BiVO_4$ in PEC for the degradation of organic pollutants in the SWTE (Tan et al., 2017). It has been established that these properties are highly dependent on its crystal and electronic structures (Garcia-Segura and Brillas, 2017). The physical properties of $BiVO_4$ are discussed in this section.

2.3.1. Structural Properties

$BiVO_4$ in the crystalline form usually occurs in three types of structures, or polymorphs, namely dreyerite, pucherite and clinobisvanite. $BiVO_4$ in nature is present in the form of pucherite, which displays an orthorhombic crystalline arrangement, whereas dreyerite and clinobisvanate usually display a tetragonal and monoclinic crystal system, respectively. The structures of $BiVO_4$, which can be synthesized in lab, are clinobisvanate, that consists of a scheelite type of structure with tetragonal and monoclinic phases, and dreyerite, that consists of zircon type of structure with tetragonal phase (Park et al., 2013). The crystal system of $BiVO_4$ is highly dependent on the method of fabrication (Park et al., 2013). The atomic arrangement of $BiVO_4$ consists of each Bi ion coordinated by eight O atoms, and each V ion coordinated by four atoms in a tetrahedral arrangement. In the scheelite type structure, each Bi ion is coordinated by eight VO_4 molecules, whereas in the zircon type structure, each Bi ion is coordinated by six VO_4 molecules (Tokunaga et al., 2001). The monoclinic scheelite phase, shown in Figure 6(b), has more distorted local environments of VO_4 and BiO_8 than the tetragonal scheelite phase, shown in Figure 6(a). It is found that the monoclinic scheelite $BiVO_4$ is the more thermodynamically favorable phase out of the two scheelite phases (Tokunaga et al., 2001). Monoclinic scheelite $BiVO_4$ can be irreversibly synthesized by heating tetrahedral zircon $BiVO_4$, shown in Figure 6(c), to approximately 400^oC to 500^oC (Orimolade and Arotiba, 2020).

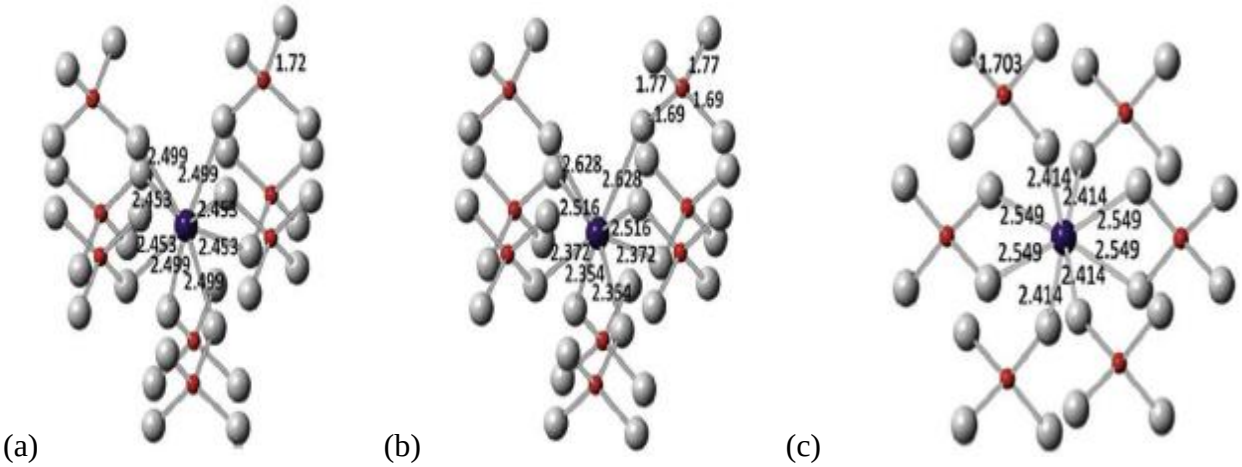

(a) (b) (c)

Figures 6: Crystalline structures of $BiVO_4$, namely (a) tetragonal scheelite; (b) monoclinic scheelite and (c) zircon structure of $BiVO_4$ (where purple is Bi, red is V and gray is O) (Orimolade and Arotiba, 2020)

2.3.2. Optical and Electronic Properties

It is noted that the monoclinic scheelite $BiVO_4$ displays highest photocatalytic activity for water oxidation to form hydroxyl radicals in the presence of visible light irradiation. This is due to the distortion of the local environments in the monoclinic scheelite $BiVO_4$ (Tokunaga et al., 2001). This is because the Bi ion in the 6s orbital is hybridized with the O 2p orbital, which increases the electron mobility, thus improving charge separation and retarding the electron-hole combination. The band width energy of the monoclinic scheelite structure also differs from tetragonal zircon structure, at 2.4 eV, with that of the latter being 2.9 eV to 3.1 eV. This is also a consequence of the distortion which facilitates the transition of electrons to the conduction band at the 3d orbitals of V (Park et al., 2013). This allows better absorption of light in the visible spectrum by the monoclinic scheelite $BiVO_4$ (Tan et al., 2017). The band structures of both the discussed forms are depicted in Figure 7.

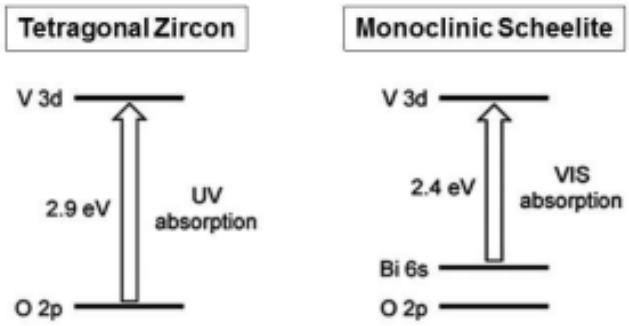

Figure 7: Band structures of $BiVO_4$, tetragonal zircon on left, and monoclinic scheelite on right (Tan et al., 2017)

2.3.3. Fabrication of $BiVO_4$ electrodes

There are various techniques used to synthesize, or fabricate $BiVO_4$ as a thin film onto an FTO substrate to prepare the photoanode for PEC. It has been established that a high value of surface area-to-volume ratio of the thin film can improve the efficiency of photocatalytic degradation (Dong et al., 2017). This is because a higher surface area of photocatalysts allows more adsorption of the organic pollutant molecules, which allows better degradation of the molecules by the generated reactive oxidizing species (Danish et al., 2020). Therefore, importance has been given to the fabrication of photocatalyst thin films in the form of nanostructures (Joseph et al., 2020). Another property that is found to be a factor in efficient photocatalytic degradation is the surface structure. The surface structure determines the quantum efficiency of the photocatalyst on irradiation, which is given by the percentage of the number of incoming photons being converted into generated electron-hole pairs (Khan et al., 2017). Thus, the quantum efficiency is an indicator of charge transfer efficiency, which determines the degradation of OMPs because the generation of radicals is by reactions involving the charge carriers (Bennani, 2017). A smoother, more uniform surface of the photocatalyst allows proper absorption of light and thus shows a higher quantum efficiency (Peleyeju and Arotiba, 2018). The methods of fabrication that will be discussed and tested in this research are dip-coating and electrodeposition.

Dip-coating is a technique of fabrication of $BiVO_4$ thin films that has generated acclaim due to the high degradation efficiency by the produced photocatalysts, along with the facile experimental method (da Silva et al., 2015). Dip-coating consists of dipping a conducting substrate into a precursor solution, and drying the successive layers, before annealing to obtain the crystalline

structure. Figure 8 illustrates the procedure for dip-coating. The $BiVO_4$ electrodes fabricated by dip-coating have reportedly been efficient in producing a monoclinic scheelite crystal structure (da Silva et al., 2016). Dip-coated $BiVO_4$ has shown efficiency in the PC of methylene blue in heterojunction with Nickel Oxide (NiO) (da Silva et al., 2015). The morphology of the dip-coated $BiVO_4$ thin films are shown to consist of uniformly distributed round shaped particles (Hernández et al., 2015). Based on literature, the structure and area of the produced electrodes may have the potential to facilitate adsorption of organic pollutants, as well as the absorption of light.

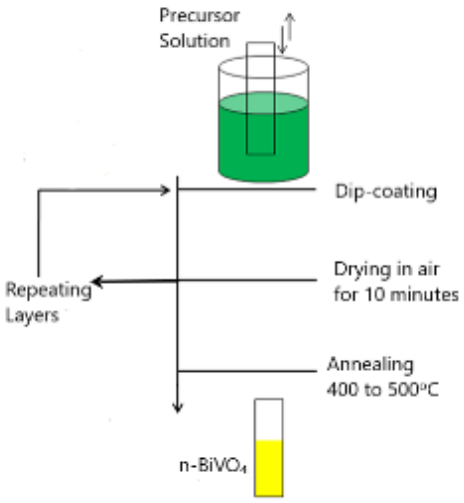

Figure 8: Simplified diagram showing the dip-coating deposition process to obtain $BiVO_4$, electrodes, adapted from (da Silva et al., 2015)

Electrodeposition of $BiVO_4$ thin films is another technique of fabrication that has been used in research for photoelectrocatalytic solar water splitting. This is a two-step process illustrated in Figure 9, that consists of the electrodeposition of bismuth oxy-iodide (BiOI), followed by the addition of a vanadium-based solution before annealing to form $BiVO_4$ (McDonald and Choi, 2012). This is considered a promising method due to the favorable porosity and uniformly distributed needle-shaped and flower shaped structure of the produced thin film, providing more surface area and photocatalytic sites (Mohamed et al., 2021). Along with facile and inexpensive experimental methods at ambient conditions, the research on electrodeposited $BiVO_4$ photoanodes shows that the photoanodes have a monoclinic scheelite crystal structure, and high photocurrent density, which signifies better charge separation and high quantum efficiency (Tolod et al., 2020).

Electrodeposited $BiVO_4$ electrodes also reportedly showed efficient photocatalytic degradation of organic pollutants (Orimolade and Arotiba, 2022).

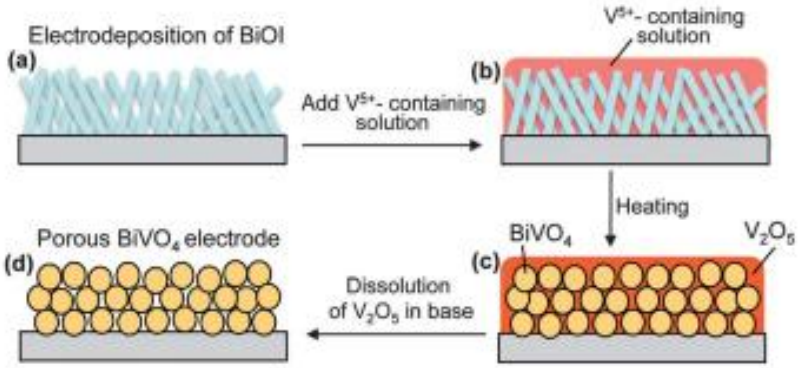

Figure 9: Schematic representation of the procedures used to prepare porous $BiVO_4$ electrodes (McDonald and Choi, 2012)

2.3.4. Review of $BiVO_4$ in Photocatalysis and Photoelectrocatalysis

Various articles have lauded $BiVO_4$ as a photocatalyst both on its own, and in a heterojunction, for the degradation of various organic pollutants (Gotić et al., 2005). A review of the current research studies done using $BiVO_4$ for the degradation of organics has been gathered in Table 1. It is seen that research for photocatalytic degradation has mostly been established for phenols, various dyes and other compounds, but fewer articles discuss the degradation of organic micropollutants.

Table 1: Review of research in applications of PC and PEC using $BiVO_4$ electrodes.

Photocatalyst	Process	Mode of Synthesis	Organic Pollutant	Duration of process (minutes)	Removal (%)	References
FTO-NiO/$BiVO_4$	PC	Dip-coating	Methylene Blue	40	75	(da Silva et al., 2015)
$BiVO_4$ microspheres	PC	Hydrothermal method	Ibuprofen	25	90	(Li et al., 2016)
$BiVO_4$ microstructures	PC	Hydrothermal method	Rhodamine B	180	99.5	(Wu et al., 2018)
$BiVO_4$/α-Fe_2O_3 composites	PC	Hydrothermal Calcination	Gaseous Benzene	210	67	(Chen et al., 2018)
g-C_3N_4/$BiVO_4$ composites	PC	Electro-spinning	Bisphenol A	120	93	(Wang et al., 2017)
$BiVO_4$ stacked nanoplate stars	PC	Hydrothermal Method	Methylene Blue	25	91	(Sun et al., 2009)
$BiVO_4$ nanoparticles	PC	Citrate-based Chemical	Acid Orange 7	180	79	(Xu et al., 2011)
FTO-$BiVO_4$/Ag_2S	PEC	Electro-deposition	Ciprofloxacin	120	80	(Orimolade and Arotiba, 2020)
FTO-$BiVO_4$/Ag_2S	PEC	Electro-deposition	Sulfamethoxazole	120	86	(Orimolade and Arotiba, 2020)
FTO-WO_3/$BiVO_4$	PEC	Electro-deposition	Methylene Blue	120	83	(Chatchai et al., 2013)
FTO-$BiVO_4$	PEC	Spray Pyrolysis	Phenol	240	70	(Bennani et al., 2016)
FTO-$BiVO_4$	PEC	Drop-coating	Methyl Orange	120	97	(Bacha et al., 2019)
FTO-$BiVO_4$	PEC	Spin-coating	Congo Red	90	86	(Deshpande et al., 2020)
FTO-$BiVO_4$	PEC	Electro-deposition	Bisphenol A	120	100%	(Shao et al., 2020)

2.4. Selected OMPs

With an increasing human population and dependency on pharmaceuticals, personal care products and enhancing industrial chemicals, there is a rising challenge in the field of water treatment. The Ministry of Infrastructure and Water Management of Netherlands has narrowed the focus on a group of OMPs including pharmaceuticals amongst others, that reportedly pose threats to the human health in the long run due to chronic exposure (STOWA, 2019) The OMPs relevant to this research have been detailed in the following sub-sections.

2.4.1. Acetaminophen

Acetaminophen (ACT), commonly known as Paracetamol, is an analgesic that is frequently used as a pain reliever for body aches and cold/flu aches. Due to its widespread consumption as over-the-counter drugs, analgesics such as ACT are observed to be one of the fastest emerging contaminants in the water matrix (Twycross et al., 2013). The chemical formula of ACT is $C_8H_9NO_2$. ACT enters the water through excretion, hospital discharge amongst others, and do not experience any change in their molecular structure after their release. Hence, depending on the type of water, they may either enter the sewage treatment plant, or the freshwater source, from where they can enter the food chain. ACT is reported to have a toxic effect at smaller concentrations and a smaller duration of exposure, of any microorganism, by reducing their reproduction rate (Żur et al., 2018).

2.4.2. Propranolol

Propranolol (PRO) is a pharmaceutical that falls under the category of β-Blockers, which serve the purpose of treatment of hypertension and heart attacks (Clinicalkey, n.d.). The chemical formula of PRO is $C_{16}H_{21}NO_2$. PRO enters the hydrosphere through excretion and urine of the human bodies that consume this chemical. Out of all the β-Blockers, PRO shows the highest bioaccumulation potential, and thus a relatively higher toxicity in water bodies. It has been seen in

the ecotoxicological studies that PRO and other β-Blockers can have negative impacts on aquatic organisms (Maurer et al., 2007).

2.4.3. Benzotriazole

Benzotriazole (BTA) is an aromatic compound that is widely used as a corrosion inhibitor in various applications, such as plastics, dyes, sunscreen and metals (Tan et al., 2022). It has the chemical formula $C_6H_5N_3$, and displays a high value of water solubility at 2 g/L. Since BTA is a prominent ingredient in many applications, it results as a pervasive contaminant in wastewater. BTA is also persistent, and poses a risk of bioaccumulation. It is shown that BTA can have adverse and toxic impacts at concentrations above 0.97 mg/L (Martín-Rilo et al., 2018) .

2.5. Usage of AOPs for OMP Removal from SWTE

Biologically treated SWTE from wastewater treatment plants has been seen as a potential source of reclaimed water to mitigate the issue of shortage in water supply, and to be further used for agricultural and irrigation purposes amongst others (Khanzada et al., 2020). The primary step consists of the removal of sediments, followed by the secondary step where the suspended and dissolved organics are degraded, along with nitrogen and phosphorus removal from the wastewater (United States Environmental Protection Agency (1998)). After secondary settling, the SWTE is reported to meet most requirements for further usage, but it still contains a mixture of a number of potentially harmful compounds. Some of these compounds are natural organic matter (NOM) and extracellular polymeric substances (EPS), apart from low concentrations of OMPs (Deng and Zhao, 2015). Various techniques have been researched for the tertiary treatment of SWTE for its discharge into surface water without any ecotoxicological effects. Such techniques are adsorption technologies, coagulation flocculation, advanced membrane technologies and AOPs (Samsudin et al., 2018). However, it is seen that in the membrane technologies, only selective OMPs are removed, due to differences in the electrostatic and hydrophobic properties of the OMPs (Khanzada et al., 2020). These processes are also energy intensive due to their pressure driven operation (Khanzada et al., 2020). It is of importance to unselectively destroy all the OMPs in the

wastewater, while following the principle of energy efficiency by utilizing solar radiation. The innovative AOPs are traditionally used for treatment of water to make it suitable for drinking purposes, and over the recent years it has gained traction in the application of various types of wastewaters (de Boer et al., 2022). Thus, the generated radicals are assumed to destroy persisting pollutants, micropollutants and inorganic pollutants as well, to oxidize and degrade them (Orimolade and Arotiba, 2020). It is reported that the process of advanced oxidation using TiO_2 under UV radiation, as well as hydrogen peroxide under UV radiation prove to be effective in the disinfection of SWTE including the removal of humic substances (Deng and Zhao, 2015). PEC using TiO_2 has been applied for the treatment of wastewaters from pharmaceutical and textile industries as well as for river water, and showed appreciable results (Garcia-Segura and Brillas, 2017). However, the application of this method using $BiVO_4$ for SWTE is to be further researched.

CHAPTER 3: RESEARCH MOTIVE

3.1. Knowledge Gaps

Although there is existing research on using PC for successful degradation of organic compounds like phenol and dyes using photocatalyst nanoparticles, (Xu et al., 2011), there is currently a lack of research on the usage of visible-light photocatalysts for the photoelectrocatalytic degradation of OMPs.

Even though there is research on the photoelectrocatalytic degradation of OMPs using the TiO_2 electrode, this has the disadvantage of a large band gap (Bennani, 2017). Hence, it is of interest to study the performance of $BiVO_4$ electrode, which is a visible-light photocatalyst with a smaller band gap, in the photoelectrocatalytic degradation of OMPs.

So far, there is only research on the photocatalytic degradation of a single OMP in a solution (Li et al., 2016). There is a lack of study in the simultaneous degradation of multiple OMPs in a solution using PEC.

Another gap in research is the study of photoelectrocatalytic removal of OMPs from SWTE, which consists of multiple OMPs along with other constituents. Thus, photoelectrocatalytic degradation of OMPs in SWTE using $BiVO_4$ photoanodes for the purification of SWTE is yet to be tested.

3.2. Research Questions

The following research questions are framed using the provided background knowledge in order to give structure for the experiments and analysis to be conducted in this project.

1) How do the structural, optical and optoelectronic behaviors differ between $BiVO_4$ electrodes fabricated by both dip-coating and electrodeposition?

2) What is the effect of the applied external bias on the photocurrent, as well as on the degradation efficiency for an OMP in an aqueous solution?

3) Which method of electrode fabrication, dip-coating or electrodeposition, leads to a better degradation efficiency of an OMP in aqueous solution, and what is the correlation between the OMP degradation and the properties observed from characterizing the electrodes?

4) How efficient is the process of PEC using $BiVO_4$ electrodes when it is carried out for a system with multiple OMPs, which is more representative of real wastewater effluent, as compared to a system with a single OMP?

3.3. Objectives

The following objectives have been developed in order to guide the direction and provide an overview of the expectations of this research project.

1) Fabrication of the $BiVO_4$ photoanodes using two different fabrication processes, namely dip-coating and electrodeposition, to be studied based on their characterization and OMP degradation.

2) Characterization of the fabricated $BiVO_4$ photoanodes from both the fabrication processes using analytical techniques for structural, optical, optoelectronic and electrochemical characterization.

3) Determination of the effect of the type of electrode fabrication used on the removal efficiency of a single OMP of 45 μg/L during their degradation.

4) Study of removal of the selected OMPs in a multiple component system at 45 μg/L, and eventually for SWTE, using the $BiVO_4$ photoanode that showed the highest degradation of ACT in the single component system.

3.4. Hypothesis

It was hypothesized that the method of depositing $BiVO_4$ thin film will influence the overall photocatalytic activity of the photoanode. Among dip coating and electrodeposition, only one of these methods will yield a thin film with higher quantum yield and adsorption surface area. The quantum efficiency determines the amount of incoming solar photons converting into photogenerated electron-hole pairs, and the holes generate hydroxyl radicals that in turn unselectively oxidizes the OMPs. Application of suitable external voltage will extract the photogenerated electrons from the photoanode hence slowing the recombination in $BiVO_4$ thin film. It was also hypothesized that the electrodeposition method will yield a more superior $BiVO_4$ film, since the particles deposited via this method are smaller in size. This will provide a larger surface area on the photoanode, leading to the production of more electron-hole pairs, and thus more hydroxyl radicals, and eventually resulting in more efficient removal of OMPs.

CHAPTER 4: MATERIALS AND METHODS

4.1. Chemicals

The $BiVO_4$ electrodes were fabricated on FTO glass electrodes (10 cm x10 cm, ~7 Ω/sq, Sigma-Aldrich) as substrates. For the fabrication process of dip-coating for the $BiVO_4$ electrode, the chemicals used were nitric acid (HNO_3) (70%, Sigma-Aldrich), bismuth nitrate pentahydrate ($Bi(NO_3)_3.5H_2O$) (98%, Sigma-Aldrich), and vanadyl acetyl acetonate ($VO(acac)_2$) (98%, Sigma-Aldrich). For the fabrication process of electrodeposition, further chemicals used were ethanol (Sigma-Aldrich) dimethyl sulfoxide (≥99.9%, Sigma-Aldrich), potassium chloride (KCl) (Sigma-Aldrich), sodium hydroxide (NaOH), (Sigma-Aldrich) and para-benzoquinone (98+%, Thermoscientific). For the degradation experiments, the electrode connections were made using carbon paste (Dycotec DM-CAP-4701S) and polyurethane resin (Electrolube), and the test degradation experiments were done using phenol (99.0-100.5%, Sigma-Aldrich). All the OMPs used in some or all photoelectrocatalytic degradation experiments consisted of acetaminophen, benzotriazole, methylbenzotriazole, carbamazepine, hydrochlorothiazide, metoprolol, sulfamethoxazole, propranolol, sotalol, trimethoprim, clarithromycin, ketoprofen, metformin, clofibric acid, sulfadimethoxine, caffeine, theophylline and gabapentin, all from Sigma-Aldrich. Sodium sulphate (Na_2SO_4) ((≥99%, Sigma-Aldrich) was used as a supporting electrolyte. Ethylenediaminetetra-acetic acid (EDTA) (99.4-100.6%, Sigma-Aldrich), para-benzoquinone and methanol (Sigma-Aldrich) were used as scavengers in the scavenging experiments.

4.2. Electrode Fabrication

The $BiVO_4$ thin films to be used in the photoelectrocatalytic degradation of the OMPs were prepared using two techniques of fabrication, namely dip-coating and electrodeposition. Prior to each process of fabrication, the FTO electrodes, also known as the substrates, were cut into an area of 4 cm x 4 cm for the experiments, and were consequently cleaned before use. The cleaning process consisted of ultrasonicating the substrates in acetone or ethanol for 5-6 minutes, and then ultrasonicating the substrate once again in demineralized water for another 5-6 minutes. The substrates were then wiped dry to be ready for use.

4.2.1. Dip-coating

The procedure of dip-coating comprised of the preparation of a precursor solution that was used for the formation of the $BiVO_4$ layer on the FTO side of the substrate, followed by annealing in the furnace. A volume of 1M HNO_3 solution was prepared as the solvent. 0.049 M of $Bi(NO_3)_3.5H_2O$ was measured and added to the solution, and mixed thoroughly. The solution was then ultrasonicated until it appeared clear and homogenous. Subsequently, 0.049 M $VO(acac)_2$ was measured, added and mixed thoroughly, and the beaker was placed once again in the ultrasonic bath, with simultaneous mixing. It was removed when the solution appeared homogenous, and acquired a bright blue color as shown in Figure 10. The pH of the solution was measured with a pH probe and multimeter.

Figure 10: Precursor solution for dip-coating

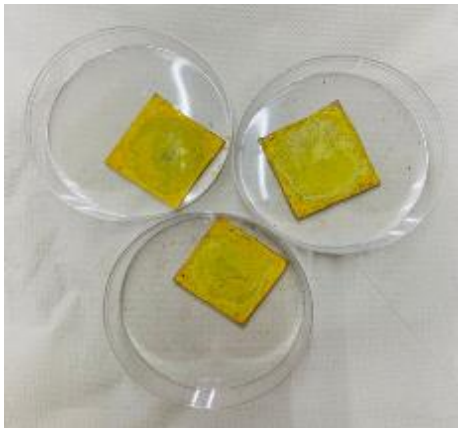

Figure 11: Annealed $BiVO_4$ electrodes by dip-coating method

The prepared substrate was taken and dipped into the solution, with the FTO side facing upward, and was allowed to stay for 5 minutes inside the solution before being removed. A pincer was used to dip the substrate into the solution. After being removed, the substrate was placed onto a hot plate magnetic stirrer for roughly 5 minutes, until the layer of $BiVO_4$ material dried. The electrode was dipped, removed and dried again in order to achieve multiple layers of the $BiVO_4$ material. The parameter varied the dip-coating process was the number of layers, which was varied from 1 layer to 5 layers. The electrodes were then annealed in the furnace at 460^oC, at a ramp rate of

2.2±0.1°C per minute. Once the furnace had cooled down to room temperature, the $BiVO_4$ electrodes were removed and displayed a bright yellow color, as shown in Figure 11.

4.2.2. Electrodeposition

The procedure for electrodeposition consisted of two steps that involved firstly preparing a precursor solution and depositing it onto the active side of the substrate via an external bias application, and secondly adding another precursor solution to the electrode before annealing it in the furnace. For the first precursor solution, two solvents were used, namely demineralized water and ethanol, in the proportions of 71.5% and 28.5% of the total end solution, respectively. 0.4 M KCl was added to demineralized water, and thoroughly mixed until the solution became clear in appearance. The pH of the solution was reduced to a value between 1.50 to 1.55, by dropwise addition of HNO_3 to the solution with simultaneous stirring. 0.04 M of $Bi(NO_3)_3.5H_2O$ was added to this solution, and mixed thoroughly. The beaker was placed in the ultrasonic bath while stirring the solution until the solution became homogenous and acquired a neon orange color, as shown in Figure 12. Meanwhile, 0.23 M para-benzoquinone was added to ethanol, mixed thoroughly and ultrasonicated until the para-benzoquinone was mixed well and the solution sported a greenish-brown color, also shown in Figure 12. The solutions of water and ethanol were finally mixed together manually to produce a new solution of wine-red color. This was the precursor solution for the formation of the layer of bismuth oxy-iodide (BiOI) on the substrate.

Figure 12: Precursor solutions for electrodeposition. The one on the left is KI and $Bi(NO_3)_3.5H_2O$ in demineralized water, and the one on the right is para-benzoquinone in ethanol

Figure 13: Electrodeposition cell setup, with all three electrodes and crocodile clips to connect them to the potentiostat

The beaker containing the precursor solution was placed on the hot plate magnetic stirrer, and the solution was stirred for 10±5 minutes. The process of electrodeposition was carried out using a three-electrode system as shown in Figure 13, where the reference electrode used is Ag/Ag^+ (4M KCl), the counter electrode used was a platinum wire, and the working electrode was the FTO substrate. The electrical connections were made to the AUTOLAB potentiostat with the help of wires with crocodile clips to clasp the electrodes. The potentiostat was used to apply the desired values of the voltage, time and other settings. The beaker was removed from the magnetic stirrer, and the electrodes were dipped into the solution. The electrodes were arranged in such a way that the FTO substrate faced the counter and reference electrodes. The voltage of the external bias and the duration of electrodeposition were set in the software, and the procedure was started. The parameters varied for the electrodeposition process were the voltage and duration of electrodeposition. The chosen voltage values were -0.2 V and -0.4 V, and the duration periods tested were 2 minutes, 5 minutes, 7 minutes, 10 minutes and 15 minutes of electrodeposition.

After the procedure, the substrate was unclasped from the crocodile clip. The BiOI electrode, which displayed a maroon color as shown in Figure 14, was mildly rinsed with distilled water to remove the loosely bound BiOI molecules on the electrodeposited layer, and subsequently air-dried. Another solution consisting of 0.2 M $VO(acac)_2$ was prepared with dimethyl sulfoxide as the solvent. Approximately 0.2 mL of this solution was added on top of the dried BiOI layer with

full coverage. The electrode was then annealed in the furnace at 460^{o}C, at a ramp rate of 2.2±0.1^{o}C per minute. On cooling down to room temperature, the $BiVO_4$ electrodes were removed and soaked in a solution of 1M NaOH to remove the excess vanadium oxide (V_2O_5) deposited on the layer. The final electrodes were air-dried and displayed a bright yellow color as shown in Figure 15.

Figure 14: BiOI electrodes produced at -0.2 V at different times of electrodeposition

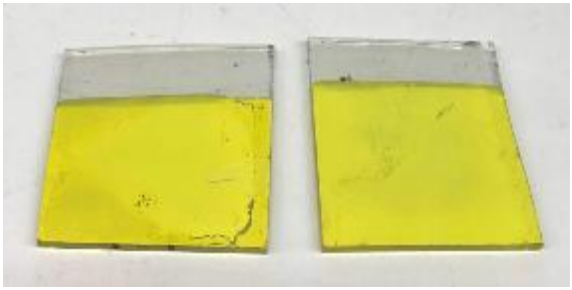

Figure 15: Final $BiVO_4$ electrodes by electrodeposition at a bias of -0.2V

4.3. Electrode Characterization

The characterization of the fabricated $BiVO_4$ electrodes was done by measuring various parameters of the electrode using analytical techniques, to get information on their properties. The structural characterization of the electrode was done using X-Ray diffraction, Surface Profilometry, Scanning Electron Microscopy, Energy Dispersive X-ray analysis and X-Ray Fluorescence. The electrode was optically characterized using Steady State Absorbance Spectroscopy. The optoelectronic behavior of the electrode was studied by measuring the Incident Photon to Current Conversion Efficiency. Finally, the electrochemical behavior of the electrode was studied using Linear Sweep Voltammetry.

4.3.1. X-Ray Diffraction

X-ray diffraction (XRD) is a powerful nondestructive technique for characterizing crystalline materials. It can provide information on structures, phases, preferred crystal orientations and other structural parameters, such as average grain size and crystal defects. X-Rays are generated on

bombarding the sample with accelerated electrons produced by heating a filament. As the electrons with the required energy displace the inherent inner shell electrons of the sample, X-Rays are produced. Each mineral has a unique value of inter-atomic spacing, and this allows the identification of the crystalline structure of the sample. This technique was used to validate the crystal structure of the $BiVO_4$ thin films (X-Ray Powder Diffraction(Xrd), n.d.). The instruments used for the XRD were the Bruker D8 Advance diffractometer Bragg-Brentano geometry and Lynxeye position sensitive detector. The X-Ray energy used for the purpose of this analysis was Cu Kα radiation. The data regarding the crystallinity was evaluated using the Bruker software DiffracSuite.EVA vs 6.0.

4.3.2. Surface Profilometry

Surface profilometry is a characterization technique that provides details on the surface profile of the sample, and can measure surface properties such as roughness, film thickness, detection of defects, and stress measurement. A thin vertical line was scratched out on the face of each electrode to expose the FTO substrate, to prepare the sample for the measurement of thickness of the $BiVO_4$ layer.

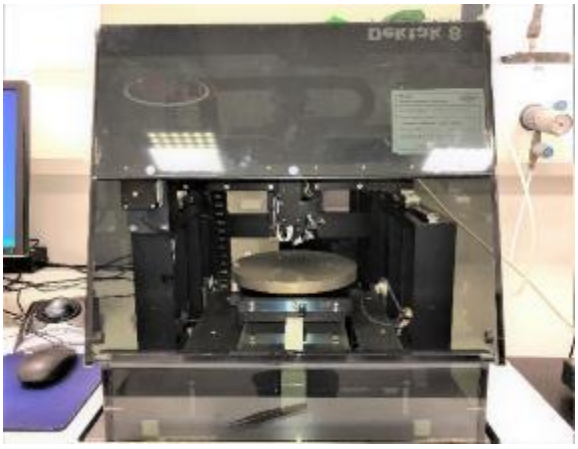

Figure 16: Veeco Dektak 8 Surface Profilometer used to measure film thickness of the $BiVO_4$ electrodes

The Veeco Dektak 8 Surface Profilometer, shown in Figure 16, was used to measure the thickness of the $BiVO_4$ electrodes. This instrument consisted of a stylus, which was in contact with the sample surface once the sample had been placed on the stage, and was moved across the surface along the exposed FTO substrate, to measure the properties in a two-dimensional or three-dimensional setting. The software Dektak 32 was used to run the profilometer, with parameters such as Scan length and Stylus Tracking Force.

4.3.3. Energy Dispersive X-Ray Analysis

The Energy Dispersive X-ray Analysis (EDX) is an analytical technique used for the elemental analysis or chemical characterization of a sample, and helps in the determination of impurities and allows elemental analysis. It relies on an interaction of a certain source of X-ray excitation and a sample. Its characterization capabilities are based on the principle that each element has a unique atomic structure that provides a unique set of peaks on its X-ray emission spectrum (The Utilization of Slag in Civil Infrastructure Construction, 2016). This allows the qualitative and quantitative identification of the atoms present in the sample, and their weight percentages. The EDX analysis of the $BiVO_4$ samples was conducted using the FEI Model Quanta 650 Field Emission Scanning Electron Microscope, and the Inca 250 SSD XMax20 detector.

4.3.4. X-Ray Fluorescence

X-ray fluorescence (XRF) is another nondestructive technique that allows the analysis of the elemental and chemical composition of the electrode. Here, the electrode material is excited with X-Ray energy, and the fluorescent X-ray energy emitted by the material is measured. On radiation, the electron in a certain atom is dislodged, and it releases a unique amount of energy when it returns to its original location. This energy is measured by the XRF technique, giving information on the elemental composition. The equipment used for the $BiVO_4$ electrodes was Panalytical Axios Max WD-XRF spectrometer and the data on composition was evaluated using the SuperQ5.0i/Omnian software.

4.3.5. Scanning Electron Microscopy

Scanning Electron Microscopy (SEM) is a characterization technique where magnified, detailed and high-resolution images of the morphology and topography of a sample are produced by scanning a focused beam of electrons that are created and fired using an electron gun. This beam accelerates down the microscope passing through a series of lenses and apertures creating a focused beam which then interacts with the surface of a sample. Various signals are generated at the interface of the sample, containing information about the surface's topography and composition, and hence the morphology of the photoanode (What Is Scanning Electron Microscopy (SEM)? ; "Membrane Characterization Equipment | Scanning Electron Microscopy", 2021).

Figure 17: Illustration of the microscope for SEM (FEI Model Quanta 650), used to study the surface morphology of the $BiVO_4$ electrodes

The FEI Model Quanta 650 Field Emission SEM, as illustrated in Figure 17, was used to analyze the surface morphology of the $BiVO_4$ samples. These samples had a surface area of 4±1 cm^2. They were attached to the sample holders, which were then placed into the equipment. They were observed at 0.497 mbar with a working distance (WD) of 10 mm, and the mode of detection was through 10 kV solid state BSE (Back Scattered Electrons) using the Circular Backscatter Detector (CBS). In the BSE detection, the electrons in the beam are scattered back or reflected, due to the elastic interactions with the atoms of the sample. The samples that consist of heavy metal atoms are shown to produce brighter images due to stronger backscattering of the electrons. The images

of the electrode surface are collected at magnification times of 1000, 5000, 10000, 25000, and 50000.

4.3.6. UV-Visible Spectroscopy

The electrodes were optically characterized using Steady state absorption spectroscopy in the Ultraviolet to Visible region of spectrum. The electrodes for a range of wavelengths from 300 nm to 700 nm, at two nm intervals. This characterization allows the measurement of the absorbance spectra of any solid compound or a component of a solution ("4.4", 2016). Here, the absorption of light by the electrode in the given range, and its consequent increase in energy on excitation of its electrons was measured as a function of the wavelength of radiation. The LAMBDA 1050+ UV/Vis/NIR spectrophotometer, shown in Figure 18, was used to measure the absorption spectrum of the electrodes. The absorption spectra were measured using the Integrating Sphere, which ensures that the effect of the scattered radiation from the sample, on the optical path, is negated. This is because the sphere cavity has a highly reflective inner surface, such that there are multiple reflections of the light, and hence a uniform intensity and optical path, that is then sensed by the detector. The absorbance spectra for all samples were measured using the UV Winlab software.

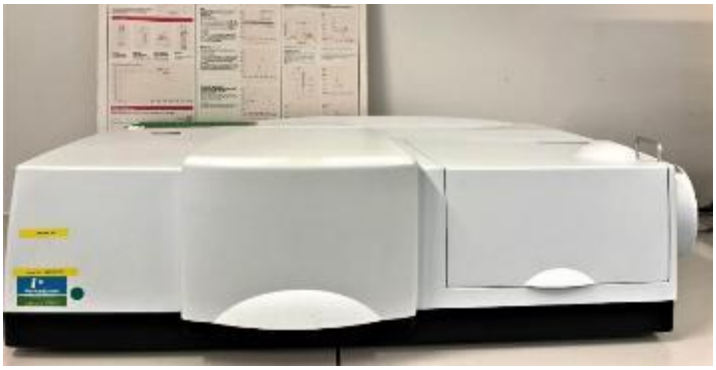

Figure 18: LAMBDA 1050+ UV/Vis/NIR spectrophotometer used to study the absorption behavior of the $BiVO_4$ electrodes

4.3.7. Incident Photon to Current Efficiency Measurement

The transient photocurrent through the photoanode is studied for measuring the Incident Photon to Current Efficiency (IPCE), also known as External Quantum Efficiency (EQE) or quantum efficiency, which is the measure of ratio of the photocurrent to the rate of incident photons as a function of wavelength of radiation (Chen et al., 2013). This analytical technique measures the ratio of the number of charge carriers on the electrode on illumination, to the number of photons from the radiation at a given wavelength. The charge carriers with respect to $BiVO_4$ electrodes are electrons and holes.

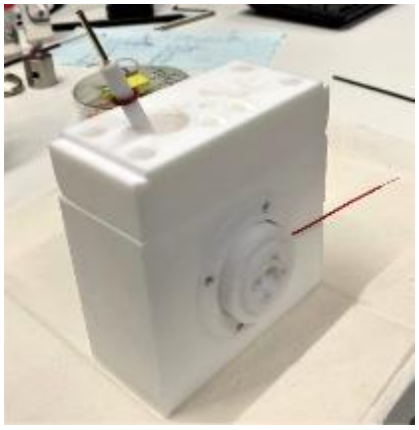

Figure 19: Cell used to place the $BiVO_4$ electrode and the counter electrode, along with the electrolyte (45 µg/L ACT and 0.1 M Na_2SO_4 in demineralized water) for IPCE measurement

Figure 20: External Quantum Efficiency setup at TU Delft

A Xenon lamp was used to produce illumination that was passed through a first-order filter, and then through a monochromator, to shorten the radiation wavelength range to one that went from 280 nm to 700 nm. It was then passed through a chopper wheel to ensure focusing of light on the sample. The signal was then measured at a source measurement unit (National Instruments) for current and voltage measurements. A shunt resistance of 47 Ω was used to maintain constant voltage. There was also a lock-in amplifier to recover the signal from the noise. The applied bias

had the function of ensuring that the carriers, or the electron-hole pairs, are generated, thus producing photocurrent.

The electrode was placed in a cell, as shown in Figure 19, and served as the working electrode, and a platinum wire served as the counter electrode, and the voltage was set at 1 V. The electrode was exposed to an electrolyte with 45 μg/L ACT and 0.1 M Na_2SO_4. The cell was connected to the setup in Figure 20, and the quantum efficiency was measured. The photogenerated current density by the electrode could also be measured with the help of the EQE setup.

4.3.8. Linear Sweep Voltammetry

Linear Sweep Voltammetry (LSV) is an electrochemical technique that is employed to provide information on the redox reactions in chemical species. This technique measures the photocurrent response of a sample while the voltage is swept up linearly in time, with a fixed rate of increase. The photoelectrochemical characterization of the $BiVO_4$ thin film was carried out using LSV. This technique allows the measurement of photocurrent across the photoanode under illumination, for a range of applied potential values. The LSV was carried out under conditions of both dark and illumination, at a scan rate of 10 mV/s, from -0.5 V to 1.5 V. The DC3 electrode was used as the working electrode, graphite electrode was used as the counter electrode, and Ag/Ag+ (4M KCl) was used as the reference electrode. This technique was carried out using a solution of 45 μg/L of ACT, with 0.1 M Na_2SO_4 as a supporting electrolyte.

4.4. Degradation Experiments

Prior to the degradation experiments, the fabricated $BiVO_4$ electrodes were made suitable to be used in electrical connections, by attaching insulated copper wires to the side of the $BiVO_4$ layer. A small amount of insulation was cut out from either end of the wires, to expose the copper wires present underneath the insulation. The carbon paste was used as the conductive glue to connect the wires to the FTO substrate, on which the $BiVO_4$ electrodes were deposited, to close the path for current flow. The carbon paste was applied under heat using the hot plate magnetic stirrer. After

the paste dried, the heat was switched off, and the electrode was left on the plate for 10 to 15 minutes for the carbon paste to solidify for a stable connection.

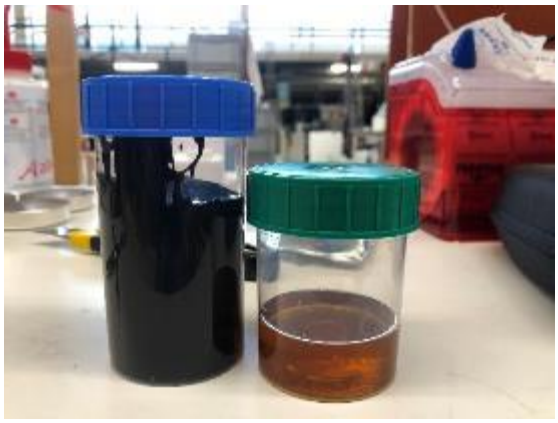

Figure 21: Epoxy resin used for insulation of connection, with polyurethane resin at the left, and hardener at the right, purchased from Electrolube

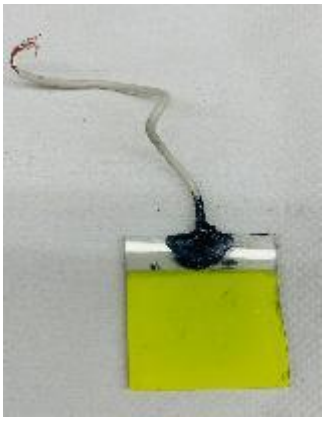

Figure 22: $BiVO_4$ electrode with connections ready for use in degradation experiments

Polyurethane epoxy was used to insulate the carbon paste connection. The package consisted of two liquids, the resin and the hardener, which were separated into plastic containers as seen in Figure 21. The required amounts of the resin and hardener were measured in the ratio of 5.21:1 respectively, and collected in a separate plastic container. It was thoroughly mixed for 5 minutes, after which it was allowed to thicken for 15 minutes. This mixture was generously applied on the carbon paste, neatly coating its full area. The electrode – wire connection was left overnight for the paste to solidify, after which the electrode as shown in Figure 22 was finally ready for usage in the degradation experiments.

Photocatalytic and photoelectrocatalytic degradation experiments were conducted to observe the reduction in the concentration of the organic pollutants in the solution, using the fabricated $BiVO_4$ electrodes. 0.1 M Na_2SO_4 was added to the solution prior to the experiments as a supporting electrolyte, to increase its conductivity, and facilitate the flow of current into the solution during the degradation processes. The required solar radiation was simulated using the Solar Simulator SUNTEST XXL+, a test chamber shown in Figure 23 consisting of three Xenon lamps that emit radiation at a wavelength within the range of 280 to 700 nm, with a radiation exposure area of

3000 cm^2, and at an intensity of 60 W/m^2. A hot plate magnetic stirrer (IKA) was used for stirring and heating purposes. The Metrohm Autolab PGSTAT128N, a potentiostat-galvanostat, was used for the observation of current and voltage for electrochemical applications. The OMP concentrations after the degradation experiments were analyzed using Liquid Chromatography – Mass Spectroscopy (Xevo TQ-S micro, Waters).

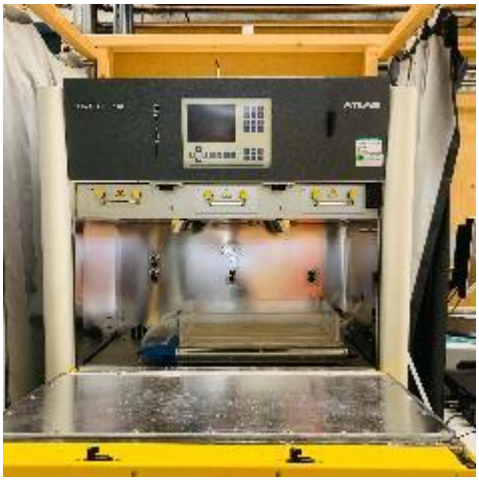

Figure 23: Solar Simulator (SUNTEST XXL+) used for the degradation of OMPs

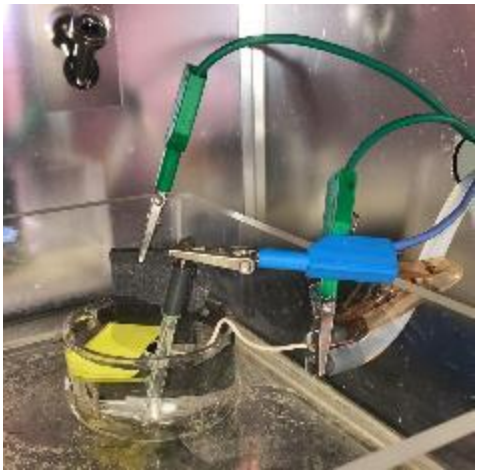

Figure 24: Reactor cell setup for PEC, with all three electrodes and the electrolyte with the OMP

The reactor setup is visually displayed in Figure 24. The $BiVO_4$ electrode was placed in a glass reactor cell onto the elevated flat surface constructed in the cell, filled with 167±1 mL of the solution facing upwards, with the attached wire dangling out of the cell. The solution was placed into the solar simulator. With the help of a stirring bar and a magnetic device, the solution was stirred for approximately 30 minutes, to allow the adsorption of organics onto the surface of the electrode. The setup for the degradation experiments consisted of a three-electrode, where the reference electrode, counter electrode and working electrode used were Ag/Ag^+ (4M KCl), graphite electrode and the $BiVO_4$ electrode. The electrical connections were made to the AUTOLAB Potentiostat as shown in Figure 25, using wires with crocodile clips to clasp the electrodes.

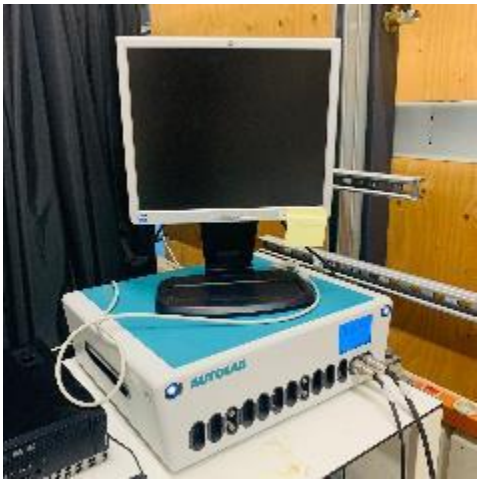

Figure 25: Autolab potentiostat for electrochemical applications located below the monitor

The value of external bias potential and the duration are set in the software. For photocatalytic experiments, the voltage was set at 0 V, and for photoelectrocatalytic experiments, the voltage was set at 1 V. The first sample of 1 mL was taken before the experiment was started at t = 0 in a labelled 40 mL plastic container (VWR), using a pipette (Thermoscientific). Ice was placed around the reactor cell inside the solar simulator to prevent the evaporation of the solution during the experiment, due to heat produced by the Xenon lamps. The process was started in the software, the solar simulator was closed, and the Xenon lamps were switched on. The solution was stirred throughout the experiment. Samples were successively collected at fixed intervals, and ice was added during sample collection. After the experiment was completed, the samples were labelled and stored in the refrigerator at 7^{o}C. The emptied reactor cell was cleansed with ethanol/acetone, followed by soap and water.

Degradation experiments were carried out to study the removal of a single OMP in a synthetically prepared solution using PEC at a concentration of 45 µg/L. The next batch of experiments was studied the degradation of multiple OMPs in a solution, at the same concentration of 45 µg/L. The final experiment was conducted to study the degradation of OMPs in real SWTE from the Wastewater Treatment Plant at Horstermeer. An experiment called photolysis was also carried out using the solution with 45 µg/L OMPs and 0.1M Na_2SO_4, to study its degradation solely due to the radiation, with the absence of a $BiVO_4$ electrode, as well as the external bias potential. Scavenging experiments were carried out as well to prove that the ROS are responsible for OMP

removal in PEC. For this purpose, a solution consisting of 45 μg/L of ACT, BTA and PRO, along with 0.1 M Na_2SO_4, was used. Three separate experiments were carried out, each with the addition of 4 mM of a single scavenger, namely EDTA, methanol and para-benzoquinone, to quench the holes, radicals and conduction band electrons, respectively. They were conducted separately to study the effect of a scavenger on the each individual OMP.

4.5. Analytical Method: LC-MS

The data of the concentration values of the OMPs, and thus the degradation efficiency of OMPs using the $BiVO_4$ electrodes, are determined by using the analytical technique of Liquid Chromatography – Mass Spectroscopy (LC-MS). This method combines the principles of two separate techniques in analytical chemistry, namely High-Performance Liquid Chromatography (HPLC) and Mass spectrometry (MS). HPLC helps to separate, identify, and quantify each component in a mixture, whereas in MS, atoms or molecules are ionized to separate them, after which these are detected in accordance with their molecular masses and charges. The combined technique LC-MS provides a higher accuracy, and involves separating mixtures in accordance with their physical and chemical properties, then identifying the components within each peak and detecting based on their mass spectrum ("Basic Principles of HPLC, MS and LC-MS", 2017). Hence, the difference in the concentration of each compound before and after photoelectrocatalytic degradation will be noted, which gives the removal efficiency.

The Internal Standard corresponding to a certain OMP allows the identification of the OMP compounds after they are ionized in the LC-MS. The calibration line that gives the range of measurement for the OMPs, is from 0.0025 μg/L to 10 μg/L. The labelled samples from the experiments using synthetic solutions are diluted to a factor of 10, whereas those from the experiments using the SWTE are left undiluted. The samples are filtered using the 0.2 μm filter (Chromafil Xtra), and poured into 1.5 mL glass vials. Using the LC-MS pipettes (Eppendorf), 495 μL of the sample is transferred to a new glass vial, to which 5 μL of the Internal Standard is added, to achieve 10% volume by volume, followed by vortex mixing of the vial contents before being run in the LC-MS. The data of concentration of OMPs is processed using the MassLynx V4.2 software.

CHAPTER 5: RESULTS AND DISCUSSION

5.1. Structural Characterization of Electrodes

5.1.1. Crystallinity

The crystallinity of the fabricated $BiVO_4$ electrodes was validated by carrying out the XRD technique, using Cu Kα radiation, within a range of 2θ = 10° - 130°, a step size of 0.040 ° 2θ, and counting time per step 2 seconds. This analysis was carried out for three electrodes, namely an electrode each from -0.2 V and -0.4 V bias of electrodeposition, as well as an electrode from the dip-coating process, to study the outcome of different fabrication methods on the crystallinity of electrodes.

Figure 26 depicts the diffraction patterns of the $BiVO_4$ electrodes prepared by electrodeposition at conditions of -0.2 V and -0.4 V, and by dip-coating respectively, and annealed at 460^{o}C, at a ramp rate of 2^{o}C per minute. The XRD patterns in Figure 26 show that for all the samples of electrodes chosen for the examination of crystallinity, the highest intensity diffraction peaks were presented at 2θ = 18.5^o, 29^o and 49^o, which were similar to the values found in (Kiama, 2018). By the usage of the ICDD pdf4 database for analyzing the peaks, the crystalline structures of Clinobisvanite and Cassiterite were detected in these samples. Clinobisvanite corresponds to scheelite – monoclinic $BiVO_4$ photoanode, whereas Cassiterite corresponds to the FTO layer on the glass substrate that was used for the deposition of the $BiVO_4$ thin film.

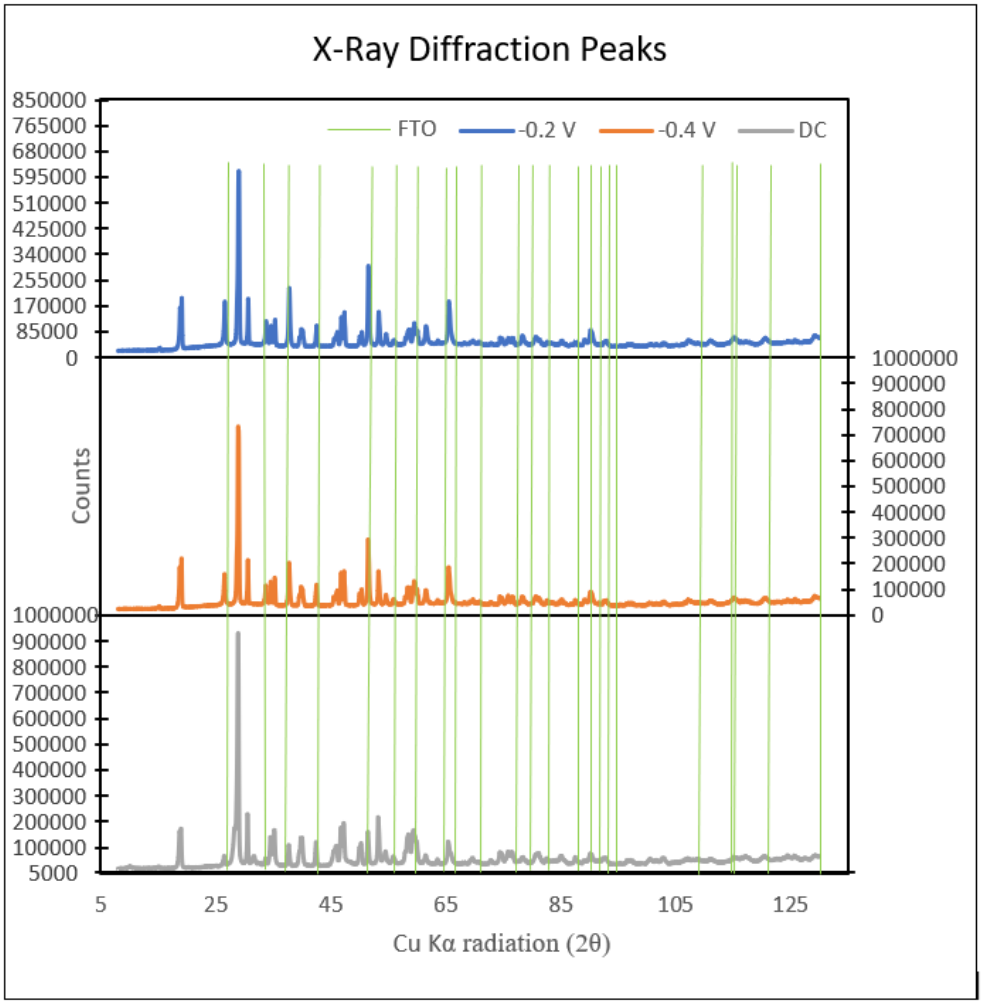

Figure 26: XRD Diffraction peaks observed for $BiVO_4$ thin films, produced by electrodeposition at -0.2 V, -0.4 V and dip-coating respectively

Clinobisvanate has a monoclinic crystallographic symmetry (Clinobisvanite Mineral Data, n.d.) and its presence confirms the monoclinic scheelite crystalline structure of the $BiVO_4$ thin film. This is the desired structure, because as previously mentioned, the band structure enables the excited electrons to move freely, proving to be beneficial in the degradation of OMPs (Zheng et al., 2019). The peak was also observed at 2θ equal to 65^o for the two electrodes produced by electrodeposition, but the peak at this value was relatively less intense for the electrode by dip-coating. This implies that there is a difference in the atomic structure in that specific region of the electrode, therefore producing a difference in the scattering of light, and thus a difference in the peak intensities (Basics to Powder X-Ray Diffraction, 2020) .

5.1.2. Film Thickness

The thickness of all 15 fabricated $BiVO_4$ thin films was measured in nanometers (nm) with the help of the surface profilometry technique, and are listed in Table 2 in micrometers (μm). For the two groups of samples consisting of electrodes fabricated by electrodeposition at -0.2 V and -0.4 V, there is a clear trend of increase in the thickness with increasing duration of electrodeposition. This verifies that a higher amount of BiOI was deposited on the FTO substrate when a longer duration of electrodeposition was applied.

Table 2: Thickness in micrometers (μm) for all 15 $BiVO_4$ electrodes

-0.2 V	**Thickness (μm)**	**-0.4 V**	**Thickness (μm)**	**Dip-coating**	**Thickness (μm)**
Durations		**Durations**		**Number of layers**	
2 minutes	0.545	2 minutes	0.894	1 layer	1.619
5 minutes	1.382	5 minutes	0.970	2 layers	2.259
7 minutes	1.548	7 minutes	2.219	3 layers	2.708
10 minutes	1.719	10 minutes	3.746	4 layers	3.075
15 minutes	1.896	15 minutes	4.536	5 layers	1.626

A similar general increasing trend was noticed within the group of electrodes fabricated by dip-coating, apart from the last electrode with 5 layers of dip-coating. This anomaly could be due to a failure during the dipping of electrode, and/or during the annealing process. The electrodes fabricated at -0.4 V had approximately 1.5 to 2.5 times higher thickness than the electrodes fabricated at -0.2 V, except for the electrodes at 5 minutes, where the thickness was higher for the electrode of -0.2 V. This error could have originated from the processes of fabrication, for which various factors include the precursor solution pH, the homogenous mixing of the chemicals into the precursor solution, and the positioning of the electrodes during electrodeposition of BiOI.

5.1.3. Chemical Composition

The chemical presence of $BiVO_4$ and other byproduct compounds in the fabricated thin films was confirmed by the elemental characterization techniques of EDX and XRF. The EDX was conducted for the qualitative and quantitative analysis of the samples, namely the electrodes

electrodeposited at -0.2 V, 5 minutes (2v5m), and at -0.4 V, 7 minutes (4v7m), and the electrode by dip-coating with 3 layers (DC3).

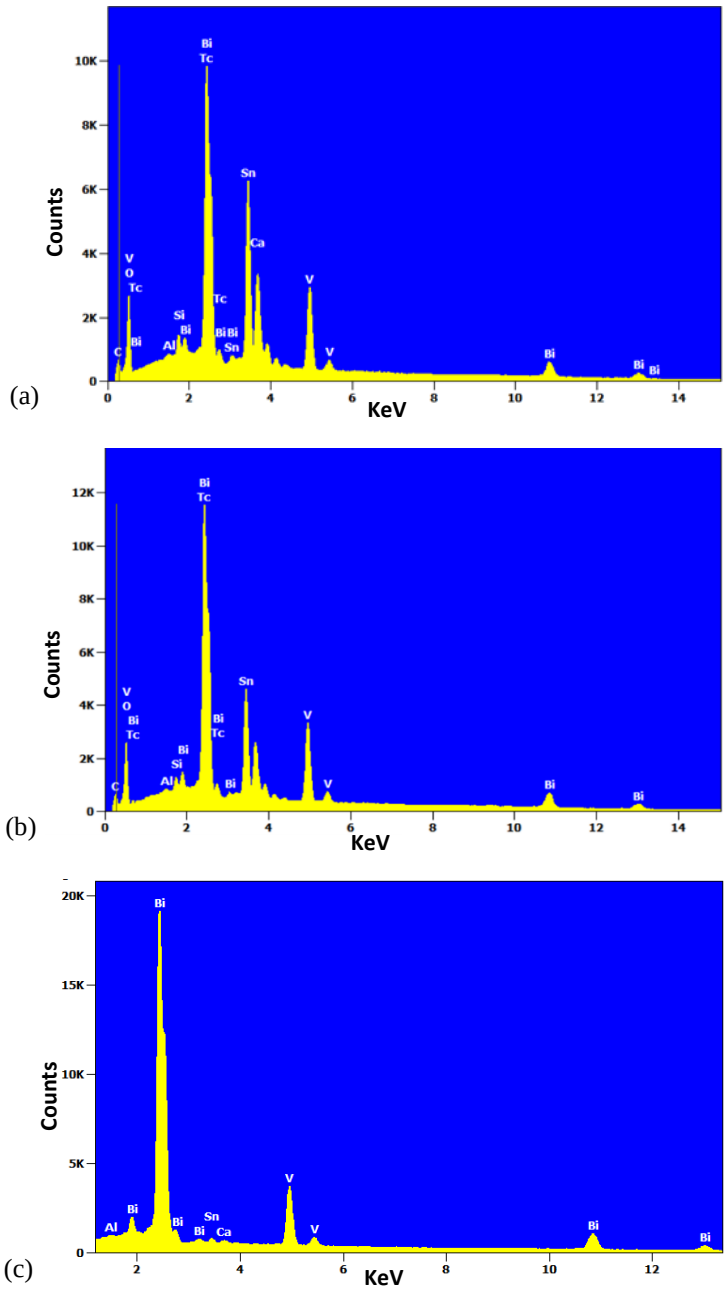

Figures 27: EDX analysis curves for $BiVO_4$ electrode, from (a) -0.2 V, 5 minutes, (b) -0.4 V, 7 minutes, and (c) dip-coating for 3 layers

From the EDX curves for all three electrodes shown in Figures 27, it was revealed that the peaks of highest intensities for Bi and V were present at approximately 2.4 keV and 5 keV, respectively. The distinct presence of the major elements further confirmed the successful deposition of the $BiVO_4$ thin film on the FTO/glass substrate (Lopes et al., 2015). It was observed from the Figure 27(c) that the peaks for Bi and V were higher for the DC3 electrode, at nearly 20,000 and 5,000 counts respectively, as compared to the peaks observed in the other two electrodes. From the Figure 27(a), the highest peaks of Bi and V in the 2v5m electrode were at nearly 10, 000 counts and 3,000 counts respectively. Meanwhile, the values of the highest peaks of Bi and V for the 4v7m electrode in the Figure 27(c) were higher than those of the other electrodeposited electrode, at nearly 12,000 and 4,000 counts respectively.

Table 3: Atomic and weight percentages of elements found in the $BiVO_4$ thin films through EDX analysis

Electrode	**2v5m**		**4v7m**		**DC3**	
Element	**Weight %**	**Atom %**	**Weight %**	**Atom %**	**Weight %**	**Atom %**
C	1.2	5.6	1.3	6.3	1.4	8
O	16.4	55.4	13.5	50.9	11.3	49.1
Al	0.1	0.2	0.1	0.3	0.1	0.2
Si	0.8	1.5	0.5	1.1	0	0
Ca	0.8	1	0	0	0.2	0.3
V	10.3	11	11.9	14.1	12.5	17.1
Tc	1.4	0.8	1.1	0.7	0	0
Sn	33.4	15.3	26.8	13.7	1.9	1.1
Bi	35.6	9.2	44.8	13	72.7	24.2
Total	**100**	**100**	**100**	**100**	**100**	**100**

A further glance at the atomic percentages at the weight percentages of Bi and V in Table 3 suggest that the weight percentages of Bi and V were higher for DC3 than for the other two samples, at approximately 73% and 13% respectively. These observations can be attributed to the thickness of the thin film in each of the chosen samples from Table 2. A correlation was observed between the thickness of the thin film, and the weight percentages of Bi measured in the thin films. From the results of the surface profilometry of the three chosen samples, the DC3 electrode had the thickest thin film at 2.708 μm, and it also showed the highest weight percentage of Bi at 72.7%. The 2v5m electrode had the lowest thickness at 1.382 μm, and also showed the lowest weight percentages of Bi at 36%. Another observation which can also be attributed to the thickness of the thin film, was

the presence of Sn in the peaks of the EDX analysis, shown in Figures 27. They were observed at over 6 keV, 4 keV, and just under 1 keV for the DC3, 2v5m and 4v7m electrodes respectively. The Sn is from the FTO substrate, on top of which the $BiVO_4$ thin film is fabricated. Therefore, with increasing thickness of the electrodes, the Sn peak decreased in intensity, and this is confirmed by the the decreasing weight percentage of Sn with increasing thickness. Other compounds such as Si and Ca were discovered in the thin films, and they corresponded to the substrate of the thin-film, which comprised of quartz glass.

Table 4: Weight percentages (wt%) of compounds found in the $BiVO_4$ thin films through XRF analysis

Compound	**Electrode**		
	2v5m	**4v7m**	**DC3**
	(wt%)	**(wt%)**	**(wt%)**
SnO_2	42.7	42	5.2
SiO_2	18.9	17.5	2.2
V_2O_5	17.3	19	40.4
CaO	12.7	11.7	5
Bi_2O_3	7	8.1	42.4
SO_3	0.4	0.3	3.5
Fe_2O_3	0.3	0.4	0.4
ZrO_2	0.3	0.3	0.8
Na_2O	0.2	0.5	0
MgO	0.1	0.1	0
SrO	0.1	0.1	0.1
Cl	0	0.1	0.1
Total	**100**	**100**	**100**

The chemical characterization of the electrodes was further carried out using the XRF technique. The presence of other oxides of Bi and V, such as Bi_2O_3 and V_2O_5 was detected in the samples, as tabulated in Table 4. It can be seen that the DC3 electrode had higher amounts of Bi_2O_3 and V_2O_5 than the other two electrodes. This observation can be correlated to the X-Ray Diffraction patterns of the fabricated electrodes in Figure 26, and explains the peaks at other values of 2θ in the DC3 sample apart from the characteristic peaks of scheelite – monoclinic $BiVO_4$. Other metal oxides such as CaO, Fe_2O_3, ZrO_2, MgO and Na_2O were found in the elemental analysis of XRF. This may be attributed to the FTO layer consisting of impurities which include the metal oxides mentioned previously.

5.1.4. Surface Morphology

The morphology and structure of the $BiVO_4$ electrodes fabricated by dip-coating and electrodeposition on FTO glass slides were observed using the SEM technique. Images of the electrode surfaces were captured at magnifications of x1000, x5000, x10000, x25000 and x50000. The surface morphology of the $BiVO_4$ electrodes made from electrodeposition are shown in Figures 28(a) to (d).

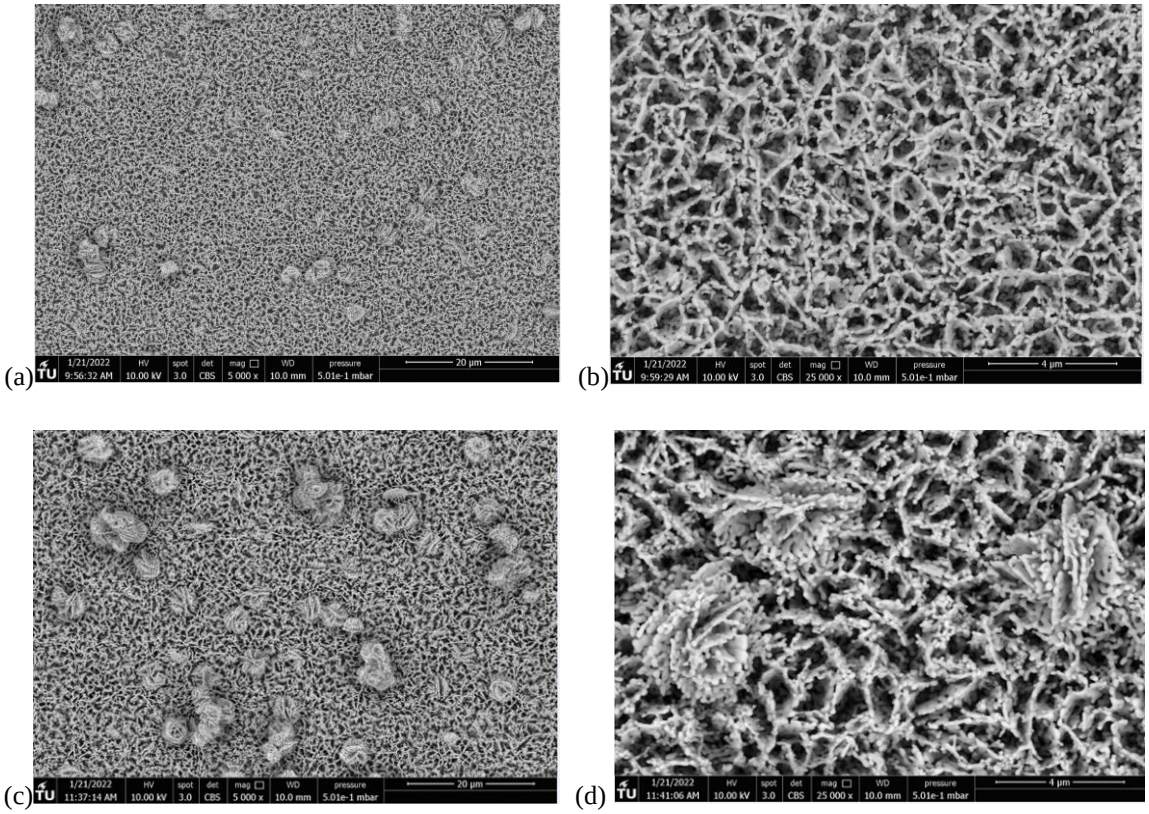

Figures 28: Surface Morphology images captured by SEM of electrodeposited $BiVO_4$ electrodes, of (a) 2v5m, at 5000x magnification, (b) 2v5m, at 25000x magnification, (c) 4v7m at 5000x magnification, and (d) 4v7m, at 25000x magnification

On observing the microstructure of the electrodeposited $BiVO_4$ layers from Figures 28, the particles of $BiVO_4$ appeared as microrods of similar size, arranged in an orderly and uniform structure, along with a few sparsely arranged clusters of the microrods. This shows the successful

fabrication of a uniform $BiVO_4$ layer through electrodeposition, regardless of the external bias used in the process. Hence, the porosity of the microstructure may be responsible for increased transfer of electrons within the layer, and thus higher charge transport in between the particles, which would result in a higher photocurrent output (Orimolade and Arotiba, 2020).

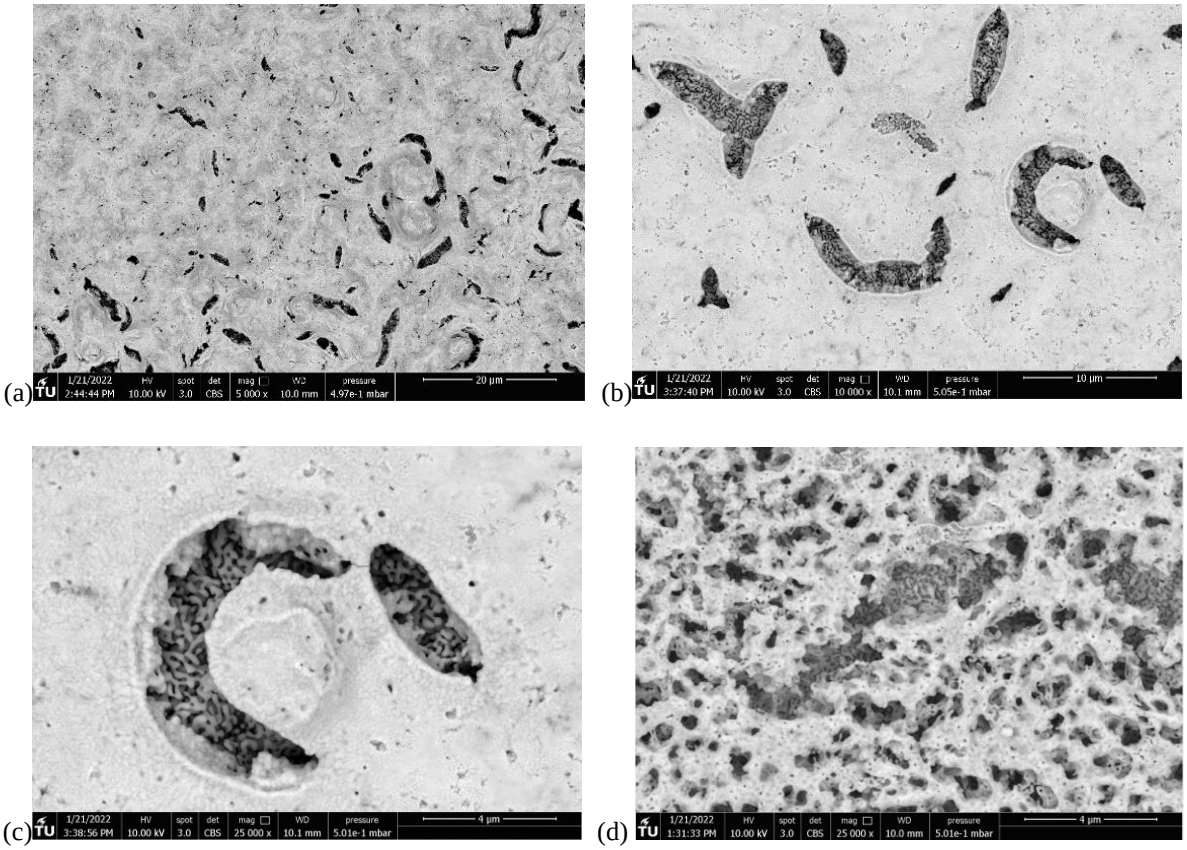

Figures 29: Surface Morphology images captured by SEM of $BiVO_4$ dip-coating electrodes, with (a) 3 layers at 5000x magnification, (b) 3 layers at 10000x magnification, (c) 3 layers at 25000x magnification, and (d) 1 layer at 25000x magnification.

The microstructure of the $BiVO_4$ layers produced by dip-coating, shown in Figures 29, was seen to significantly differ from the ones produced by electrodeposition, in the aspects of structure, shape and arrangement of the particles. Here, the $BiVO_4$ surface was complex, consisting of an upper layer with bubble-shaped variations on the surface, with deep micro-gaps and macro-gaps that revealed another inner layer of aggregates of particles, and crescent-shaped protrusions from

the surface. The Figure 29(d) exhibited the surface morphology of the $BiVO_4$ electrode produced by dip-coating with 1 layer. In this case, it was seen that the upper layer was thinner than the one in the electrode produced by dip-coating with 3 layers, which again indicates the increasing thickness of the surface with increasing number of layers. It was observed that the arrangement of the upper layer revealing an inner layer was visible in all the electrodes of different layers of dip-coating. The presence of the upper layer that served as a partial cover for the inner layer, along with the highly varied structure of the inner layer, provide sites for the target organic pollutants to get adsorbed, and subsequently attacked by the holes, the •OH radicals and the $O_2•^-$ radicals, which agrees with research by (Kamble & Ling, 2020). The upper layer allows to secure the organic pollutant molecule and prevents its escape. With a higher number of layers of dip-coating, the upper layer is thick, and more OMP molecules are trapped inside the $BiVO_4$ thin film, which implies that more OMP molecules would be degraded. However, the aggregate structure of the upper layer showed low porosity. Hence, there may be lesser amount of electrolyte perforating the layer, implying reduced electron transfer across the layer for dip-coating electrodes as compared to the electrodes by electrodeposition, as discussed in (Cristino et al., 2019).

5.2. Optical Characterization of Electrodes

The optical characterization of the $BiVO_4$ thin films was conducted using Steady State Absorption Spectroscopy in the Ultraviolet-Visible region of spectrum, ranging from 300 nm to 700 nm. The absorption patterns of all 15 electrodes are depicted in Figures 30. It was observed that all the electrodes followed a similar pattern in absorbing photons within 300 nm to 500 nm, in the UV to visible light region, with the absorption edge of each curve at 500 nm. This is a desirable range for the optical response of the thin films, since it facilitates better photoelectrocatalytic activity in the visible range. It was noticed that the absorption curve for every electrode showed the highest peak at 370 nm. The extension of the absorption curve till beyond 650 nm may be attributed to anomalies in the crystal structure of the overall scheelite – monoclinic $BiVO_4$ (Zulkifili et al., 2018).

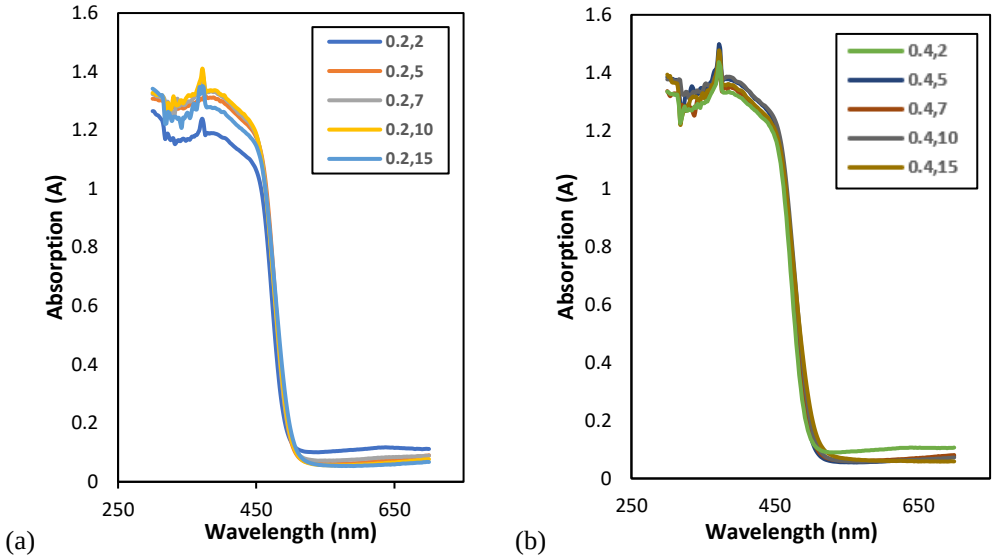

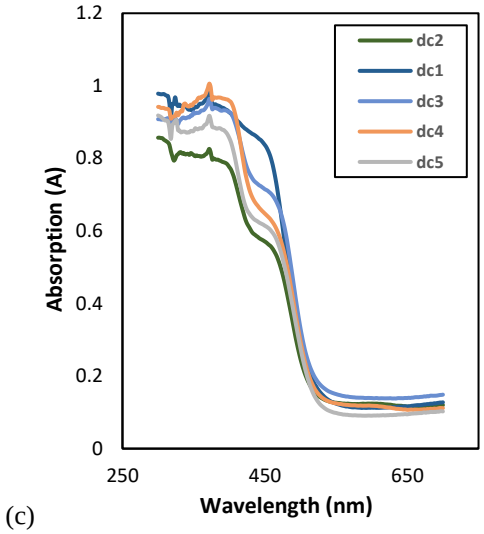

Figures 30: UV-Visible absorption spectra of all $BiVO_4$ electrodes at (a) -0.2 V (b) -0.4V, and (c) dip-coating.

With regard to the thin films fabricated by electrodeposition seen in Figures 30(a) and 30(b), the thin films electrodeposited at -0.4 V absorbed more photons in the same range of wavelengths, despite the fact that the patterns of the curve were indistinguishable. Within each group of electrodes from -0.2 V and -0.4 V, the duration of electrodeposition of the fabricated thin film does not seem to be a factor in the amount of absorption of light by the thin film. The absorption of light by the thin films fabricated by dip-coating was lower than that of their electrodeposited

counterparts. The patterns of absorption for the electrodes by dip-coating exhibited more anomalies relative to one another, as compared to the electrodes produced by electrodeposition. These differences can be attributed to the variation in crystal structure of the prepared thin films. According to (Bakhtiarnia et al., 2021), an optimum film thickness is of great importance to ensure a good balance between the light absorption and charge separation ability.

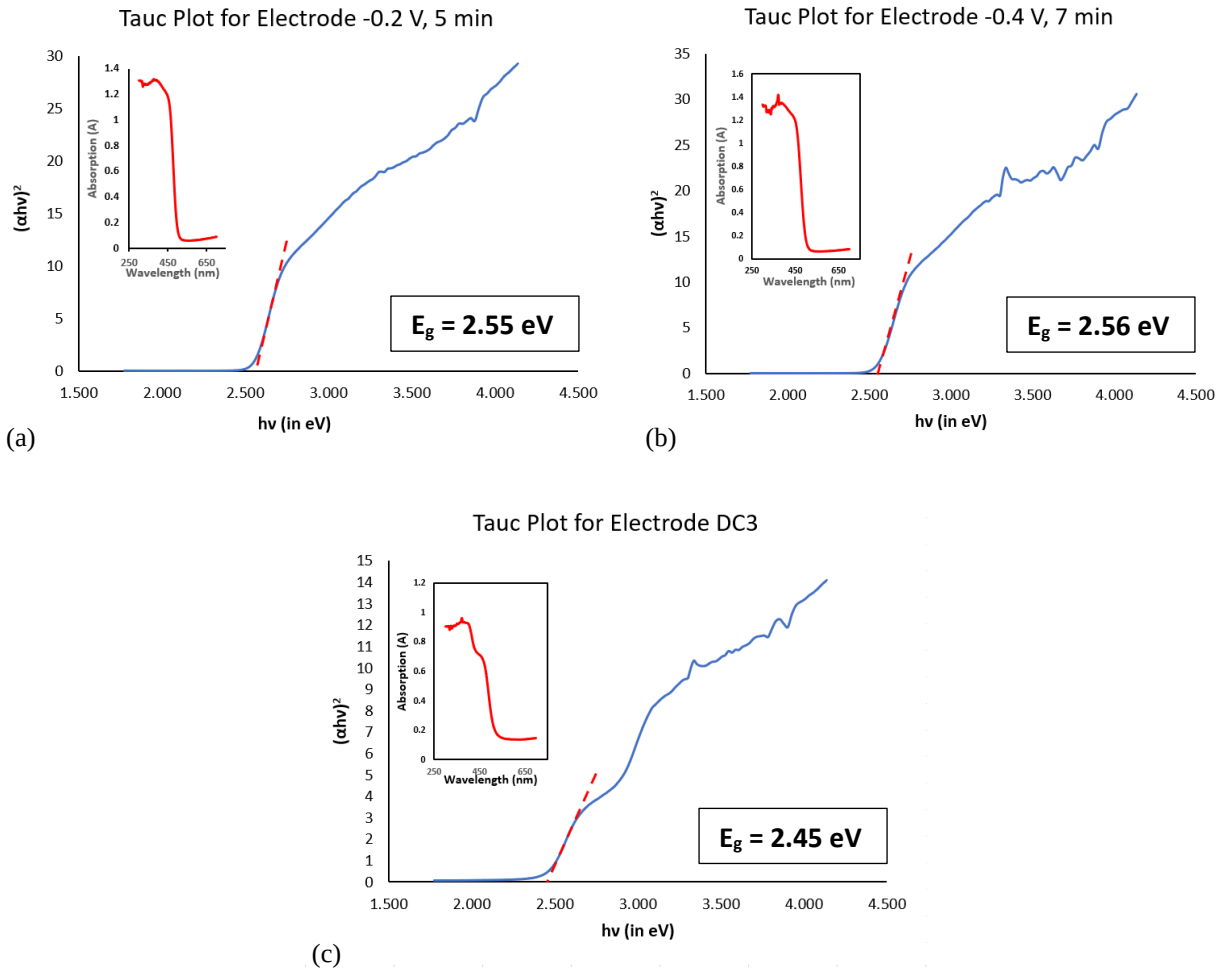

Figures 31: Tauc plots and calculated band gap energy values of $BiVO_4$ electrodes, namely the (a) 2v5m (b) 4v7m, and (c) DC3 electrodes

The absorption spectra of the $BiVO_4$ thin films also served another purpose by enabling the calculation of the band gap energies E_g of the thin films. This is done by fitting the absorption data

from the optical characterization, into the Tauc equation for semiconductors. The Tauc equation demonstrates the calculation of E_g for semiconductors as follows:

$$\alpha h\nu = (h\nu - E_g)^{n/2} \quad (7)$$

where α is the absorption of radiation, h is the Planck's constant at 6.626 x 10^{-34} m^2kg/s, ν is the frequency of the radiation, and n is a constant that depends on the nature of electron transition in the semiconductor (Xu et al., 2018). $BiVO_4$ is a considered to be a direct transition semiconductor, and so the value of the constant n is assumed to be 1 (Zhang et al., 2018). Figures 31 shows the Tauc plots of the 2v5m, 4v7m and DC3 electrodes. The band gap energies E_g of the 2v5m, 4v7m and DC3 electrodes were calculated from the Tauc plots to be 2.55 eV, 2.56 eV and 2.45 eV, respectively. These values of E_g are in accordance with what was studied in the literature review that established the general band gap energy values of the $BiVO_4$ thin film. It was also seen that the electrode of DC3 had the lowest band gap energy.

5.3. Optoelectronic Characterization of Electrodes

5.3.1. Band Potentials

When a photocatalyst such as $BiVO_4$ is illuminated with radiation in the UV-Visible range, the electrons are excited and migrate from the valence band to the conduction band, for which the energy required is the band gap energy. The band gap energy E_g of the DC3 electrode was calculated to be 2.45 eV from the Tauc plot. It is possible to calculate the conduction band edge potential and valence band edge potential of the $BiVO_4$ electrode, by the following equations according to (Cai et al., 2018).

$$E_{CB} = E_N - E_{FE} - 0.5E_g \quad (8)$$

$$E_{VB} = E_{CB} + E_g \quad (9)$$

Here, E_{CB} is the conduction band edge potential of the photocatalyst, E_N is the geometric mean of the absolute electronegativity values of all elements present in the photocatalyst, and equal to 6.04

for $BiVO_4$, E_{FE} is the energy occupied by free electrons (vs Normal Hydrogen Electrode) and equal to 4.5 eV, and E_{VB} is the valence band potential of the photocatalyst.

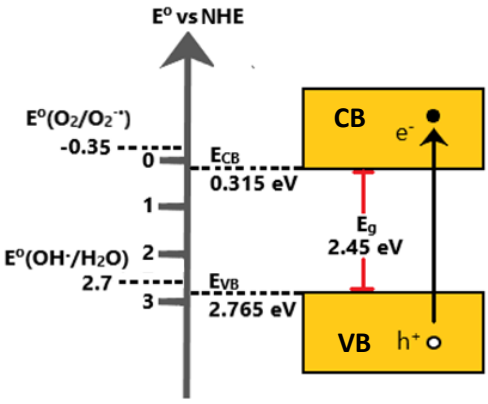

Figure 32: Illustration of the band edge potential values of the DC3 $BiVO_4$ electrode

The conduction band edge potential and valence band edge potential of $BiVO_4$ were calculated to be 0.315 eV and 2.765 eV, respectively. Figure 32 shows the illustration of the band diagram of the $BiVO_4$ electrode. Here, as stated in literature, the electrons are excited to the conduction band, where either they are held by the positive external bias applied during PEC, or they react with O_2 to form $O_2^{\bullet -}$ radicals. Whereas, the holes remain in the valence band and either directly oxidize the pollutants, or react with H_2O to form the powerful •OH radicals.

5.3.2. Incident Photon to Current Efficiency

In order to measure the optoelectronic performance of the fabricated $BiVO_4$ thin films, the IPCE was measured for the 15 electrodes within the range of 280 nm to 700 nm of wavelength of the irradiation. This technique measured the efficiency of the electron-hole pairs generation on the electrode by the photons absorbed. A higher quantum efficiency indicates that a higher number of holes are generated, which would react with more water molecules to produce a higher number of •OH radicals, and would thus lead to the enhancement of the photoelectrocatalytic degradation of OMPs (Sahu, 2019). This technique also provided a measure of the current density across the

photoanode, which indicates the status of the electron-hole recombination. A higher value of current density indicates better charge separation (Sun et al., 2015).

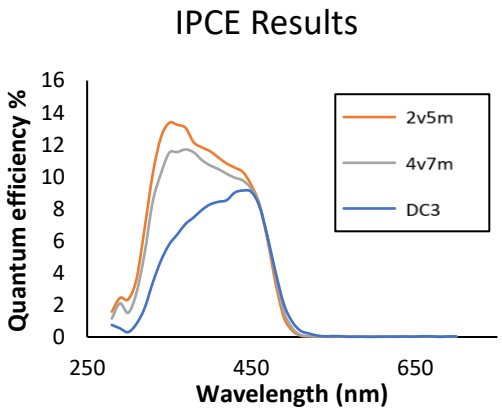

Figure 33: Quantum efficiency vs wavelength of $BiVO_4$ electrodes of 2v5m, 4v7m and DC3 together

From Figure 33, it is noticed that the onset of the IPCE of all the electrodes was from approximately 250 to 300 nm, and its termination was at 500 nm. The $BiVO_4$ 2v5m electrode had the greatest IPCE at a given wavelength out of all the electrodes, with the quantum efficiency curve showing the highest peak at 13.5% at 350 nm. The electrodes produced by electrodeposition tended to have ranges with higher IPCE values than the electrode produced by dip-coating, for which the maximum IPCE value was 9%. This increased magnitude of the IPCE curve area, as well as the peak value of the quantum efficiency, can be correlated with the results for the absorption of radiation in the UV-Visible region by the same electrodes, since the amount of light absorbed by the electrodes were in the same order as the peak IPCE values of these electrodes. Although the electrodeposited thin films had higher maximum IPCE values, the IPCE of the dip-coated electrode peaked at 450 nm in the visible light spectrum, unlike the former cases, where the wavelength values of peak quantum efficiency were in the UV spectrum. This result also correlated with the results from the Tauc plot from Figure 31(c), where it was seen that the dip-coating electrode had the lowest calculated band gap energy at 2.45 eV. This could explain why the peak IPCE of DC3 is at a wavelength in the visible light spectrum. The IPCE value of DC3 shown in Figure 33 could be low due to optical losses by reflection, which leads to ineffective absorption of light (Bennani,

2017). This result is backed by the surface morphology result of DC3 from Figures 29(a) to (c), which showed that the surface was uneven and less structured as compared to its electrodeposited counterparts. The surface results may also explain the reduced absorption intensity for DC3 in UV-Visible spectroscopy. The photocurrent density values of the 2v5m, 4v7m, and DC3 electrodes were 0.53, 0.5 and 0.43 mA/cm^2 respectively. A higher value of current density implies that there is better charge separation due to easier charge transport, and thus it can be assumed from the results of current density that the electrodeposited electrodes have better charge separation than the dip-coated electrode. This is also backed by the results of the surface morphology of the electrodes in Figures 28 and 29, where the surface analysis implied that the charge transfer may take place more readily for electrodeposited electrodes than the dip-coated electrodes.

5.4. Photoelectrochemical Characterization of Electrodes

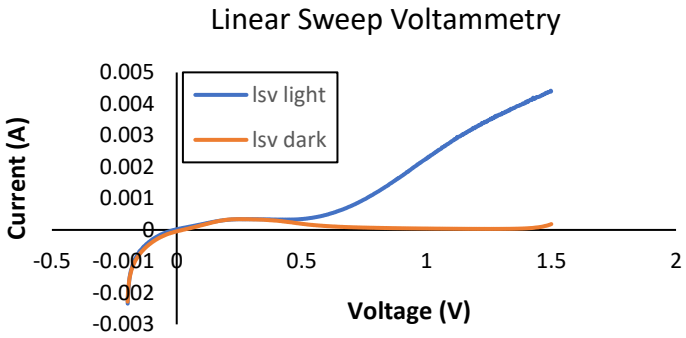

Figure 34: LSV curves in dark and illuminated conditions.

The behavior of the photocurrent with increasing bias potential applied to the $BiVO_4$ electrode in the solution can be observed in Figure 34. The photocurrent under illuminated condition stayed constant at a very small value until the voltage reached 0.5 V. From this value of potential, a significant and linear rise in the photocurrent was observed with increasing value of potential until 1.5 V. It can be inferred that at a higher potential, since the photocurrent was found to be higher, the charge separation is better and thus the charge transfer is feasible, which ultimately reduces

the recombination of electron-hole pairs. The external bias to be used for the photoelectrocatalytic degradation experiments was chosen to be 1.0 V, in order to allow sufficient degradation of the OMPs, without compromising energy efficiency by limiting the electrical consumption.

5.5. Degradation of Single Component System

5.5.1. Degradation of Phenol

The degradation phase is initiated with the organic compound phenol, dissolved in demineralized water at a concentration of 30 mg/L, along with 0.1 M Na_2SO_4 as a supporting electrolyte. The rate of degradation of a compound can be evaluated by looking at its removal percentage after a certain number of hours. Two experiments were carried out to study the degradation of phenol, namely PC and PEC.

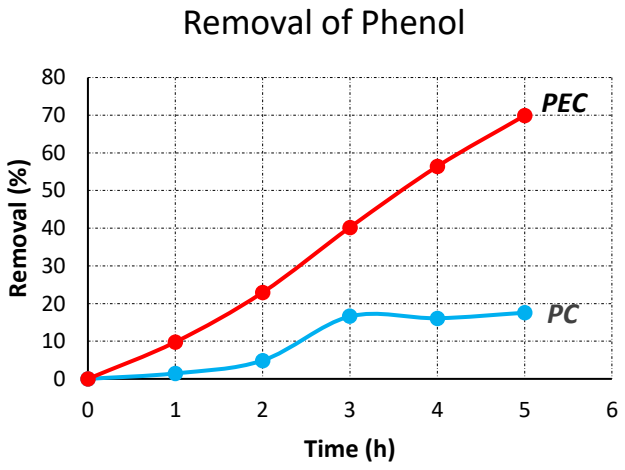

(a)

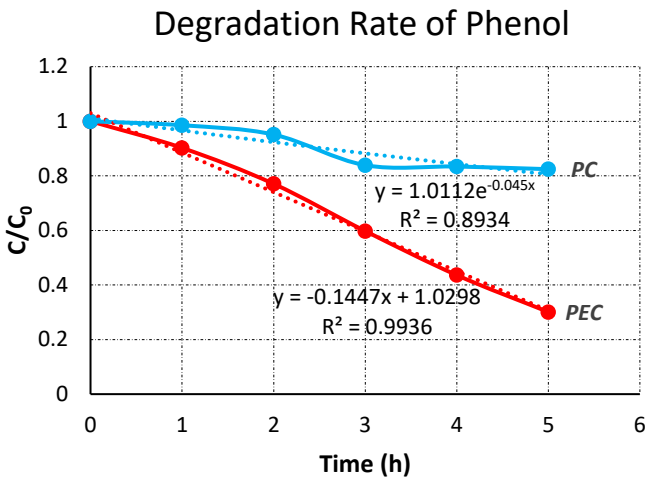

(b)

Figures 35: Results of degradation of phenol using $BiVO_4$ electrode. (a) Removal percentages of Phenol using photocatalysis (PC) and photoelectrocatalysis (PEC), and (b) Degradation rates of Phenol using photocatalysis (PC) and photoelectrocatalysis (PEC)

From the Figures 35, it was observed that photoelectrocatalytic degradation of phenol, conducted with an external bias of +1.0 V, resulted in a higher removal efficiency than the photocatalytic degradation of phenol. The rate of the reaction was also higher in the PEC experiment of phenol at 0.145 h^{-1}, than the PC experiment at 0.045 h^{-1}. This may be explained by the reduced recombination of electrons and holes and enhanced charge separation, due to the electrons being captured into the conduction band, thereby allowing the formation of more •OH radicals that effectively degrade the organic substances. This is further backed by the results from the LSV characterization of the electrode, where a higher positive external bias produced a higher current response under illuminated condition, showing enhanced charge separation. Hence, the results displayed in Figures 35 serve as proof of concept that PEC is a more effective process than PC in the degradation of organics. The experimentation was consequently continued using PEC for the degradation of OMPs.

5.5.2. Effect of Electrode Fabrication on Degradation

Once the benefit of PEC over PC is proven, the next step was the photoelectrocatalytic degradation of a single OMP in a solution, for which ACT was chosen. With an initial concentration of 45

μg/L, along with 0.1 M Na_2SO_4, the degradation of ACT was conducted using all 15 $BiVO_4$ electrodes. The range of duration of electrodeposition was optimized to be from 2 minutes to 15 minutes, since preliminary experiments showed the highest ACT degradation within this range. An additional experiment was done to test the photolysis of ACT under illumination, which resulted in a removal percentage of only 7%, this proving that the $BiVO_4$ photocatalyst, and thereby the process of PEC, is chiefly responsible for the effective degradation of ACT.

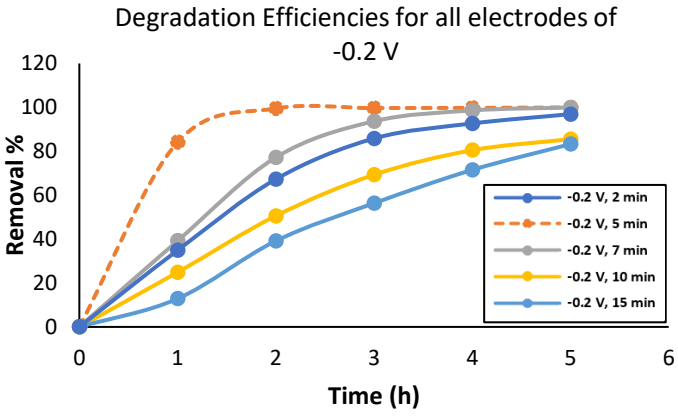

(a)

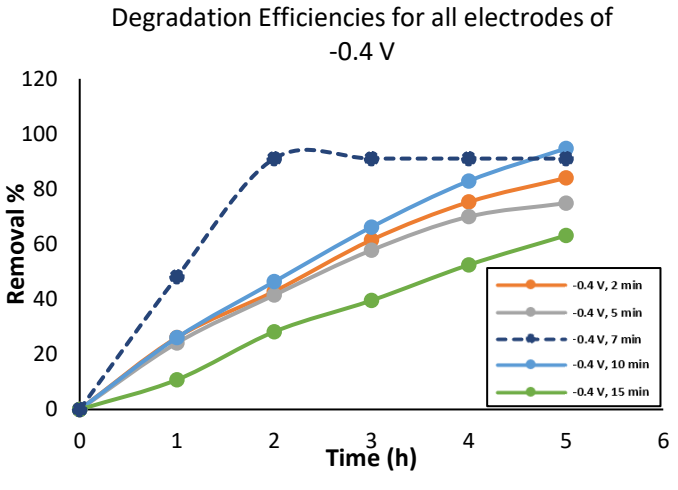

(b)

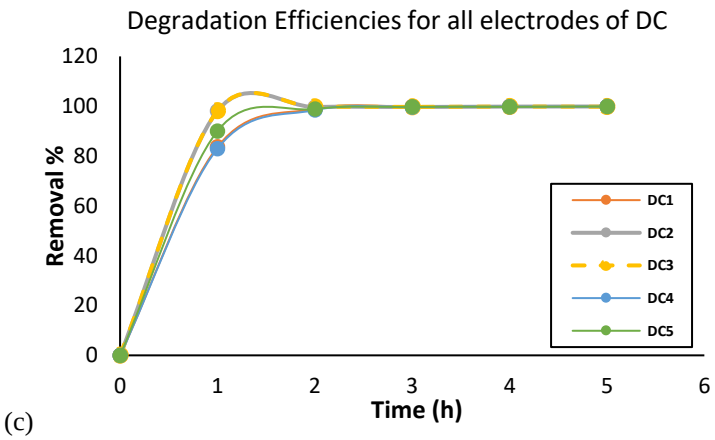

(c)

Figures 36: Removal of ACT using $BiVO_4$ electrodes at (a) -0.2 V at all five durations, (b) -0.4 V at all five durations, and (c) Dip-coating at all five numbers of layers

The results for the ACT degradation are displayed in Figures 36 on the basis of mode of fabrication, voltage of electrodeposition, and the duration of electrodeposition. A general observation was the decrease in pH of the solution after the degradation experiments, with the initial pH values of the solutions falling in between 7 to 8. This was agreeable with Equation 3, which showed the release of H^+ ions with the production of •OH radicals. The degradation of ACT concentration for all the electrodes showed exponential decay over 5 hours, and thus the reactions followed first order kinetics. The rate law is given by the equation:

$$y = Ae^{-kt} \quad (10)$$

Where y is the concentration of the OMP (µg/L) at time t (h), A is the initial concentration of the OMP (µg/L), and k is the rate constant of the reaction (h^{-1}).

The electrodes produced at 15 minutes of duration for both -0.2 V and -0.4 V, as seen in Figures 36(a) and 36(b), were responsible for the lowest degradation efficiencies of ACT, as well as the slowest rates of degradation, in their respective groups. This further affirms the choice of not fabricating electrodes for an electrodeposition duration of longer than 15 minutes. However, apart from the increasing thickness of electrodes at higher durations of electrodeposition, the duration of electrodeposition had no clear trend with regard to OMP removal. For the voltage of -0.2 V, it was observed from Figure 36(a) that the $BiVO_4$ electrode at 5 minutes achieved the highest removal of ACT at approximately 99% It also showed a quicker rate of degradation than the other

durations of electrodes, since over 80% removal was achieved in the first hour. As for the electrodes of -0.4 V, it was seen from Figure 36(b) that the electrode of 7 minutes was responsible for the highest rate of ACT removal out of the group, accomplishing 90% removal within the first 2 hours of degradation. Even though the electrode at 10 minutes showed the highest removal of almost 95% after 5 hours, it showed slower degradation with only 25% removal within the first 2 hours.

For the electrodes fabricated by dip-coating, it was seen from the figure 36(c) that all the electrodes showed relatively rapid rates of degradation of ACT. It was noted that within the first hour, all the electrodes showed ACT removal of over 80%. The degradation rate reduced after the first 2 hours, and the graphs showed slower degradation for the remaining 3 hours. Although all electrodes showed over 99% removal of ACT, the removal rate by the DC3 electrode was noted to be the quickest at 1.124 h^{-1}. The dip-coating electrodes with 1 and 4 layers showed the slowest degradation of ACT, with removal percentages of roughly 83% in the first hour, in comparison to the other electrodes, which reported removal percentages all of roughly 99%. Even for the process of dip-coating, apart from the increasing thickness of electrodes with increasing number of layers, the number of layers had no clear trend with regard to OMP removal.

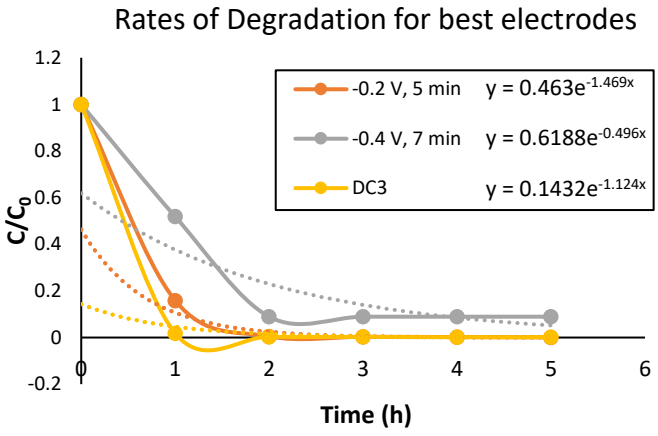

Figure 37: Degradation rates for electrodes with highest ACT degradation from each group, namely 2v5m, 4v7m, and DC3 electrodes

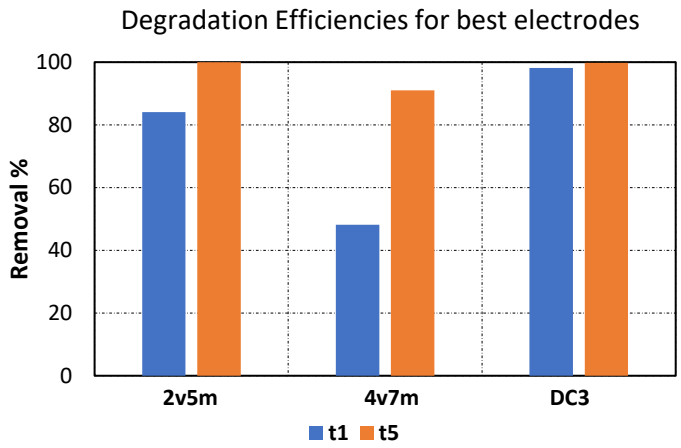

Figure 38: Degradation efficiencies for electrodes with highest ACT degradation in each group. t1 signifies the value after 1 hour, and t5 signifies the value after 5 hours

Figures 37 and 38 show a comparison of the electrode from each group with the highest degradation of ACT, namely the 2v5m, 4v7m, and DC3 electrodes. This is further represented by Figure 38 that shows the removal of ACT after the first hour (t1) and the fifth hour (t5), where the DC3 electrode had the highest removal in t1. However, the 2v5m electrode had the highest overall removal at 99.9%, with the DC3 electrode showing 99.8% removal at the end of the experiment (t5). Between the two voltages of electrodeposition, -0.2 V electrodes showed better degradation overall of ACT than the electrodes of -0.4 V.

It was observed from the results of all 15 electrodes that the electrode of the maximum thickness in each group, namely -0.2 V and 15 minutes, -0.4 V and 15 minutes, and dip-coating with 4 layers, resulted in the least amount of degradation of ACT, as was shown in Table 2. The reason for degradation performance of ACT reducing with increasing thickness could be due to reduced hole production with too thick layers, which can reduce photocatalytic activity (Zhao et al., 2021). It can be inferred from the profilometry results that the electrodes with the best performance of ACT degradation, namely by the three electrodes previously mentioned, had values of surface thickness within the range 1.3 µm to 2.8 µm. Thus, it can be understood that there is a certain range of thickness of the $BiVO_4$ thin films, within which the highest degradation of ACT is achieved. A significant result was seen from Figure 36(c), which shows that all the dip-coating electrodes produced high degradation efficiencies of ACT. This can be further explained by the analysis of

the surface morphology of the electrodes produced by dip-coating shown in Figures 29, which showed the presence of an upper layer with open spaces, to reveal an inner layer of varied structure and socket-like sites. This may provide more area for the adsorption of the ACT molecules than the surface of the electrodeposited electrodes, which showed a uniform and constant surface morphology. The ACT may be secured from leaving the position by the upper layer, and hence the attack by radicals and holes is further facilitated, which may lead to degradation of more adsorbed OMP molecules.

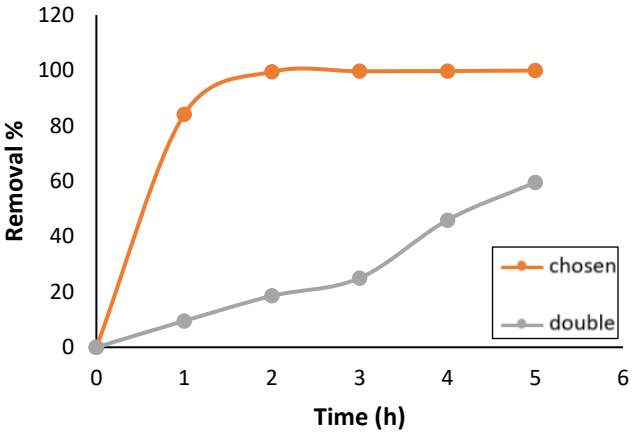

(a)

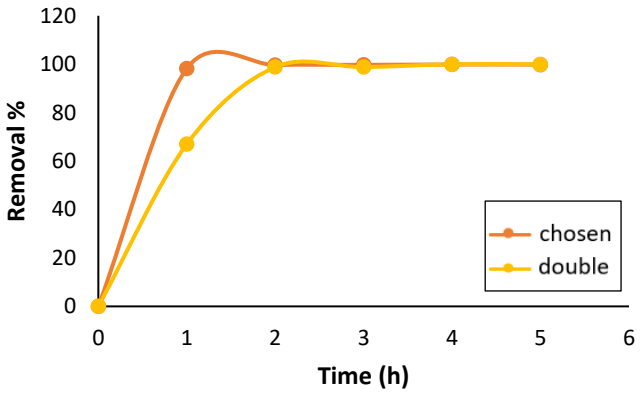

(b)

Figures 39: Results for two PEC experiments of ACT carried out using the (a) 2v5m electrode and (b) DC3 electrode. 'Chosen' and 'Double' represent the removal of ACT during the first and second experiments, respectively.

Out of the three electrodes that lead to the highest degradation of ACT, the 2v5m electrode and the DC3 electrode showed the quickest rates and highest removal percentages of ACT degradation.

Hence, the degradation experiments were carried out in duplicates using these two electrodes, to test the reliability of the results. Repeated experiments conducted under the same conditions using the DC3 electrode was the most consistent with regard to the reaction kinetics, as well as the removal of ACT as shown in Figures 39. Hence, the DC3 electrode was chosen to be used in further experiments involving PEC of OMPs.

5.6. Degradation of Multiple Component System

5.6.1. Photoelectrocatalytic Degradation of Multiple OMPs

After the degradation of ACT by PEC using the DC3 electrode was established, the degradation of multiple OMPs in a system was investigated under the same operational conditions. The OMPs used for this purpose apart from ACT were propranolol (PRO), benzotriazole (BTA), hydrochlorothiazide (HCT), sulfamethoxazole (SFX), trimethoprim (TRI), metoprolol (MTO), sotalol (STO), carbamazepine (CBM), clarithromycin (CLA), and methylbenzotriazole (MBT). The experiment with PEC of 11 OMPs was conducted for a duration of 5 hours, with the initial concentration of OMPs at 45 μg/L. This experiment was conducted in order to study the behavior of degradation of all the OMPs, and mainly to provide an overview of the degradation pattern of the OMPs that were chosen for further experimentation and detailed studies.

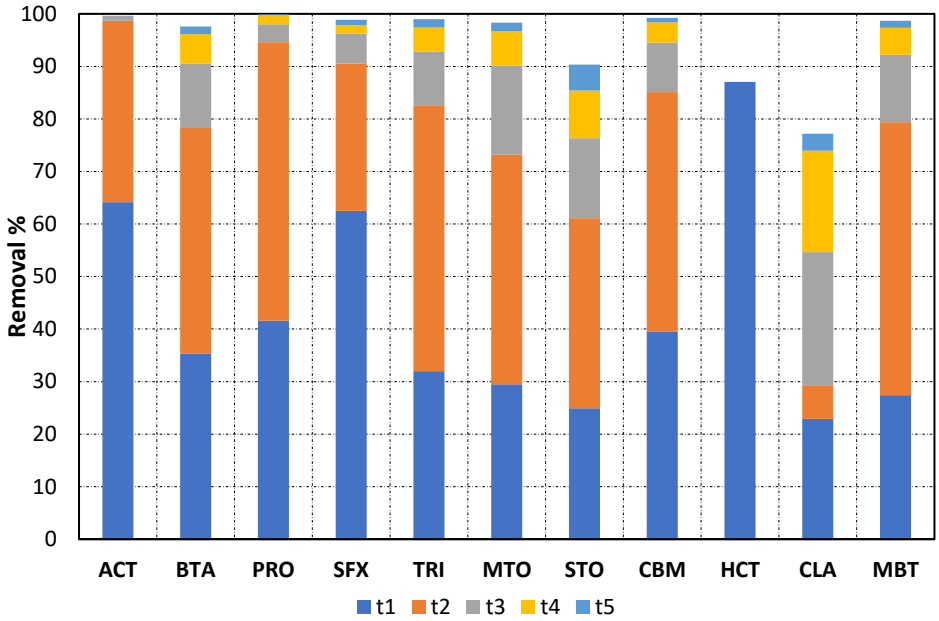

Figure 40: Degradation percentages of 11 OMPs, where t1, t2, t3, t4 and t5 signify the degradation of the OMP after 1,2,3,4 and 5 hours respectively.

From the Figure 40, it was seen that ACT, SFX and HCT had the highest removal within the first hour, at 64%, 62% and 87% respectively. After the second hour, all the OMPs showed the achievement of removal percentages over 70%, except for STO and CLA. It was noted that the OMPs with the highest removal at the end of the experiments were ACT (99.6%), PRO (99.8%), SFX (98.9%), CBM (99.2%), TRI (99%) and MBT (98.7%). Figure 41 shows the results from the photolysis of the OMPs, which was conducted alongside PEC for the same solution. This experiment revealed that SFX and HTA had tendencies to get photodegraded, with removal percentages of 40% and 87%, respectively. From (Willach et al., 2018), it can be seen that SFX has a tendency to degrade under direct illumination. Hence, the results of SFX and HCT degradation from PEC cannot be chiefly attributed to the $BiVO_4$ photoanode, and cannot be used in further experiments of PEC, due to the photolysis taking place. The list of OMPs for further experimentation consists of ACT as the analgesic, BTA as the corrosion inhibitor and PRO as the beta-blocker.

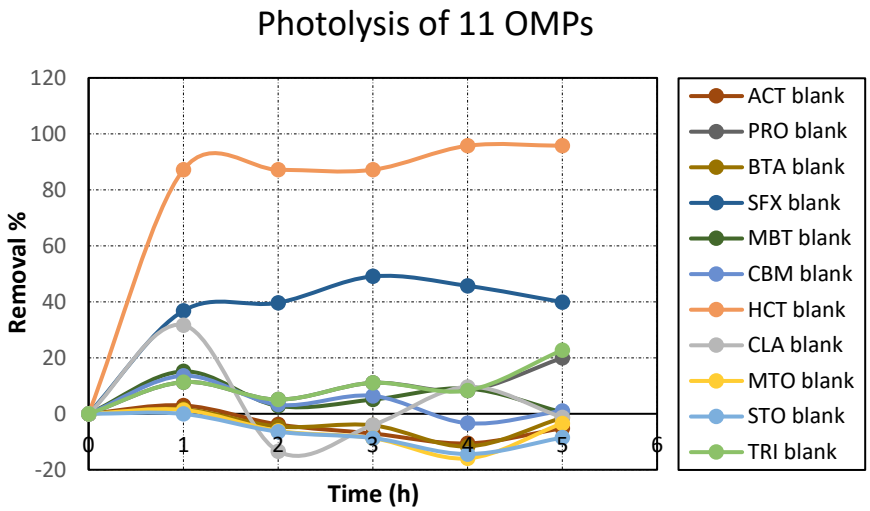

Figure 41: Photolysis experiment with 11 OMPs. The word 'blank' after the names of OMPs in the legend refers to the degradation results of OMPs with time under photolysis

5.6.2. Photoelectrocatalytic Degradation of ACT, PRO and BTA

The photoelectrocatalytic degradation of the three OMPs was carried out for a total duration of 2 hours. The DC3 electrodes were used for this purpose, and three experiments were carried out under the same conditions for studying the degradation of OMPs.

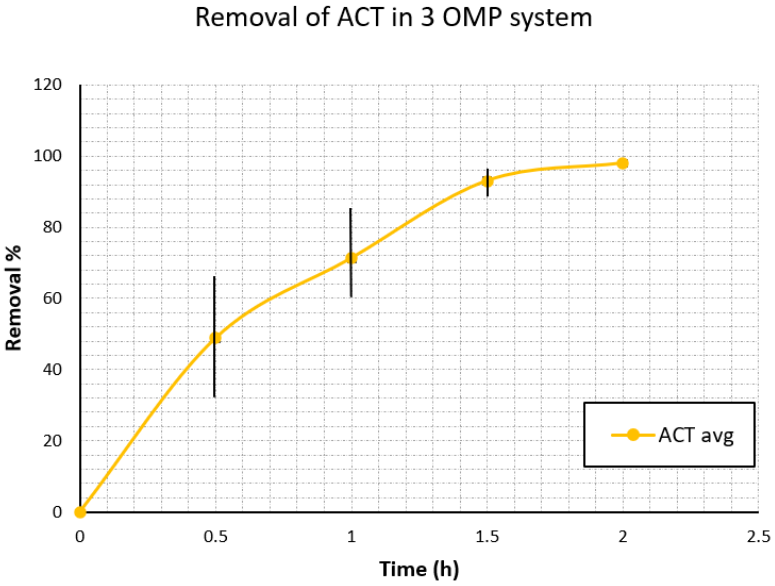

(a)

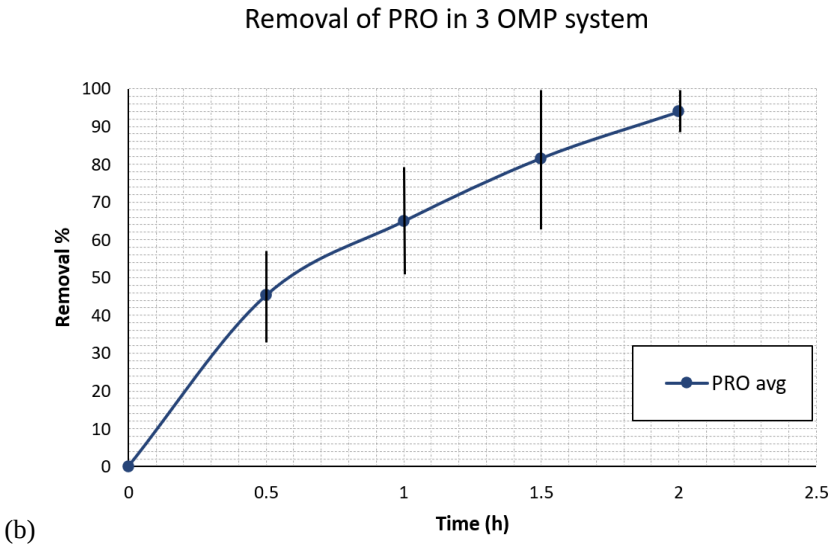

(b)

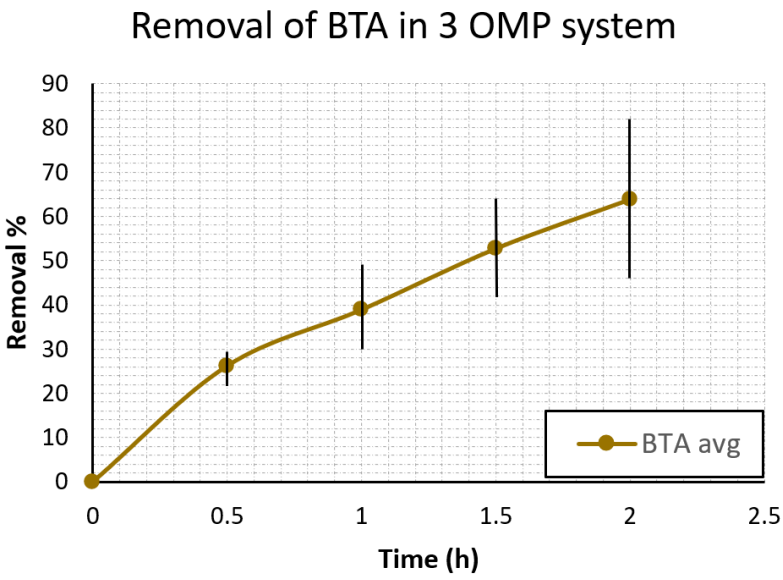

(c)

Figures 42: Results of average degradation from three experiments of three OMPs, namely (a) ACT, (b) PRO and (c) BTA. The vertical black lines indicate the standard deviation errors of the removal percentage at each time interval.

It is seen from the Figures 42 that the average removal percentages of ACT, PRO and BTA over three experiments were 98%, 94% and 64% respectively. On observing the values from all three experiments, the degradation efficiencies of ACT and PRO were both above 85% in all three experiments, and the degradation efficiencies of BTA were roughly 72% and 77% for two of the experiments, and roughly 43% for the other experiment. It can be inferred from these results that

ACT and PRO were degraded more easily, both in terms of a quicker rate, and the removal percentage, in comparison to BTA. This can be further solidified by observing the results from the photolysis of 11 OMPs in Figure 41. The photolysis experiment was conducted over a duration of 5 hours, as opposed to the 2 hours duration of the experiment referred to in Figure 42. The results for the 11 OMPs experiment shown in Figure 40 after 2 hours showed removal of ACT, PRO and BTA to be 98.7%, 94.6% and 78.3% respectively. Thus, the degradation patterns were similar and resembled the results of ACT, PRO and BTA in Figure 42.

Two factors were considered to explain the difference in the behavior of degradation of the three OMPs, namely the variations from usage of different electrodes, and the chemical nature of OMPs. However, in the experiments conducted using the DC3 electrode, the degradation of OMPs showed similar patterns for all the degradation experiments of ACT, namely the experiments with 11 OMPs, as well as those with three OMPs. Therefore, it can be assumed that the usage of different electrodes does not cause the unique pattern of BTA degradation. Thus, it can be hypothesized that the unique chemical properties of each OMP affect their degradation by PEC and the generated radicals and holes. It is known from literature that •OH radicals are unselective in nature and are thermodynamically capable of degrading pollutants that can be oxidized (Siraki et al., 2018). However, it is seen from (Sauter et al., 2021) that the oxidation is preferential, and favors the pathway that is more energetically feasible, with the compound with the weakest bonds. It was derived from literature that the pathway of photocatalytic degradation of ACT by •OH radicals involved the cleavage of the C-N bond, to oxidize the C atom, after which there is further oxidation of the parent compound (Villamena, 2017). Meanwhile, a common pathway of degradation of PRO and other beta-blockers was the cleavage of the C-O bond at the side chain, with an OH group being added to the parent compound (Marothu et al., 2019). It was also reported that the pathway of degradation of BTA was initially by the hydroxylation of the aromatic ring, which involves the cleavage of a C=C bond (Yao and Luan, 2022). The bond enthalpies of the C-N, C-O and C=C bonds are 305, 358 and 614 kJ/mol, respectively (Average Bond Energies(KJ/mol), n.d.). The bond to be cleaved in BTA for hydroxylation requires significantly more energy than the bonds in ACT and PRO, due to which the •OH radicals attack ACT and PRO first. This is concluded to be the reason for the lower degradation efficiency of BTA over 2 hours of degradation, as compared to PRO and ACT. Finally, the results from Figure 40 show that with a longer duration of PEC, BTA

was degraded with an efficiency of over 97%, which reaffirmed that •OH radicals were indeed unselective in nature, and that BTA requires more time for high degradation.

5.6.3. Reusability of Electrode in Photoelectrocatalytic Degradation

The reusability of the $BiVO_4$ photocatalyst, specifically the DC3 electrodes, was tested for the photoelectrocatalytic degradation of OMPs. A used DC3 electrode was mildly rinsed with demineralized water and airdried at room temperature before being reused. The experiment was carried out with the same initial conditions of concentration of the three OMPs and volume of the electrolyte.

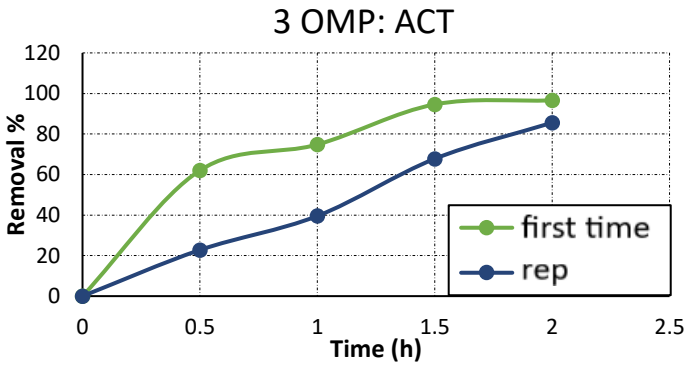

(a)

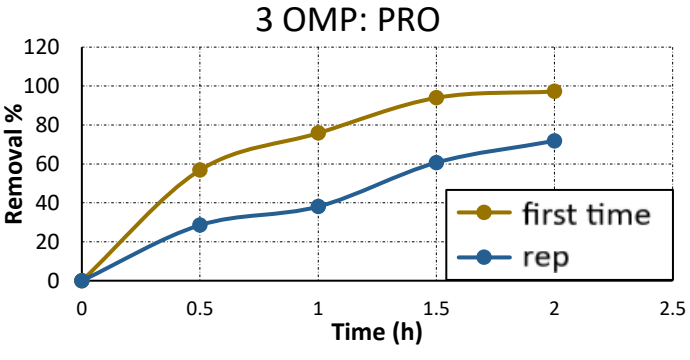

(b)

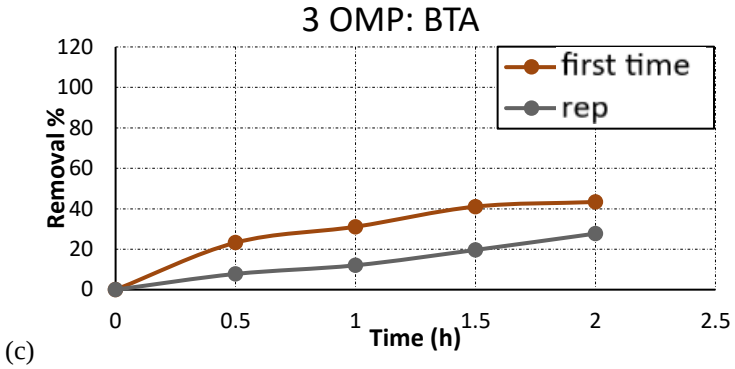

(c)

Figures 43: Results of removal efficiencies from electrode reuse experiment for (a) ACT, (b) PRO and (c) BTA, where 'first time' and 'rep' signify the degradation of an OMP during the first and second experiments respectively with an electrode.

From Figures 43, it was seen that the removal efficiency of ACT was reduced by 11%, from 96.6% to 85.6%. The removal at each 30-minute interval was reduced, and thus the overall efficiency of degradation was reduced. The reduction in degradation was more pronounced in the case of PRO, with a decrease of 25%, from 97% to 72%. With BTA, the final removal after reuse was seen to almost half of the original removal rate, which could also be attributed to its slow degradation. Based on the results, it can therefore be concluded that the $BiVO_4$ electrodes can be reused for the degradation of ACT. A longer duration of photoelectrocatalytic degradation experiments achieved higher removal of OMPs, as depicted for the removal of BTA in the PEC of 11 OMPs shown in Figure 40.

5.7. Scavenger Studies

The photoelectrocatalytic degradation of the OMPs is chiefly attributed to the production of three main ROS, namely •OH radicals, $O_2^{\bullet -}$ radicals and the positively charged holes. The scavenger studies involved the addition of certain reagents called scavengers to the solution, which quench the ROS responsible for the degradation, thereby inhibiting the action of ROS in degrading the OMPs. The results of three separate experiments, with the addition of EDTA, methanol and para-benzoquinone, to quench the holes, radicals and conduction band electrons, respectively, were

studied, to verify that the ROS are indeed responsible in the photoelectrocatalytic removal of OMPs.

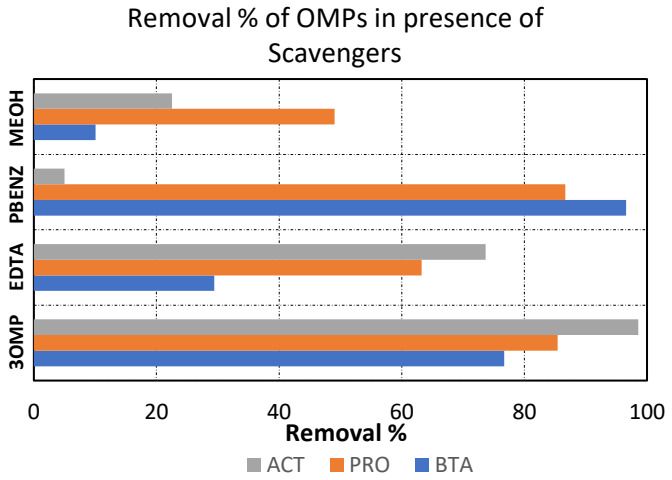

Figure 44: Removal percentage of three OMPs in presence and absence of Scavengers. The scavengers EDTA, para-benzoquinone and methanol are denoted by EDTA, PBENZ and MEOH respectively. 3OMP refers to the degradation of the OMP in the absence of scavengers.

The information regarding how each scavenger affected the degradation of each OMP, can be obtained from the Figures 44 and 45. For ACT, the removal was reduced to 74% on addition of EDTA, and the rate of degradation was reduced by a small amount. However, on addition of para-benzoquinone, the removal of ACT was reduced rapidly to 5%, and the addition of Methanol reduced the degradation of ACT to 22.5%. Hence, it can be concluded that the degradation of ACT takes place chiefly due to the •OH radicals, and the O_2•$^-$ radicals. In the case of PRO, the addition of EDTA and methanol reduced the degradation rate, and the removal was decreased to 63% and 49% respectively. With the addition of para-benzoquinone, a slight increase in removal of PRO was noticed, to a value of 87% from the original 86%. However, there was an unexpected significant increase in the rate of degradation of PRO, mainly in the first 30 minutes of degradation. Thus, it can be concluded that PRO is degraded chiefly by the attack of •OH radicals, and holes play a smaller role. In BTA, the addition of methanol and EDTA bring about a significant reduction in removal, namely 10% and 29% respectively, and thus it can be confirmed that •OH radicals and holes play the major roles in the degradation of BTA. However, it was noticed that the addition of

para-benzoquinone showed a rapid increase in the removal of BTA from 76.6% to 96.6%, with a clear increase in rate of degradation.

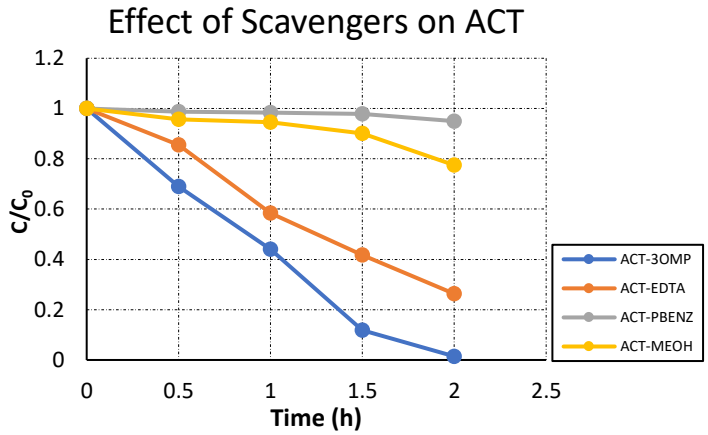

(a)

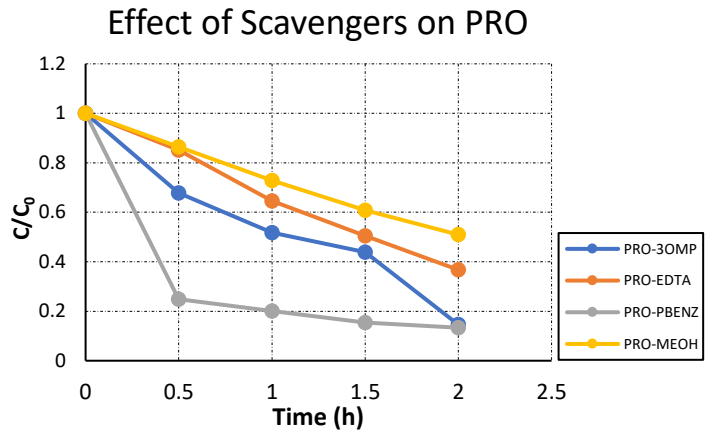

(b)

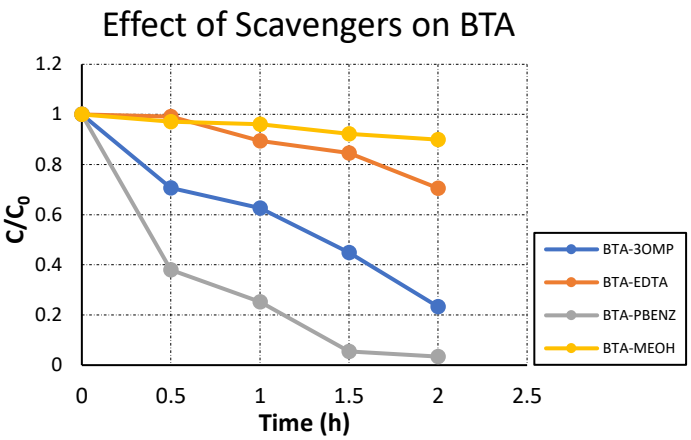

(c)

Figure 45: Effect of scavengers on degradation rates of (a) ACT, (b) PRO and (c) BTA. The scavengers EDTA, para-benzoquinone and methanol are denoted by EDTA, PBENZ and MEOH respectively. 3OMP refers to the degradation of the OMP in the absence of scavengers

It can be understood by the results of OMP degradation under the scavenging by adding methanol, that •OH radicals play a vital role in the degradation of all the OMPs. Once again, the unselective nature of the •OH radicals in the oxidation of OMPs is reaffirmed by these results. An unexpected observation was that the addition of para-benzoquinone had a reverse effect on BTA and PRO, where the overall degradation of BTA rapidly increased. An increased rate of degradation was also observed in PRO in this experiment. It is reported that the addition of para-benzoquinone not only captures the electrons, but it also produces •OH radicals and holes in secondary reactions (Schneider et al., 2020). It is possible for photoreduction of quinones to take place in solutions under illumination (Schneider et al., 2020), and hence the para-benzoquinone is reduced to form •OH radicals. Another side reaction is assumed to take place that involves the formation of semiquinone radicals by the trapping of conduction band electrons, thereby preventing the electron – hole recombination and leaving the vacant holes available for oxidizing the OMPs. These reactions are depicted in Equations 11 and 12.

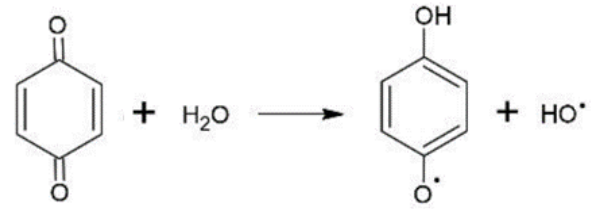

(11)

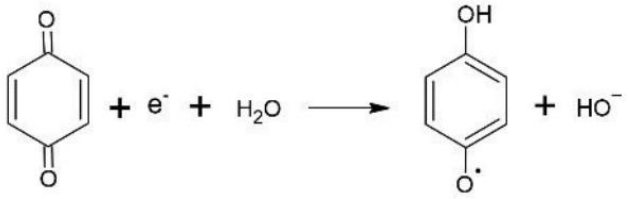

(12)

Hence, it can be concluded during the scavenging process using para-benzoquinone, the •OH radical significantly increases the degradation of BTA and PRO. This is backed by the results from Figures 45 with scavenging by methanol, thus showing that •OH radicals played the most important role in degradation of BTA and PRO. It was also seen that holes played a smaller role in the degradation of these two OMPs, and hence this further improved the degradation of BTA and PRO. The increase in BTA degradation with scavenging by para-benzoquinone also agrees with the decrease in BTA degradation with holes scavenging by EDTA, since it implies that the vacant holes from para-benzoquinone addition also improved BTA degradation. The increase in removal of BTA was higher than that of PRO. It is also concluded that the effect of $O_2^{\bullet -}$ radical quenching on ACT dominates the effect of the simultaneous production of •OH radicals on ACT. This is solidified by the results of the quenching experiments of ACT under scavenging by para-benzoquinone and methanol, with 5% and 22% removal respectively.

A higher removal of PRO was observed under both EDTA and Methanol scavenging, than BTA, and PRO showed the highest removal percentages out of all three OMPs under Methanol scavenging, despite •OH radicals being responsible in the degradation of all three OMPs. The cause of this behavior can be explained by the results of photolysis from Figure 41, as well as the PC experiment of three OMPs, shown in Figure 45. Removal percentages of PRO under direct illumination were found to be 20% and 16% in the photolysis experiments with 11 OMPs, and three OMPs, respectively. Thus, it can be concluded that photolysis also plays a minor role in the degradation of PRO, which explains the higher removal percentages.

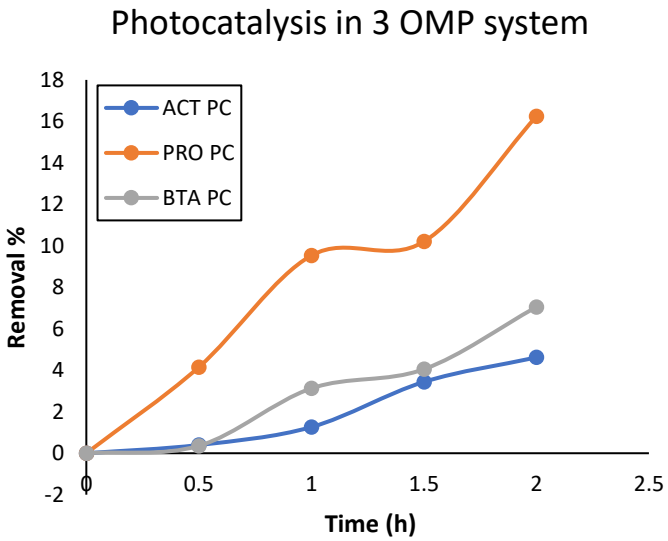

Figure 45: Photocatalysis of three OMPs, namely ACT, PRO and BTA, denoted by ACT PC, PRO PC and BTA PC respectively.

5.8. Photoelectrocatalytic degradation of OMPs in SWTE

The final step of the experimentation was to test PEC for the degradation of OMPs in real SWTE. The SWTE used in this experiment was obtained from WWTP Horstermeer, and its characteristics are described in Table 5. The SWTE was filtered using a 0.45 µm membrane disc filter (X100 Supor, 0.45 µm, 47 mm) to remove the bigger solid particles.

Table 5: SWTE (WWTP Horstermeer) Characteristics

Characteristics	Unit	Values
pH	-	8.03
EC	µS/cm	499
COD	mg/L	26.9±1.4
Ca^{2+}	mg/L	0.27±0.004
Mg^{2+}	mg/L	0.064±0.007
NO_3^-	mg/L	2.535±0.06
SO_4^{2-}	mg/L	24.05±0.5
PO_4^{3-}	mg/L	0

The OMPs studied for degradation are acetaminophen, sulfamethoxazole, sulfadimethoxine, trimethoprim, propranolol, metoprolol, sotalol, ketoprofen, hydrochlorothiazide, clofibric acid, clarithromycin, carbamazepine, benzotriazole, methylbenzotriazole, caffeine, gabapentin, theophylline and metformin. The concentrations of the OMPs were spiked to 15 μg/L, which was decided to be just enough to facilitate the studying of the degradation of OMPs in SWTE, without using a higher concentration such as 45 μg/L that may stray away further from the real conditions of SWTE. The results of the degradation of OMPs in the SWTE are listed in Table 6, for an experiment with a duration of 2 hours. Apart from ketoprofen and hydrochlorothiazide, which showed removal of 98.9% and 71% respectively, the OMPs showed a low removal efficiency, not surpassing 40%. It was noted from the photolysis experiment of 11 OMPs from Figure 40, that hydrochlorothiazide was degraded under direct illumination, which explains its high removal percentage. It is seen in literature that ketoprofen was rapidly degraded under solar radiation in different types of waters (Matamoros et al., 2009), and this can explain the excellent degradation of ketoprofen shown in Table 6.

Table 6: Removal performance of OMPs in SWTE using PEC with $BiVO_4$ electrode

OMP	**Removal %**	**Removal Range**
Ketoprofen	98.9	**Above 70%**
Hydrochlorothiazide	70.9	
Propranolol	36.9	**Between 20% and 40%**
Acetaminophen	36.1	
Clarithromycin	28.3	
Sulfamethoxazole	27.3	
Theophylline	22.3	
Sotalol	18	**Below 20%**
Metoprolol	15.7	
Trimethoprim	13.6	
Sulfadimethoxine	10.5	
Metformin	9	
Caffeine	8.9	
Clofibric Acid	5.5	
Methylbenzotriazole	5.2	
Benzotriazole	3.9	
Gabapentin	3.2	
Carbamazepine	0.8	

It has been established by (de Boer et al., 2022) that one of the disadvantages of heterogenous PC is the low mass transfer kinetics between the photocatalyst and the bulk solution, which leads to low removal rates. Since the concentration of the OMPs was very low at 15 µg/L, this may have affected the diffusion of OMPs and thus the reaction rate of degradation. It is also seen from Table 5 that COD and inorganic ions were present in the SWTE. The presence of organic matter like COD is seen to interfere with OMP removal during tertiary treatment methods such as ozonation (van Gijn et al., 2021). Thus, it can be assumed that COD presence has an impact on the PEC process too. It is also established that inorganic ions affect the degradation of organics by quenching the reactive oxidative species (Hu et al., 2003), which could be another explanation for the reduced degradation. Finally, natural organic matter (NOM) may be present in the SWTE, and since it is studied that NOM interacts with the photocatalyst surface (Ye et al., 2019), its presence may be harmful to OMP degradation.

CHAPTER 6: CONCLUSION

This research aimed to test PEC as a combined technique of PC with electrochemistry, using the $BiVO_4$ electrode with a low band gap of 2.4 eV, for its application in OMP removal. The $BiVO_4$ electrodes were fabricated using two techniques, namely dip-coating and electrodeposition. All the electrodes were characterized using analytical techniques to provide an understanding of their structural, optical and optoelectronic properties. The results indicated that all electrodes had the monoclinic scheelite crystal structure, which was desired for optimum optoelectronic performance. The electrodes by electrodeposition had a more uniform surface morphology, and a higher average quantum efficiency at 14%, than those by dip-coating. The electrochemical characterization of the $BiVO_4$ electrodes, as well as the PC and PEC of phenol, showed the proof that applying an external bias in PEC leads a better efficiency of degradation than PC.

Overall, the process of PEC using $BiVO_4$ electrodes accomplished success in the degradation of ACT in an aqueous solution, with 11 out of 15 electrodes showing over 90% removal of ACT in 5 hours. The degradation of ACT was seen to be dependent on the mode of electrode fabrication, electrode surface structure and the film thickness. It was hypothesized that the electrodes produced by the electrodeposition method would have thin films with smaller and uniform particles, which would allow higher light absorption, and thus higher quantum efficiency, and also a higher surface area. However, in an unexpected turn of events, the electrodes produced by dip-coating, especially the DC3 electrode, showed better overall performance in the degradation of ACT than the electrodes produced by electrodeposition, all showing over 99.5% removal of ACT in 5 hours. This result is due to the surface morphology of the electrodes produced by dip-coating, which consists of a surface structure that has a high adsorption surface area, with the upper layer securing the adsorbed OMP molecules in place to be attacked by ROS.

Finally, this research tested the possibility of application of PEC in solutions of multiple OMPs, including the SWTE. The process of PEC using $BiVO_4$ electrodes was overall successful in the degradation of ACT, PRO and BTA in synthetic solutions. However, the degradation of BTA was found to be slower than the other OMPs, due to its chemical structure. The scavenging experiments provided an insight into the degradation mechanism of each OMP, and affirmed the contribution of •OH radicals in OMP degradation. However, the PEC of the real SWTE was not efficient in

removing most of the OMPs due to the presence of other contaminants such as NOM and inorganic ions that interfere in the degradation of the OMPs.

CHAPTER 7: RECOMMENDATIONS

Although the $BiVO_4$ electrodes produced by dip-coating and electrodeposition showed a variation of average to excellent performance in OMP degradation, there are methods of fabrication that are more facile and have proven to produce superior thin films and effective degradation results, such as the hydrothermal method. Hence, it would be recommended to fabricate electrodes with this method, for enhanced quantum efficiency and surface area relative to those of dip-coating and electrodeposition.

It was seen in this research that the surface of the $BiVO_4$ thin films produced by dip-coating consisted of a microstructure that led to high degradation efficiency of the OMPs. Thus, it would be beneficial to take this research forward by fabricating the $BiVO_4$ electrodes with a complex varied nanostructure, such as stacked nanoplates or nanospheres, which were shown in the literature review section to have excellent performance in the degradation of organic pollutants. Another recommendation for the future is to measure the RMS roughness of the electrode using Atomic Force Microscopy (AFM), and correlate that with the surface morphology and thickness of that electrode, to further the knowledge on the adsorption and degradation of OMP molecules.

Although the photoelectrocatalytic degradation of OMPs was carried out with successful results, the degradation pathway and thus the degradation products were not studied as part of this thesis. Since it is desired to apply the technology of PEC to allow water reuse, another recommendation would be to conduct a qualitative and quantitative analysis of the degradation products of the chosen OMPs and evaluate their toxicity, to decide if water reuse is possible.

This research also involved the addition of scavenging agents to identify the dominant species responsible in the degradation of each OMP out of ACT, PRO and BTA. A stronger explanation could be provided by also using the Electron Spin Resonance (ESR) Spectroscopy, which facilitates the study of materials having unpaired electrons, and hence could serve as a powerful tool in studying the behavior of radicals in the future of photocatalytic research.

Finally, given that the presence of other contaminants like NOM and inorganic ions in the SWTE that interfered with the photoelectrocatalytic degradation of the OMPs, it is advised to read further into the mechanisms that interfere with the degradation of OMPs in the SWTE, and to optimize the process accordingly to mitigate these mechanisms.

REFERENCES

Anjum, N. A., Gill, S. S., & Tuteja, N. (Eds.). (2017). Enhancing cleanup of environmental pollutants. Springer International Publishing. https://doi.org/10.1007/978-3-319-55426-6

Ashton, D., Hilton, M., & Thomas, K. V. (2004). Investigating the environmental transport of human pharmaceuticals to streams in the United Kingdom. Science of The Total Environment, 333(1–3), 167–184. https://doi.org/10.1016/j.scitotenv.2004.04.062

Atchudan, R., Edison, T. N. J. I., Perumal, S., Karthik, N., Karthikeyan, D., Shanmugam, M., & Lee, Y. R. (2018). Concurrent synthesis of nitrogen-doped carbon dots for cell imaging and ZnO@nitrogen-doped carbon sheets for photocatalytic degradation of methylene blue. Journal of Photochemistry and Photobiology A: Chemistry, 350, 75–85. https://doi.org/10.1016/j.jphotochem.2017.09.038

Average bond energies(Kj/mol). (n.d.). Retrieved May 11, 2022, from http://butane.chem.uiuc.edu/cyerkes/Chem104ACSpring2009/Genchemref/bondenergies.html

Bacha, A.-U.-R., Cheng, H., Han, J., Nabi, I., Li, K., Wang, T., Yang, Y., Ajmal, S., Liu, Y., & Zhang, L. (2019). Significantly accelerated PEC degradation of organic pollutant with addition of sulfite and mechanism study. Applied Catalysis B: Environmental, 248, 441–449. https://doi.org/10.1016/j.apcatb.2019.02.049

Bakhtiarnia, S., Sheibani, S., Billard, A., Sun, H., Aubry, E., & Yazdi, M. A. P. (2021). Enhanced photocatalytic activity of sputter-deposited nanoporous BiVO4 thin films by controlling film thickness. Journal of Alloys and Compounds, 879, 160463. https://doi.org/10.1016/j.jallcom.2021.160463

Basics to powder X-ray diffraction: How to achieve high-quality XRD patterns - Q&A - Materials Talks. (2020, May 14). https://www.materials-talks.com/basics-to-powder-x-ray-diffraction-how-to-achieve-high-quality-xrd-patterns-qa/

Bennani, Y. (2017). Photoelectrocatalysis in water treatment [Delft University of Technology]. https://doi.org/10.4233/UUID:5BF8B3C7-D069-4C64-90FD-3B2A5889F95D

Bennani, Y., Perez-Rodriguez, P., Alani, M. J., Smith, W. A., Rietveld, L. C., Zeman, M., & Smets, A. H. M. (2016). Photoelectrocatalytic oxidation of phenol for water treatment using a BiVO 4 thin-film photoanode. Journal of Materials Research, 31(17), 2627–2639. https://doi.org/10.1557/jmr.2016.290

Bordbar, M., Sharifi-Zarchi, Z., & Khodadadi, B. (2017). Green synthesis of copper oxide nanoparticles/clinoptilolite using Rheum palmatum L. root extract: High catalytic activity for reduction of 4-nitro phenol, rhodamine B, and methylene blue. Journal of Sol-Gel Science and Technology, 81(3), 724–733. https://doi.org/10.1007/s10971-016-4239-1

Cai, H., Cheng, L., Xu, F., Wang, H., Xu, W., & Li, F. (2018). Fabrication of the heterojunction catalyst BiVO 4 /P25 and its visible-light photocatalytic activities. Royal Society Open Science, 5(8), 180752. https://doi.org/10.1098/rsos.180752

Cattarin, S., & Decker, F. (2009). Electrodes | semiconductor electrodes. In Encyclopedia of Electrochemical Power Sources (pp. 121–133). Elsevier. https://doi.org/10.1016/B978-044452745-5.00031-9

Chatchai, P., Nosaka, A. Y., & Nosaka, Y. (2013). Photoelectrocatalytic performance of WO3/BiVO4 toward the dye degradation. Electrochimica Acta, 94, 314–319. https://doi.org/10.1016/j.electacta.2013.01.152

Chemistry LibreTexts: Uv-visible spectroscopy. (2016, July 13). https://chem.libretexts.org/Bookshelves/Analytical_Chemistry/Physical_Methods_in_Chemistry_and_Nano_Science_(Barron)/04%3A_Chemical_Speciation/4.04%3A_UV-Visible_Spectroscopy

Chemyx Inc.: Basic principles of hplc, ms & lc-ms. (2017, November 8). https://www.chemyx.com/support/knowledge-base/application-reference-by-topic/basic-principles-hplc-ms-lc-ms/

Chen, R., Zhu, C., Lu, J., Xiao, J., Lei, Y., & Yu, Z. (2018). BiVO4/α-Fe2O3 catalytic degradation of gaseous benzene: Preparation, characterization and photocatalytic properties. Applied Surface Science, 427, 141–147. https://doi.org/10.1016/j.apsusc.2017.08.153

Clinicalkey. (n.d.). Retrieved May 11, 2022, from https://www.clinicalkey.com/#!/content/book/3-s2.0-B9780323401159000062

Clinobisvanite mineral data. (n.d.). Retrieved May 11, 2022, from http://webmineral.com/data/Clinobisvanite.shtml#.YnuaYehBw2w

Cristino, V., Pasti, L., Marchetti, N., Berardi, S., Bignozzi, C. A., Molinari, A., Passabi, F., Caramori, S., Amidani, L., Orlandi, M., Bazzanella, N., Piccioni, A., Kopula Kesavan, J., Boscherini, F., & Pasquini, L. (2019). Photoelectrocatalytic degradation of emerging contaminants at WO 3 /BiVO 4 photoanodes in aqueous solution. Photochemical & Photobiological Sciences, 18(9), 2150–2163. https://doi.org/10.1039/C9PP00043G

da Silva, M. R., Scalvi, L. V. A., Neto, V. S. L., & Dall'Antonia, L. H. (2015). Dip-coating deposition of BiVO4/NiO p–n heterojunction thin film and efficiency for methylene blue degradation. Journal of Materials Science: Materials in Electronics, 26(10), 7705–7714. https://doi.org/10.1007/s10854-015-3412-6

da Silva, M. R., Scalvi, L. V. A., Neto, V. S. L., & Dall'Antonia, L. H. (2016). Dip-coating deposition of resistive BiVO4 thin film and evaluation of their photoelectrochemical parameters

under distinct sources illumination. Journal of Solid State Electrochemistry, 20(6), 1527–1538. https://doi.org/10.1007/s10008-016-3166-y

Danish, M. S. S., Bhattacharya, A., Stepanova, D., Mikhaylov, A., Grilli, M. L., Khosravy, M., & Senjyu, T. (2020a). A systematic review of metal oxide applications for energy and environmental sustainability. Metals, 10(12), 1604. https://doi.org/10.3390/met10121604

Danish, M. S. S., Bhattacharya, A., Stepanova, D., Mikhaylov, A., Grilli, M. L., Khosravy, M., & Senjyu, T. (2020b). A systematic review of metal oxide applications for energy and environmental sustainability. Metals, 10(12), 1604. https://doi.org/10.3390/met10121604

de Boer, S., González-Rodríguez, J., Conde, J. J., & Moreira, M. T. (2022). Benchmarking tertiary water treatments for the removal of micropollutants and pathogens based on operational and sustainability criteria. Journal of Water Process Engineering, 46, 102587. https://doi.org/10.1016/j.jwpe.2022.102587

Deng, Y., & Zhao, R. (2015). Advanced oxidation processes (Aops) in wastewater treatment. Current Pollution Reports, 1(3), 167–176. https://doi.org/10.1007/s40726-015-0015-z

Deshpande, N. G., Ahn, C. H., Koli, R. R., Jamadar, A. S., Kim, D. S., Kim, Y. B., Jung, S. H., & Cho, H. K. (2020). Controlled nanostructured morphology of BiVO4 photoanodes for efficient on-demand catalysis in solar water-splitting and sustainable water-treatment. Applied Surface Science, 514, 146075. https://doi.org/10.1016/j.apsusc.2020.146075

Dong, P., Hou, G., Xi, X., Shao, R., & Dong, F. (2017). WO 3 -based photocatalysts: Morphology control, activity enhancement and multifunctional applications. Environmental Science: Nano, 4(3), 539–557. https://doi.org/10.1039/C6EN00478D

Edebali, S., Oztekin, Y., & Arslan, G. (2018). Metallic engineered nanomaterial for industrial use. In Handbook of Nanomaterials for Industrial Applications (pp. 67–73). Elsevier. https://doi.org/10.1016/B978-0-12-813351-4.00004-3

Egerton, T. A., Christensen, P. A., Kosa, S. A. M., Onoka, B., Harper, J. C., & Tinlin, J. R. (2006). Photoelectrocatalysis by titanium dioxide for water treatment. International Journal of Environment and Pollution, 27(1/2/3), 2. https://doi.org/10.1504/IJEP.2006.010450

Fujishima, A., & Honda, K. (1972). Electrochemical photolysis of water at a semiconductor electrode. Nature, 238(5358), 37–38. https://doi.org/10.1038/238037a0

Garcia-Segura, S., & Brillas, E. (2017). Applied photoelectrocatalysis on the degradation of organic pollutants in wastewaters. Journal of Photochemistry and Photobiology C: Photochemistry Reviews, 31, 1–35. https://doi.org/10.1016/j.jphotochemrev.2017.01.005

Geissen, V., Mol, H., Klumpp, E., Umlauf, G., Nadal, M., van der Ploeg, M., van de Zee, S. E. A. T. M., & Ritsema, C. J. (2015). Emerging pollutants in the environment: A challenge for

water resource management. International Soil and Water Conservation Research, 3(1), 57–65. https://doi.org/10.1016/j.iswcr.2015.03.002

Gotić, M., Musić, S., Ivanda, M., Šoufek, M., & Popović, S. (2005). Synthesis and characterisation of bismuth(Iii) vanadate. Journal of Molecular Structure, 744–747, 535–540. https://doi.org/10.1016/j.molstruc.2004.10.075

Hernández, S., Thalluri, S. M., Sacco, A., Bensaid, S., Saracco, G., & Russo, N. (2015). Photo-catalytic activity of BiVO4 thin-film electrodes for solar-driven water splitting. Applied Catalysis A: General, 504, 266–271. https://doi.org/10.1016/j.apcata.2015.01.019

Hu, C., Yu, J. C., Hao, Z., & Wong, P. K. (2003). Effects of acidity and inorganic ions on the photocatalytic degradation of different azo dyes. Applied Catalysis B: Environmental, 46(1), 35–47. https://doi.org/10.1016/S0926-3373(03)00139-5

Huang, C.-K., Wu, T., Huang, C.-W., Lai, C.-Y., Wu, M.-Y., & Lin, Y.-W. (2017). Enhanced photocatalytic performance of BiVO 4 in aqueous AgNO 3 solution under visible light irradiation. Applied Surface Science, 399, 10–19. https://doi.org/10.1016/j.apsusc.2016.12.038

Hummel, T. J. : Student solutions guide [to accompany] chemistry, ninth edition steven s. Zumdahl, susan arena zumdahl (9th ed). Brooks/Cole Gengage Learning.(2014).

Jafar, A. & Al-Amarah, K. & Lafta, F. & Fayyadh, I. (2013). Fabrication and Characterization of Fluorine-Doped Tin Oxide Transparent Conductive Nano-Films. 20107-20111

Joseph, J. A., Nair, S. B., John, K. A., Babu, S., Shaji, S., Shinoj, V. K., & Philip, R. R. (2020). Aluminium doping in iron oxide nanoporous structures to tailor material properties for photocatalytic applications. Journal of Applied Electrochemistry, 50(1), 81–92. https://doi.org/10.1007/s10800-019-01371-6

Kamble, G. S., & Ling, Y.-C. (2020). Solvothermal synthesis of facet-dependent BiVO4 photocatalyst with enhanced visible-light-driven photocatalytic degradation of organic pollutant: Assessment of toxicity by zebrafish embryo. Scientific Reports, 10(1), 12993. https://doi.org/10.1038/s41598-020-69706-4

Khan, S. B., Hou, M., Shuang, S., & Zhang, Z. (2017). Morphological influence of TiO 2 nanostructures (Nanozigzag, nanohelics and nanorod) on photocatalytic degradation of organic dyes. Applied Surface Science, 400, 184–193. https://doi.org/10.1016/j.apsusc.2016.12.172

Khanzada, N. K., Farid, M. U., Kharraz, J. A., Choi, J., Tang, C. Y., Nghiem, L. D., Jang, A., & An, A. K. (2020). Removal of organic micropollutants using advanced membrane-based water and wastewater treatment: A review. Journal of Membrane Science, 598, 117672. https://doi.org/10.1016/j.memsci.2019.117672

Kiama, N. (2018). Improvement the bivo4 photoanode fabricated for water oxidation by electrodeposition technique. International Journal of GEOMATE, 14(46). https://doi.org/10.21660/2018.46.7317

Kumar, S., Thakur, P., & Kumar, V. (2019). Kinetics and thermodynamic studies for removal of methylene blue dye by biosynthesize copper oxide nanoparticles and its antibacterial activity. Journal of Environmental Health Science and Engineering, 17(1), 367–376. https://doi.org/10.1007/s40201-019-00354-1

Li, F., Kang, Y., Chen, M., Liu, G., Lv, W., Yao, K., Chen, P., & Huang, H. (2016). Photocatalytic degradation and removal mechanism of ibuprofen via monoclinic BiVO4 under simulated solar light. Chemosphere, 150, 139–144. https://doi.org/10.1016/j.chemosphere.2016.02.045

Li, H., Su, Z., Hu, S., & Yan, Y. (2017). Free-standing and flexible Cu/Cu2O/CuO heterojunction net: A novel material as cost-effective and easily recycled visible-light photocatalyst. Applied Catalysis B: Environmental, 207, 134–142. https://doi.org/10.1016/j.apcatb.2017.02.013

Lopes, O. F., Carvalho, K. T. G., Macedo, G. K., de Mendonça, V. R., Avansi, W., & Ribeiro, C. (2015). Synthesis of BiVO 4 via oxidant peroxo-method: Insights into the photocatalytic performance and degradation mechanism of pollutants. New Journal of Chemistry, 39(8), 6231–6237. https://doi.org/10.1039/C5NJ00984G

Malathi, A., Ashokkumar, M., & Arunachalam, P. (2018). A review on BiVO 4 photocatalyst: Activity enhancement methods for solar photocatalytic applications. Applied Catalysis A: General, 555, 47–74. https://doi.org/10.1016/j.apcata.2018.02.010

Marothu, V. K., Gorrepati, M., Idris, N. F., Idris, S. A. M., & Lella, R. K. C. (2019). Photocatalysis of β-blockers – An overview. Arabian Journal of Chemistry, 12(7), 1290–1297. https://doi.org/10.1016/j.arabjc.2014.10.044

Martín-Rilo, S., Coimbra, R., Escapa, C., & Otero, M. (2018). Treatment of dairy wastewater by oxygen injection: Occurrence and removal efficiency of a benzotriazole based anticorrosive. Water, 10(2), 155. https://doi.org/10.3390/w10020155

Matamoros, V., Duhec, A., Albaigés, J., & Bayona, J. M. (2009). Photodegradation of carbamazepine, ibuprofen, ketoprofen and 17α-ethinylestradiol in fresh and seawater. Water, Air, and Soil Pollution, 196(1–4), 161–168. https://doi.org/10.1007/s11270-008-9765-1

Maurer, M., Escher, B., Richle, P., Schaffner, C., & Alder, A. (2007). Elimination of β-blockers in sewage treatment plants. Water Research, 41(7), 1614–1622. https://doi.org/10.1016/j.watres.2007.01.004

McDonald, K. J., & Choi, K.-S. (2012). A new electrochemical synthesis route for a BiOI electrode and its conversion to a highly efficient porous BiVO4 photoanode for solar water oxidation. Energy & Environmental Science, 5(9), 8553. https://doi.org/10.1039/c2ee22608a

Mohamed, N. A., Arzaee, N. A., Mohamad Noh, M. F., Ismail, A. F., Safaei, J., Sagu, J. S., Johan, M. R., & Mat Teridi, M. A. (2021). Electrodeposition of BiVO4 with needle-like flower architecture for high performance photoelectrochemical splitting of water. Ceramics International, 47(17), 24227–24239. https://doi.org/10.1016/j.ceramint.2021.05.134

Mou, H., Song, C., Zhou, Y., Zhang, B., & Wang, D. (2018). Design and synthesis of porous Ag/ZnO nanosheets assemblies as super photocatalysts for enhanced visible-light degradation of 4-nitrophenol and hydrogen evolution. Applied Catalysis B: Environmental, 221, 565–573. https://doi.org/10.1016/j.apcatb.2017.09.061

Nunes, D. (2019). Metal oxide nanostructures: Synthesis, properties, and applications /.

Optical materials. (2021). Elsevier. https://doi.org/10.1016/C2018-0-04435-7

Orimolade, B. O., & Arotiba, O. A. (2020a). Bismuth vanadate in photoelectrocatalytic water treatment systems for the degradation of organics: A review on recent trends. Journal of Electroanalytical Chemistry, 878, 114724. https://doi.org/10.1016/j.jelechem.2020.114724

Orimolade, B. O., & Arotiba, O. A. (2020b). Towards visible light driven photoelectrocatalysis for water treatment: Application of a FTO/BiVO4/Ag2S heterojunction anode for the removal of emerging pharmaceutical pollutants. Scientific Reports, 10(1), 5348. https://doi.org/10.1038/s41598-020-62425-w

Orimolade, B. O., & Arotiba, O. A. (2022). Enhanced photoelectrocatalytic degradation of diclofenac sodium using a system of Ag-BiVO4/BiOI anode and Ag-BiOI cathode. Scientific Reports, 12(1), 4214. https://doi.org/10.1038/s41598-022-08213-0

Park, Y., McDonald, K. J., & Choi, K.-S. (2013). Progress in bismuth Vdate photoanodes for use in solar water oxidation. Chem. Soc. Rev., 42(6), 2321–2337. https://doi.org/10.1039/C2CS35260E

Peleyeju, M. G., & Arotiba, O. A. (2018). Recent trend in visible-light photoelectrocatalytic systems for degradation of organic contaminants in water/wastewater. Environmental Science: Water Research & Technology, 4(10), 1389–1411. https://doi.org/10.1039/C8EW00276B

Rahman, M. A. (2014). A review on semiconductors including applications and temperature effects in semiconductors. American Academic Scientific Research Journal for Engineering, Technology, and Sciences, 7(1), 50–70. https://asrjetsjournal.org/index.php/American_Scientific_Journal/article/view/693

Ren, G., Han, H., Wang, Y., Liu, S., Zhao, J., Meng, X., & Li, Z. (2021). Recent advances of photocatalytic application in water treatment: A review. Nanomaterials, 11(7), 1804. https://doi.org/10.3390/nano11071804

Sahu, S. (2019). Electrical modeling of dye-sensitized solar cells for improving the overall photoelectric conversion efficiency. Journal of Ravishankar University (PART-B), 32(1), 84–89. https://doi.org/10.52228/JRUB.2019-32-1-12

Samsudin, M. F. R., Sufian, S., & Hameed, B. H. (2018). Epigrammatic progress and perspective on the photocatalytic properties of BiVO4-based photocatalyst in photocatalytic water treatment technology: A review. Journal of Molecular Liquids, 268, 438–459. https://doi.org/10.1016/j.molliq.2018.07.051

Sánchez-Polo, M., Salhi, E., Rivera-Utrilla, J., & von Gunten, U. (2006). Combination of ozone with activated carbon as an alternative to conventional advanced oxidation processes. Ozone: Science & Engineering, 28(4), 237–245. https://doi.org/10.1080/01919510600714170

Sauter, D., Dąbrowska, A., Bloch, R., Stapf, M., Miehe, U., Sperlich, A., Gnirss, R., & Wintgens, T. (2021). Deep-bed filters as post-treatment for ozonation in tertiary municipal wastewater treatment: Impact of design and operation on treatment goals. Environmental Science: Water Research & Technology, 7(1), 197–211. https://doi.org/10.1039/D0EW00684J

Schneider, J. T., Firak, D. S., Ribeiro, R. R., & Peralta-Zamora, P. (2020). Use of scavenger agents in heterogeneous photocatalysis: Truths, half-truths, and misinterpretations. Physical Chemistry Chemical Physics, 22(27), 15723–15733. https://doi.org/10.1039/D0CP02411B

Shao, H., Wang, Y., Zeng, H., Zhang, J., Wang, Y., Sillanpää, M., & Zhao, X. (2020). Enhanced photoelectrocatalytic degradation of bisphenol a by BiVO4 photoanode coupling with peroxymonosulfate. Journal of Hazardous Materials, 394, 121105. https://doi.org/10.1016/j.jhazmat.2019.121105

Siraki, A. G., Klotz, L.-O., & Kehrer, J. P. (2018). Free radicals and reactive oxygen species. In Comprehensive Toxicology (pp. 262–294). Elsevier. https://doi.org/10.1016/B978-0-12-801238-3.01895-X

STOWA. (2019). Innovation Program Removal of Micropollutants At WWTPs. 24.

Sun, M., Qu, S., Ji, W., Jing, P., Li, D., Qin, L., Cao, J., Zhang, H., Zhao, J., & Shen, D. (2015). Towards efficient photoinduced charge separation in carbon nanodots and TiO 2 composites in the visible region. Physical Chemistry Chemical Physics, 17(12), 7966–7971. https://doi.org/10.1039/C5CP00444F

Sun, S., Wang, W., Zhou, L., & Xu, H. (2009). Efficient methylene blue removal over hydrothermally synthesized starlike bivo 4. Industrial & Engineering Chemistry Research, 48(4), 1735–1739. https://doi.org/10.1021/ie801516u

Tan, B., Guo, L., Yin, D., Ma, T., Zhang, S., & Wang, C. (2022). Environmentally sustainable corrosion inhibitors used for electronics industry. In Environmentally Sustainable Corrosion Inhibitors (pp. 359–381). Elsevier. https://doi.org/10.1016/B978-0-323-85405-4.00007-0

Tan, H. L., Amal, R., & Ng, Y. H. (2017). Alternative strategies in improving the photocatalytic and photoelectrochemical activities of visible light-driven BiVO 4: A review. Journal of Materials Chemistry A, 5(32), 16498–16521. https://doi.org/10.1039/C7TA04441K

The utilization of slag in civil infrastructure construction. (2016). Elsevier. https://doi.org/10.1016/C2014-0-03995-0

Tokunaga, S., Kato, H., & Kudo, A. (2001). Selective preparation of monoclinic and tetragonal bivo 4 with scheelite structure and their photocatalytic properties. Chemistry of Materials, 13(12), 4624–4628. https://doi.org/10.1021/cm0103390

Tolod, K. R., Hernández, S., Castellino, M., Deorsola, F. A., Davarpanah, E., & Russo, N. (2020). Optimization of BiVO4 photoelectrodes made by electrodeposition for sun-driven water oxidation. International Journal of Hydrogen Energy, 45(1), 605–618. https://doi.org/10.1016/j.ijhydene.2019.10.236

Trześniewski, B. J., & Smith, W. A. (2016). Photocharged BiVO 4 photoanodes for improved solar water splitting. Journal of Materials Chemistry A, 4(8), 2919–2926. https://doi.org/10.1039/C5TA04716A

Twycross, R., Pace, V., Mihalyo, M., & Wilcock, A. (2013). Acetaminophen(Paracetamol). Journal of Pain and Symptom Management, 46(5), 747–755. https://doi.org/10.1016/j.jpainsymman.2013.08.001

United States Environmental Protection Agency: How Wastewater Treatment Works... The Basics. (1998).

van Gijn, K., Chen, Y. L., van Oudheusden, B., Gong, S., de Wilt, H. A., Rijnaarts, H. H. M., & Langenhoff, A. A. M. (2021). Optimizing biological effluent organic matter removal for subsequent micropollutant removal. Journal of Environmental Chemical Engineering, 9(5), 106247. https://doi.org/10.1016/j.jece.2021.106247

Villamena, F. A. (2017). Reactive species detection in biology: From fluorescence to electron paramagnetic resonance spectroscopy. Elsevier.

Wang, L., Zhao, J., Liu, H., & Huang, J. (2018). Design, modification and application of semiconductor photocatalysts. Journal of the Taiwan Institute of Chemical Engineers, 93, 590–602. https://doi.org/10.1016/j.jtice.2018.09.004

Wang, Y., Sun, J., Li, J., & Zhao, X. (2017). Electrospinning Preparation of Nanostructured g-C 3 N 4 /BiVO 4 Composite Films with an Enhanced Photoelectrochemical Performance. Langmuir, 33(19), 4694–4701. https://doi.org/10.1021/acs.langmuir.7b00893

What is conduction and valence band in semiconductors—Definition. (2019, December 14). Radiation Dosimetry. https://www.radiation-dosimetry.org/what-is-conduction-and-valence-band-in-semiconductors-definition/

Willach, S., Lutze, H. V., Eckey, K., Löppenberg, K., Lüling, M., Wolbert, J.-B., Kujawinski, D. M., Jochmann, M. A., Karst, U., & Schmidt, T. C. (2018). Direct photolysis of sulfamethoxazole using various irradiation sources and wavelength ranges—Insights from degradation product analysis and compound-specific stable isotope analysis. Environmental Science & Technology, 52(3), 1225–1233. https://doi.org/10.1021/acs.est.7b04744

Wu, M., Jing, Q., Feng, X., & Chen, L. (2018). BiVO4 microstructures with various morphologies: Synthesis and characterization. Applied Surface Science, 427, 525–532. https://doi.org/10.1016/j.apsusc.2017.07.299

X-ray powder diffraction(Xrd). (n.d.). Methods. Retrieved May 11, 2022, from https://serc.carleton.edu/msu_nanotech/methods/XRD.html

Xu, X., Sun, Y., Fan, Z., Zhao, D., Xiong, S., Zhang, B., Zhou, S., & Liu, G. (2018). Mechanisms for ·o2- and ·oh production on flowerlike bivo4 photocatalysis based on electron spin resonance. Frontiers in Chemistry, 6, 64. https://doi.org/10.3389/fchem.2018.00064

Xu, Y. H., Liu, C. J., Chen, M. J., & Liu, Y. Q. (2011). A review in visible-light-driven BiVO<SUB align=right>4 photocatalysts. International Journal of Nanoparticles, 4(2/3), 268. https://doi.org/10.1504/IJNP.2011.040513

Yao, Y., & Luan, J. (2022). Preparation, property characterization of gd2ysbo7/znbinbo5 heterojunction photocatalyst for photocatalytic degradation of benzotriazole under visible light irradiation. Catalysts, 12(2), 159. https://doi.org/10.3390/catal12020159

Ye, Y., Bruning, H., Liu, W., Rijnaarts, H., & Yntema, D. (2019). Effect of dissolved natural organic matter on the photocatalytic micropollutant removal performance of TiO2 nanotube array. Journal of Photochemistry and Photobiology A: Chemistry, 371, 216–222. https://doi.org/10.1016/j.jphotochem.2018.11.012

Yoon, J., Sun, Y., & Rogers, J. A. (2010). Flexible solar cells made of nanowires/microwires. In Semiconductor Nanomaterials for Flexible Technologies (pp. 159–196). Elsevier. https://doi.org/10.1016/B978-1-4377-7823-6.00006-4

Yu, P. Y., & Cardona, M. (2005). Introduction. In P. Y. Yu & M. Cardona, Fundamentals of Semiconductors (pp. 1–15). Springer Berlin Heidelberg. https://doi.org/10.1007/3-540-26475-2_1

Zhang, L., Dai, Z., Zheng, G., Yao, Z., & Mu, J. (2018). Superior visible light photocatalytic performance of reticular BiVO 4 synthesized via a modified sol–gel method. RSC Advances, 8(19), 10654–10664. https://doi.org/10.1039/C8RA00554K

Zhang, M., Pu, W., Pan, S., Okoth, O. K., Yang, C., & Zhang, J. (2015a). Photoelectrocatalytic activity of liquid phase deposited α-Fe2O3 films under visible light illumination. Journal of Alloys and Compounds, 648, 719–725. https://doi.org/10.1016/j.jallcom.2015.07.026

Zhang, M., Pu, W., Pan, S., Okoth, O. K., Yang, C., & Zhang, J. (2015b). Photoelectrocatalytic activity of liquid phase deposited α-Fe2O3 films under visible light illumination. Journal of Alloys and Compounds, 648, 719–725. https://doi.org/10.1016/j.jallcom.2015.07.026

Zhao, T., Yanagi, R., Xu, Y., He, Y., Song, Y., Yang, M., & Hu, S. (2021). A coating strategy to achieve effective local charge separation for photocatalytic coevolution. Proceedings of the National Academy of Sciences, 118(7), e2023552118. https://doi.org/10.1073/pnas.2023552118

Zhao, Y., Tao, C., Xiao, G., & Su, H. (2017). Controlled synthesis and wastewater treatment of Ag 2 O/TiO 2 modified chitosan-based photocatalytic film. RSC Advances, 7(18), 11211–11221. https://doi.org/10.1039/C6RA27295A

Zulkifili, A., Fujiki, A., & Kimijima, S. (2018). Flower-like bivo4 microspheres and their visible light-driven photocatalytic activity. Applied Sciences, 8(2), 216. https://doi.org/10.3390/app8020216

Żur, J., Piński, A., Marchlewicz, A., Hupert-Kocurek, K., Wojcieszyńska, D., & Guzik, U. (2018). Organic micropollutants paracetamol and ibuprofen—Toxicity, biodegradation, and genetic background of their utilization by bacteria. Environmental Science and Pollution Research, 25(22), 21498–21524. https://doi.org/10.1007/s11356-018-2517-x

APPENDICES

Appendix A: Molecular structures of ACT, PRO and BTA

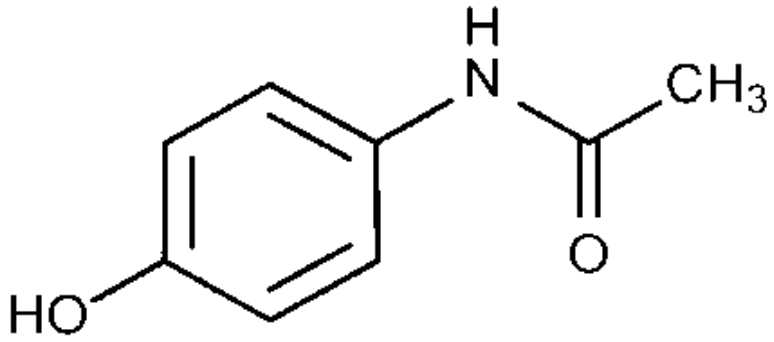

Figure 47: Molecular Structure of ACT

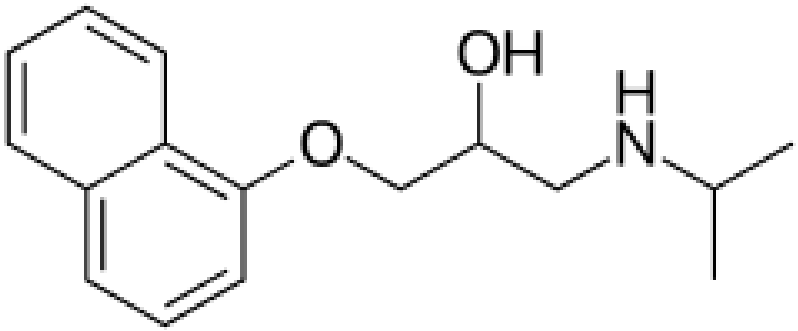

Figure 48: Molecular Structure of PRO

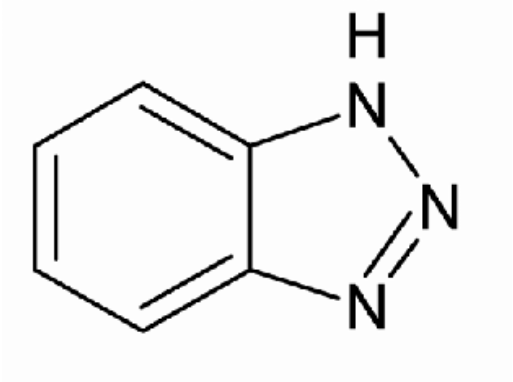

Figure 49: Molecular Structure of BTA

Appendix B: Fabrication of $BiVO_4$ electrodes

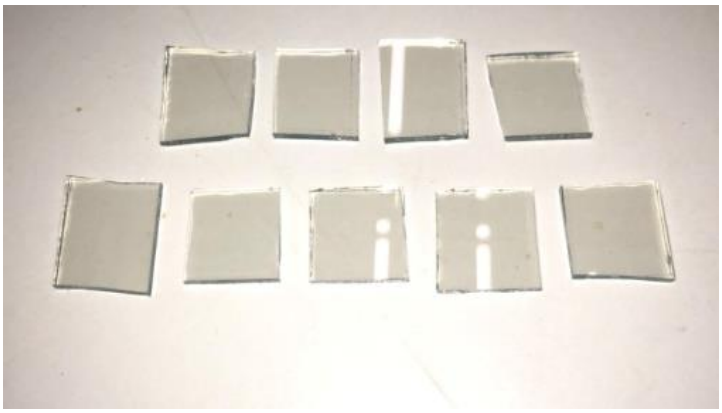

Figure 50: Multiple FTO substrates cut into an area of 4 cm by 4 cm

Figure 51: Digital multimeter used to indicate the conducting FTO side of the glass subtrates

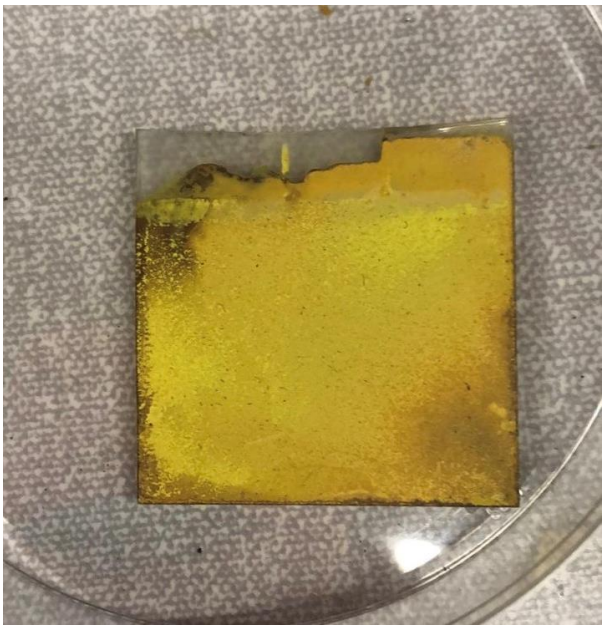

Figure 52: $BiVO_4$ electrode by electrodeposition after being taken out of the furnace, before being soaked in 1 M NaOH to remove the excess V_2O_5

Figure 53: Furnace (Nabeltherm) used for annealing the $BiVO_4$ electrodes

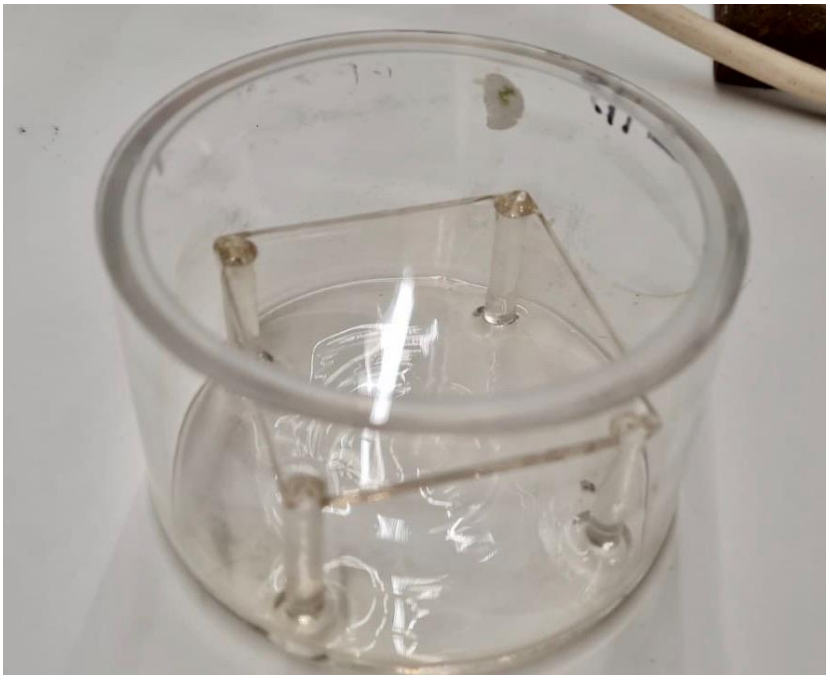

Figure 54: Reactor cell used for degradation experiments (175 mL capacity)

Appendix C: Characterization of $BiVO_4$ electrodes

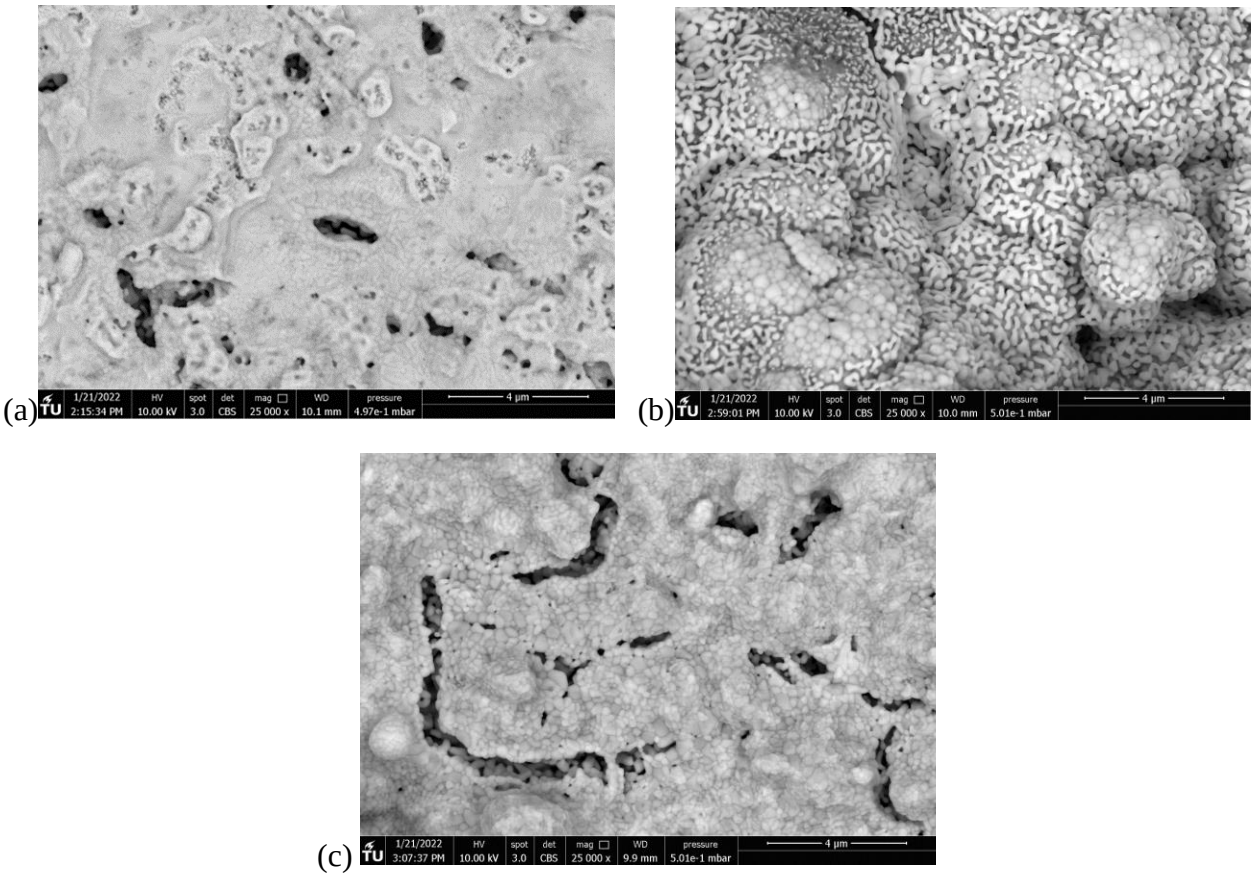

Figure 55: SEM images of dip-coating electrodes with (a)2 layers, (b)4 layers and (c)5 layers, at 25000x magnitude

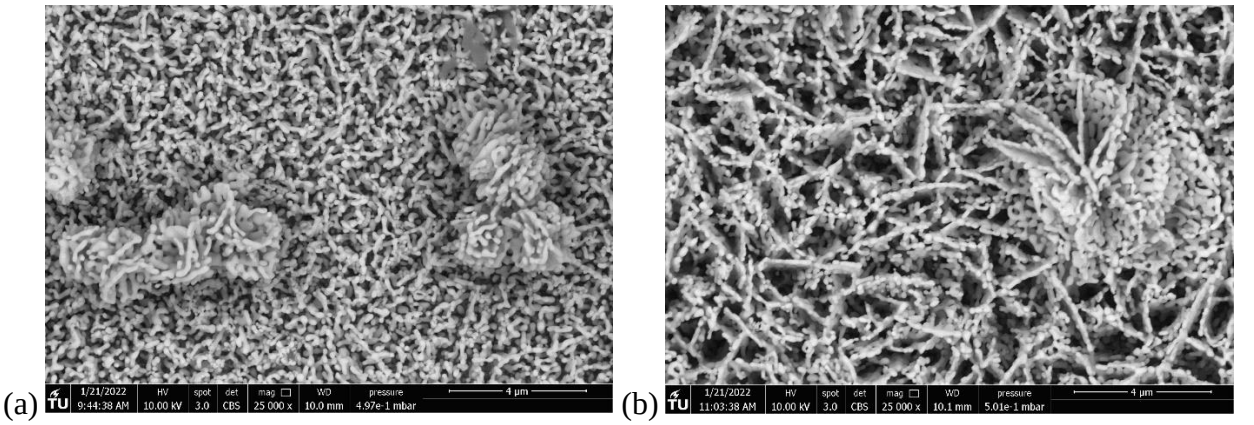

Figure 56: SEM images of electrodeposition electrodes at (a) – 0.2 V, 2 minutes and (b) – 0.2 V, 15 minutes, at 25000x magnitude

(a) 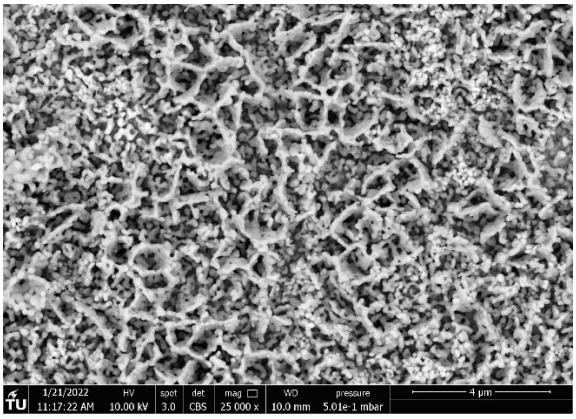

(b) 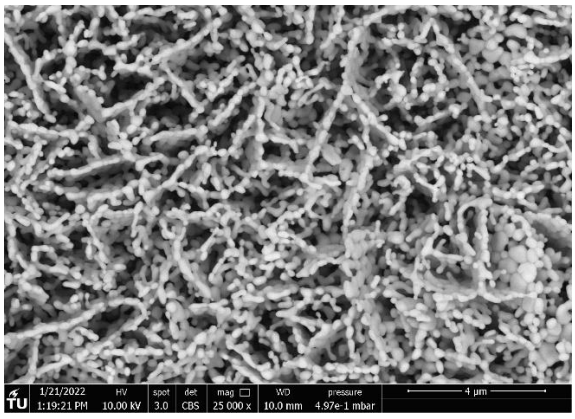

Figure 57: SEM images of electrodeposition electrodes at (a) – 0.4 V, 2 minutes and (b) – 0.4 V, 15 minutes, at 25000x magnitude

Table 7: Maximum IPCE in % measured for all the $BiVO_4$ electrodes

-0.2 V electrodes	**Maximum IPCE (%)**	**-0.4 V electrodes**	**Maximum IPCE (%)**	**Dip-coating electrodes**	**Maximum IPCE (%)**
2 minutes	15.2	**2 minutes**	14.5	**1 layer**	6.4
5 minutes	13.4	**5 minutes**	12.4	**2 layers**	9.2
7 minutes	14.5	**7 minutes**	11.7	**3 layers**	9.1
10 minutes	15.2	**10 minutes**	13.2	**4 layers**	2.3
15 minutes	10.8	**15 minutes**	18.4	**5 layers**	6.5

Appendix D: Photoelectrocatalytic degradation using $BiVO_4$ electrodes

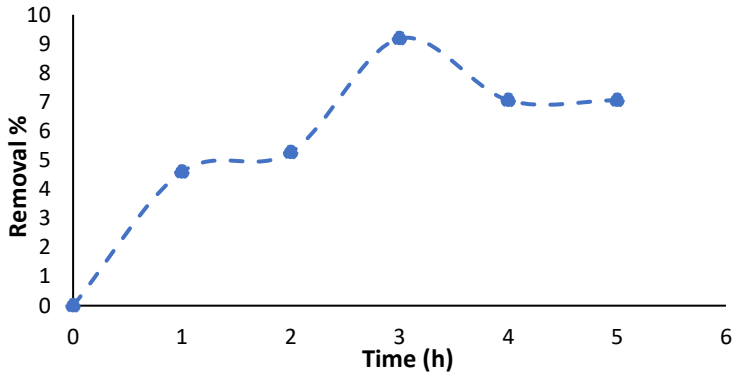

Figure 58:Photolysis of Acetaminophen

Table 8: Rate constants of the reactions of photoelectrocatalytic degradation of ACT for all the $BiVO_4$ electrodes

-0.2 V electrodes	**Rate constant (h^{-1})**	**-0.4 V electrodes**	**Rate constant (h^{-1})**	**Dip-coating electrodes**	**Rate constant (h^{-1})**
2 minutes	0.708	**2 minutes**	0.367	**1 layer**	1.56
5 minutes	1.469	**5 minutes**	0.286	**2 layers**	1.203
7 minutes	1.519	**7 minutes**	1.207	**3 layers**	1.124
10 minutes	0.408	**10 minutes**	0.559	**4 layers**	1.367
15 minutes	0.361	**15 minutes**	0.202	**5 layers**	1.366

Table 9: pH values of the solution after the photoelectrocatalytic degradation of ACT of 5 hours

Electrode	Parameters	Final solution pH
-0.2 V	2 minutes	4
	5 minutes	4
	7 minutes	4
	10 minutes	4.4
	15 minutes	4.3
-0.4 V	2 minutes	4.3
	5 minutes	4.3
	7 minutes	4.2
	10 minutes	4.2
	15 minutes	4.6
Dip-coating	1 layer	5.4
	2 layers	4.7
	3 layers	4.3
	4 layers	4.4
	5 layers	4.4

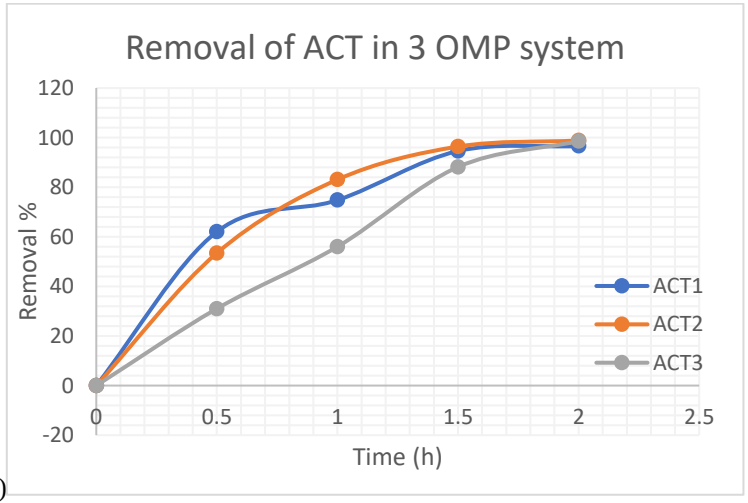

(a)

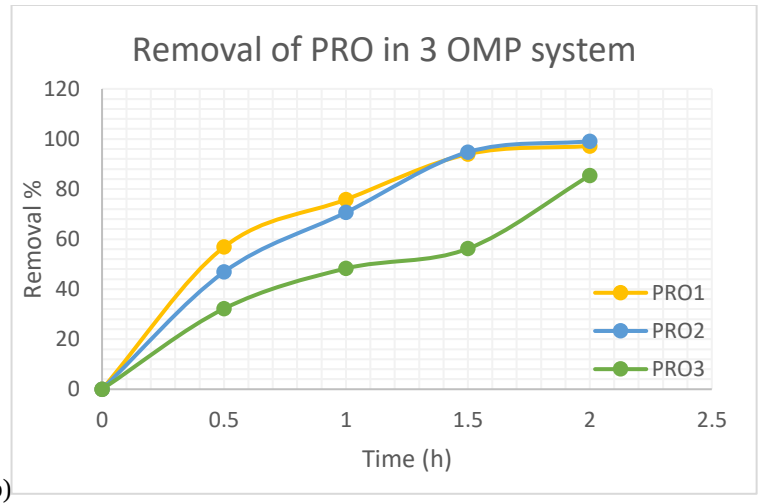

(b)

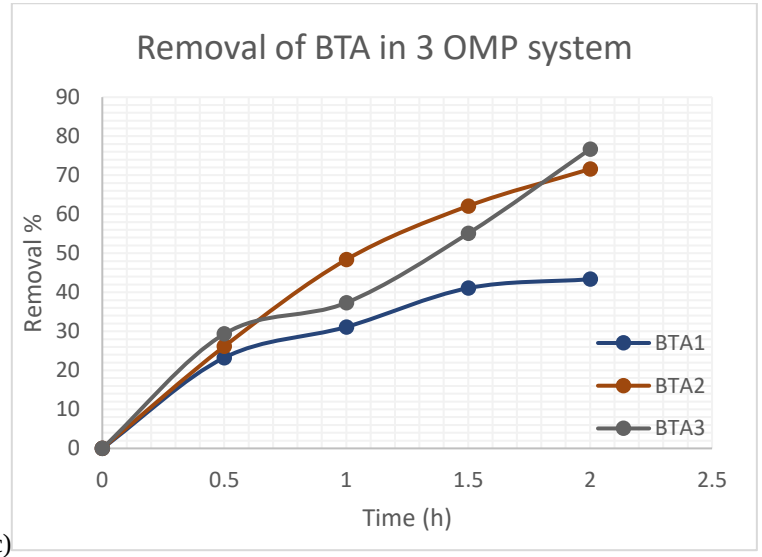

(c)

Figures 59: Results of three experiments of degradation of three OMPs,namely (a) ACT, (b) PRO and (c) BTA, where 1,2 and 3 after the OMP name in the legends describe the removal of that OMP in the first, second and third experiments respectively.